TISSUE ENGINEERING APPROACHES FOR STUDYING THE EFFECT OF BIOCHEMICAL AND PHYSIOLOGICAL STIMULI ON CELL BEHAVIOR

A Dissertation

by

ANDREA CAROLINA JIMENEZ VERGARA

Submitted to the Office of Graduate Studies of
Texas A&M University
in partial fulfillment of the requirements for the degree of

DOCTOR OF PHILOSOPHY

August 2012

Major Subject: Materials Science and Engineering

Tissue Engineering Approaches for Study the Effect of Biochemical and Physiological Stimuli on Cell Behavior

TISSUE ENGINEERING APPROACHES FOR STUDYING THE EFFECT OF BIOCHEMICAL AND PHYSIOLOGICAL STIMULI ON CELL BEHAVIOR

A Dissertation

by

ANDREA CAROLINA JIMENEZ VERGARA

Submitted to the Office of Graduate Studies of
Texas A&M University
in partial fulfillment of the requirements for the degree of

DOCTOR OF PHILOSOPHY

Approved by:

Chair of Committee,	Mariah Hahn
Committee Members,	Melissa Grunlan
	Roland Kaunas
	Arul Jayaraman
Intercollegiate Faculty Chair,	Ibrahim Karaman

August 2012

Major Subject: Materials Science and Engineering

ABSTRACT

Tissue Engineering Approaches for Studying the Effect of Biochemical and Physiological Stimuli on Cell Behavior. (August 2012)

Andrea Carolina Jimenez Vergara, B.S., Universidad Industrial de Santander

Chair of Advisory Committee: Dr. Mariah Hahn

Tissue engineering (TE) approaches have emerged as an alternative to traditional tissue and organ replacements. The aim of this work was to contribute to the understanding of the effects of cell-material and endothelial cell (EC) paracrine signaling on cell responses using poly(ethylene glycol) diacrylate (PEGDA) hydrogels as a material platform. Three TE applications were explored. First, the effect of glycosaminoglycan (GAG) identity was evaluated for vocal fold restoration. Second, the influence of GAG identity was explored and a novel approach for stable endothelialization was developed for vascular graft applications. Finally, EC paracrine signaling in the presence of cyclic stretch, and hydrophobicity and inorganic content were studied for osteogenic applications.

In terms of vocal fold restoration, it was found that vocal fold fibroblast (VFF) phenotype and extracellular matrix (ECM) production were impacted by GAG identity. VFF phenotype was preserved in long-term cultured hydrogels containing high molecular weight hyaluronan (HA_{HMW}). Furthermore, collagen I deposition, fibronectin production and smooth muscle α-actin (SM-α-actin) expression in PEG–HA, PEG–

chondroitin sulfate C and PEG– heparan sulfate (HS) gels suggest that CSC and HS may be undesirable for vocal fold implants.

Regarding vascular graft applications, the impact of GAG identity on smooth muscle cell (SMC) foam cell formation was explored. Results support the increasing body of literature that suggests a critical role for dermatan sulfate (DS)-bearing proteoglycans in early atherosclerosis. In addition, an approach for fabricating bi-layered tissue engineering vascular grafts (TEVGs) with stable endothelialization was validated using PEGDA as an intercellular ‘‘cementing’’ agent between adjacent endothelial cells (ECs).

Finally, mesenchymal stem cell (MSC) differentiation toward osteogenic like cells was evaluated. ECM and cell phenotypic data showed that elevated scaffold inorganic content and hydrophobicity were indeed correlated with increased osteogenic differentiation. Moreover, the present results suggest that EC paracrine signaling enhances MSC osteogenesis in the presence of cyclic stretch.

DEDICATION

To my parents, Omaira and Ricardo and to my brothers Camilo, David, Diego and Ricardo.

To my husband Dany Jair.

ACKNOWLEDGEMENTS

I would like to express my gratitude to my advisor and committee chair, Dr. Mariah Hahn, for her support, patience and guidance during the course of my research. I would also like to thank my committee members, Dr. Grunlan, Dr. Kaunas and Dr. Jayaraman, for their guidance and support.

Thanks also go to my friends and colleagues and the department faculty and staff for making my time at Texas A&M University a great experience. I also want to extend my gratitude to Dr. Sonia Giraldo at Universidad Industrial de Santander who encouraged me to start my graduate studies at Texas A&M.

TABLE OF CONTENTS

CHAPTER Page

CHAPTER Page

CHAPTER Page

CHAPTER Page

CHAPTER Page

LIST OF FIGURES

LIST OF TABLES

CHAPTER I

INTRODUCTION AND

LITERATURE REVIEW

1.1. Problem Statement

Annually tissue damage or loss and organ failure related diseases affect millions of people around the world. These health problems are commonly treated by tissue and organ transplantation from a donor. However, these treatments have limitations such as availability and immune response. Based on the high demand for suitable tissue and organ donors, research efforts have focused on alternative treatments that promote fast body healing or devices that mimic tissue function.

Tissue engineering approaches have emerged as an alternative to traditional tissue and organ replacements. The use of engineered materials capable of closely mimicking the cell microenvironment opens a vast number of possibilities to address the need for tissue replacement.

This dissertation follows the style of Acta Biomaterialia.

Ideal tissue engineering scaffolds should fulfill three major challenges: first, fill the defect caused by tissue damage; second, stimulate new tissue growth, and finally, have the ability to be resorbed over time and be replaced by newly formed tissue [1]. In order to develop a graft with such characteristics it is fundamental to understand the effect of scaffold properties and physiological stimuli on cell behavior.

This work focuses on the understanding of cell material interactions with the systematic and controlled design of material properties and the controlled introduction of endothelial cell (EC) paracrine signaling and their effect on cell response for 3D tissue engineering applications: vocal fold restoration, small diameter vascular graft, and bone regeneration. Cell responses were analyzed at the biochemical, histological and microstructural levels. The specific aims and rationale for this work were:

- Verify the ability of vocal fold fibroblasts (VFFs) to respond consistently to biochemical stimuli despite the abnormal cell shapes imposed by poly (ethylene glycol) diacrylate (PEGDA) hydrogels. Rationale: PEGDA hydrogels have been examined as VFF regeneration scaffolds due to their injectability and tunable viscoelastic properties [2-6]. However, a limitation of PEGDA scaffolds is that they force cells to take on round morphology, whereas VFFs are natively elongated. Thus, to further evaluate the potential utility of PEGDA hydrogels as vocal fold regeneration scaffolds, the ability of VFFs encapsulated in PEGDA hydrogels to respond appropriately (i.e. as if elongated) to scaffold biochemical stimuli was examined. Since hyaluronan (HA) based hydrogels have been extensively studied as VF regeneration scaffolds [4, 7, 8], PEGDA-HA hybrid hydrogels were examined so

as to permit direct comparison with previous studies involving scaffolds permissive of cell elongation. Alterations in VFF phenotype were examined by evaluating the relative expression of collagen III versus collagen I (with a higher collagen III:collagen I ratio being desirable), elastin expression (with lower levels of elastin being desirable), and SM-α-actin expression (with lower levels of this myofibroblast marker being desirable).

- Evaluate the effects of chondroitin sulfate C (CSC) and heparin sulfate (HS) incorporation on the mechanical response of PEG gels and VFF behavior relative to HA. Rationale: PEG-based hydrogels have recently begun to be examined as vocal fold augmentation substances [9-14], due to their tailorable mechanical properties and resistance to fibroblast-mediated contraction. However, pure PEG hydrogels lack intrinsic biochemical signals to guide cell behavior and generally fail to mimic the frequency- dependent viscoelastic response critical to normal superficial lamina propia (SLP) function [10-12, 14, 15]. Recent results suggest that conjugating viscoelastic bioactive substances, such as GAGs, into PEG networks may allow these hydrogels to more closely approach the mechanical responses of normal SLP while stimulating desired VFF behaviors [10, 16]. GAGs are a family of charged polysaccharides which play key roles in inflammation, cell migration, and cell phenotype modulation [19] and which include unsulfated forms (e.g. HA) as well as sulfated forms (e.g. HS, CSC). While a number of vocal fold studies have examined the impact of HA on implant mechanics and/or fibroblast behavior [10, 11, 13, 16-19], the influence of sulfated GAGs has been relatively unexplored. CSC and HS

were selected for investigation over other sulfated GAGs for several reasons including recent quantitative measures which suggest that expression of CSC, rather than dermatan sulfate (DS), is substantially decreased in scarred lamina propria [20]. In addition, a separate study has shown that levels of specific HS proteoglycans are altered in scarred lamina propria [21].

- Investigate the regulation of smooth muscle cell (SMC) foam cell formation by glycosaminoglycan identity within a hydrogel environment mimetic of early atherosclerosis. Rationale: Recently, it has been recognized that the early accumulation of lipids associated with atherosclerosis arises primarily from enhanced lipoprotein retention by the ECM of the arterial intima [22-24]. In particular, studies suggest that proteoglycans (PGs) play a key role in the enhanced retention of low density lipoproteins (LDL) [25, 26]. For example, versican has been shown to have high affinity for apolipoprotein B (apoB) and decorin has been related to LDL binding [27]. Recent studies indicate that the ionic interactions between the negatively charged GAG side-chains of these PGs and the positively charged apolipoprotein residues of LDL are critical to early atherosclerotic lipid retention [25-27]. Although it is recognized that GAG retention of lipoproteins is a key event in SMC foam cell formation [22], the extent to which specific GAG types contribute to this process is relatively poorly understood. This study has been designed to compare the effects of CSC, DS, and HS side chains on SMC foam cell formation.
- Validate an approach for generating a thin, mechanically stable EC layer in the lumen of PEG hydrogel-based tissue engineered vascular grafts (TEVGs). Rationale:

Achieving endothelialization of PEG-based hydrogels that is stable under physiological loading conditions is challenging, and engineered EC layers frequently delaminate upon exposure to high shear pulsatile flow [28, 29]. A range of methods have been employed to enhance stable vascular graft endothelialization, including specialized EC seeding methods [29] and luminal coatings [30]. However, only moderate long-term success has been attained with these approaches. In the present study, an approach which utilizes PEGDA as an intercellular "cementing" agent rather than as an encapsulating agent is developed.

- Examine the effects of simultaneous increases in scaffold hydrophobicity and inorganic content on mesenchymal stem cell (MSC) osteogenic fate decisions in a 3D culture environment. Rationale: A number of studies have shown that the addition of inorganic components to organic scaffolds can enhance both their osteoconductivity and osteoinductivity [31-33]. These inorganic additives have included not only hydroxyapatite, but also a range of silicon-containing compounds, such as silica, silane, and siloxane [33-36]. In addition, scaffold hydrophobicity has been demonstrated to influence osteogenic differentiation [37-39]. However, the combined effects of scaffold inorganic content and hydrophobicity have not been systematically explored. Furthermore, most of the aforementioned studies were performed in two-dimensional (2D) culture, and, thus, may not be indicative of the effects of the same scaffold variables in more biomimetic, three-dimensional (3D) culture systems. The aim of the present study was therefore to examine the impact of

simultaneous increases in scaffold hydrophobicity and inorganic content on MSC osteogenic lineage progression in a 3D culture environment.

- Examine the effect of EC paracrine signaling on osteogenesis in the context of scaffolds with "osteogenic" moduli and in the presence of mechanical stimulation. Rationale: Neovascularization and mechanical stress play critical roles in endochondral ossification, a key bone formation mechanism during bone growth and fracture healing [40]. Indeed, in endochondral ossification, blood vessels invade hyaline cartilage, and MSCs associated with invading vessels differentiate into osteoblasts which begin depositing bone matrix [40]. In addition, physiological loading during endochondral ossification enhances the rate and quality of bone matrix deposition [41, 42]. Consistent with the endochondral ossification process, studies have shown MSC osteogenic differentiation to be separately influenced by cyclic loading [43, 44] and EC presence [45-47]. However, potential synergistic interactions between mechanical stimulation and EC presence on MSC osteogenesis remain to be elucidated. The goal of the present study is to examine the effects of EC paracrine signaling on MSC osteogenesis in the presence of physiological loading.

These goals are designed to elucidate the relevance of scaffold properties and EC paracrine signaling on cell behavior and tissue regeneration. This work represents a novel strategy for the tuning and optimization of scaffold properties and physiological stimuli for tissue engineering applications in 3D contexts, which was accomplished by the use of PEG hybrid hydrogels as a material platform. Understanding the relative impact of each individual stimulus on cell response allows the design of more efficient

scaffolds by narrowing down the number of variables and range of stimuli needed for a specific application. In addition, it is important understand not only the effect of each individual factor, but also the combined effect of these factors on cell behavior particularly on MSC differentiation.

1.2. Background

Tissue regeneration is a complex process that is regulated by local microenvironment. This specific microenvironment involves different factors such as ECM and EC paracrine signaling that guide cell fate.

ECM is the material that surrounds the cells which is responsible for tissue mechanical support, organization and cell behavior [48]. ECM is mostly composed of proteins such as collagen and elastin and polysaccharides such as hyaluronic acid and glycosaminoglycans. ECM plays a role in regulating water content, selecting and retaining different growth factors as well as interacting with the cells through cell receptors.

Research efforts have focused on engineering scaffolds that mimic the ECM microenvironment using biomaterials. Scaffold properties such as chemical composition, surface chemistry and mechanical properties can be used to control cell adhesion, migration, differentiation, diffusion of nutrients and waste, and matrix composition. A variety of materials have been developed for controlling cell behavior such as natural and synthetic polymers, metals and ceramics materials. These materials have been used

to induce stem cell (SC) differentiation toward specific cell linage [49]. Several studies of natural and synthetic polymers in SC differentiation have also been reported. Natural materials are biocompatible and biodegradable, and provide biochemical and biophysical cues that influence cell behavior. Natural materials such as agarose, alginate, hyaluronic acid, fibrin, collagen and matrigel have been used to support SC differentiation [50]. On the other hand, despite the fact that synthetic materials lack the biochemical cues present in natural materials, they offer a great deal of controllability and potential for the understanding of SC behavior. Synthetic materials are easy to control, consistent across batches, have good mechanical properties, and the desired biochemical stimuli can be incorporated as a design parameter. One of the most widely used synthetic biomaterials for the study of cell behavior are polymers. Mechanical properties, chemical composition and specific degradation rate of these biomaterials can be controlled [51]. In addition, they have high purity and reproducibility Poly(ethylene glycol) (PEG), poly(vinyl alcohol) (PVA), poly(lactic acid) (PLA), poly(lactic-co-glycolic acid) (PLGA), poly(hydroxyl ethyl methacrylate) (PHEMA), and poly(anhydride) are the most common synthetic polymers used in tissue engineering applications [50].

PEG is a synthetic polymer with high hydrophilicity, biocompatibility, and resistance to protein absorption, and it is considered to behave as a biological blank slate. A commonly used form of PEG hydrogels involves vinyl chemistry in order to create a 3D environment by crosslinking under UV exposure. A brief description of PEG modification end vinyl groups as well as an idealized PEG network is presented in Fig. 1. PEG based hydrogel platforms can be used to understand the isolated effect of

material properties such as mesh size, mechanical properties, biochemical and EC paracrine signaling interactions on cell behavior.

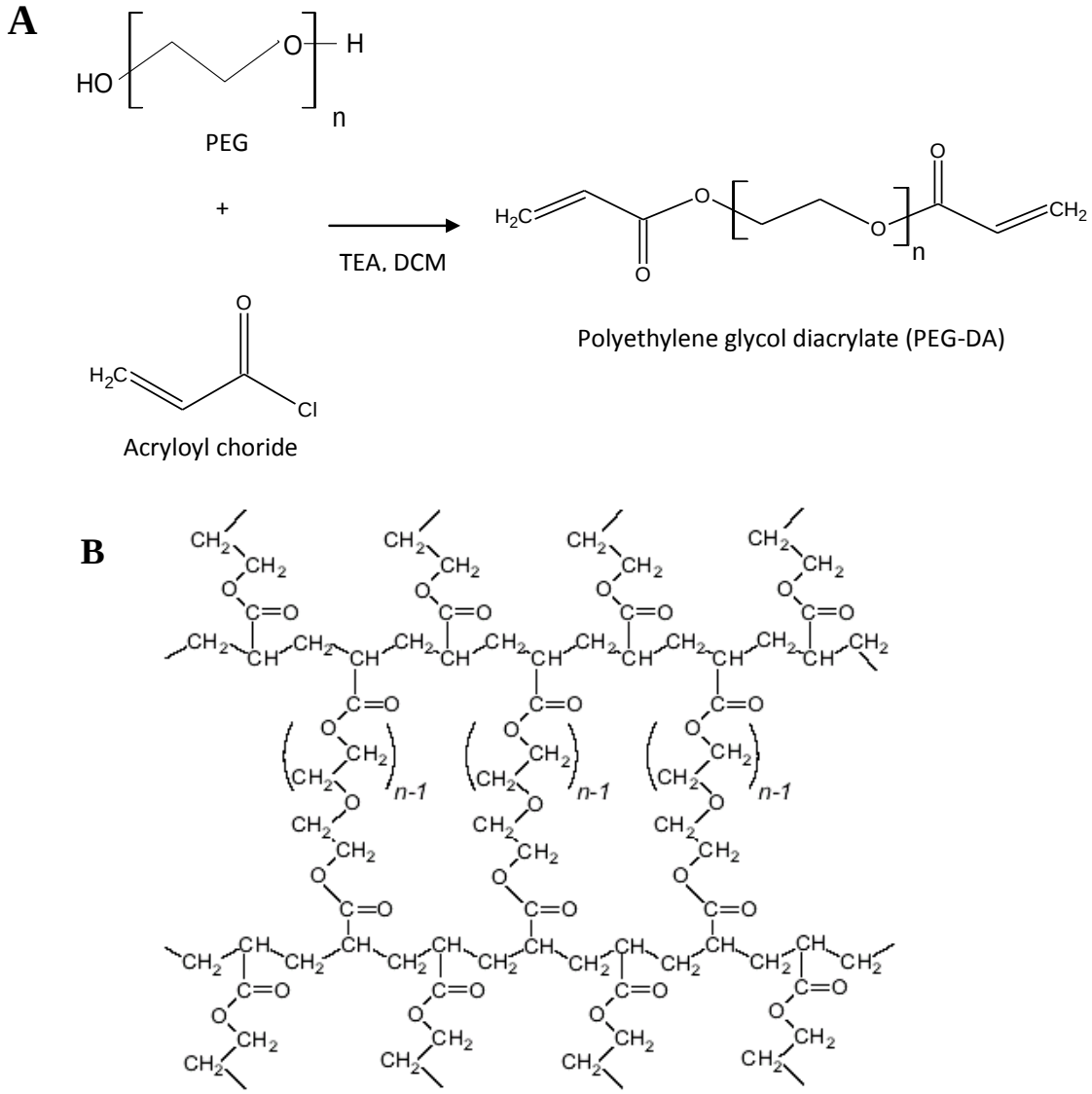

Fig. 1. (A) Schematic representation of PEGDA synthesis and (B) idealized 3D network [52].

An additional advantage of PEG-based hydrogels is that the “blank state” feature of PEGDA can be modified with the addition of biomolecules, peptides, small functional groups and other polymers. These modifications could change hydrogel chemical functionality and hydrophobicity/hydrophilicity which have shown to play a role in cell adhesion, function and differentiation [53].

Additional studies have focused on EC paracrine signaling which seem to play an important role in organ formation, especially on MSC differentiation. Several research works have been directed to evaluate the role of these interactions on MSCs fate commitment [54]. For instant, MSCs direct contact with other cell types has demonstrated to have an influence in MSC behavior [55]. Furthermore, it has been shown that EC express several factors such as BMP-2 [45] and VEGF [56] in contact with MSCs, which could induce osteogenic differentiation [57].

CHAPTER II

PROBING VOCAL FOLD FIBROBLAST RESPONSE TO HYALURONAN IN 3D CONTEXTS*

2.1. Overview

A number of treatments are being investigated for VF scar, including designer implants. The aim of the present study was to validate a 3D model system for probing the effects of various bioactive moieties on VFF behavior toward rational implant design. We selected PEGDA hydrogels as our base-scaffold due to their broadly tunable material properties. However, since cells encapsulated in PEGDA hydrogels are generally forced to take on rounded/ stellate morphologies, validation of PEGDA gels as a 3D VFF model system required that the present work directly parallel previous studies involving more permissive scaffolds. We therefore chose to focus on HA, a polysaccharide that has been a particular focus of the VF community.

*Reprinted with permission from "Probing vocal fold fibroblast response to hyaluronan using PEG-based hydrogels" by Dany J. Munoz-Pinto, Andrea Carolina Jimenez-Vergara, L. Marcela Gelves, Rebecca E. McMahon, Viviana Guiza-Arguello, Mariah S. Hahn, 2008, Biotechnology and bioengineering (2009) 821-31, Copyright 2009, Wiley Periodicals, Inc.

Toward this end, porcine VFFs were encapsulated in PEGDA hydrogels containing consistent levels of high M_w HA (HA_{HMW}), intermediate M_w HA (HA_{IMW}), or the control polysaccharide, alginate, and cultured for 7 and 21 days.

HA_{HMW} promoted sustained increases in active ERK1/2 relative to HA_{IMW}. Furthermore, VFFs in HA_{IMW} gels displayed a more myofibroblast-like phenotype, higher elastin production, and greater protein kinase C (PkC) levels at day 21 than VFFs in HA_{HMW} and alginate gels.

The present results are in agreement with a previous 3D study of VFF responses to HA_{IMW} relative to alginate in collagen-based scaffolds permissive of cell elongation, indicating that PEGDA hydrogels may serve as an effective 3D model system for probing at least certain aspects of VFF behavior.

2.2. Introduction

Voice disorders resulting from scarring of the VF lamina propria (LP) affect millions in the US alone and can significantly impact quality of life [58]. VF scar has proven difficult to treat with current surgical techniques and standard augmentation substances, such as collagen and fat [59-61]. Researchers are actively exploring alternative treatment routes, including the development of designer implants for functional LP regeneration [2, 4, 6, 62].

HA has been a particular focus as a component of these designer implants due to its role in wound healing and in VF mechanical properties [3, 4, 6]. Although several in

vivo studies suggest HA to be a promising material for VF regeneration [4, 7, 8], to rationally improve the design and formulation of these HA-based implants requires a deeper understanding of the impact of HA on VFF ECM production and phenotype.

A number of studies have examined cellular response to HA in 2D scenarios [63-66]. However, evaluating the specific influence of HA in more physiolo-gically relevant 3D contexts has proven challenging due to the additional, often interdependent, matrix variables introduced in 3D. To understand this, examine a recent study in which mesenchymal stem cells encapsulated within collagen beads displayed an increased tendency to differentiate into chondrocytes as collagen density increased [67]. Whether this increased chondrocytic potential was due primarily to the increased spatial density of bioactivity (collagen) or to the increased matrix stiffness associated with heightened collagen concentration is unclear. Being able to make such distinctions is important since both scaffold modulus [68] and bioactivity [69] have been shown to exert profound effects on cell behavior in 2D.

To begin to uncouple the effects of various stimuli on VFF behavior in 3D requires a scaffold whose material properties can be more tightly controlled. Hydrogels prepared from PEGDA are intrinsically resistant to cell attachment and spreading [70]. This biological ‘‘blank slate’’ character of PEGDA hydrogels permits the controlled introduction of desired bioactivity and examination of its effects on cell behavior [71]. Furthermore, the initial bulk average mesh size and modulus of PEGDA hydrogels can be tuned in an uncoupled manner by simultaneously varying both the molecular weight (Mw) and/or concentration of PEGDA [72]. PEGDA gels have been widely employed

in cartilage tissue engineering due to their tailorable material properties [73-75]. However, they are rarely used for encapsulation of natively elongated cells, such as fibroblasts, due to the fact that encapsulated cells are generally forced to take on rounded/stellate morphologies. Thus, validation of PEGDA gels as a 3D VFF model system requires that the present study be performed so as to permit direct comparison with previous studies involving scaffolds permissive of cell elongation.

We therefore designed the current work to be a direct analog of a previous 3D study of the influence of HA on VFF behavior by Hahn et al.[76]. In that work, porcine VFF responses to intermediate M_w HA (HA_{IMW}, ~490 kDa) relative to the control polysaccharide alginate (~300– 350 kDa, 65–75% guluronate) were investigated in basehydrogels of collagen type I. In the present work, porcine VFFs from the same explant population employed in Hahn et al.[76] were encapsulated in PEGDA hydrogels containing high M_w HA (HA_{HMW}, ~$1.65x10^3$ kDa), HA_{IMW} (~600 kDa), or alginate (~300–350 kDa, 65–75% guluronate). The promiscuous integrin adhesion peptide RGDS [77] was used in place of collagen type I. Following 7 and 21 days of culture, VFF ECM production and phenotype in each formulation was assessed biochemically and histologically. Furthermore, the modulation of two primary signaling pathways (protein kinase C (PkC) and ERK) triggered by HA interactions with cell receptors, CD44 and RHAMM [78-80], was semi-quantitatively evaluated.

2.3. Material and Methods

2.3.1. Polymer Synthesis and Characterization

2.3.1.1. PEG-Diacrylate Synthesis

PEGDA was prepared as previously described [71] by combining 0.1mmol ml^{-1} dry PEG (10 kDa, Sigma, St. Louis, MO), 0.4 mmol ml^{-1} acryloyl chloride, and 0.2 mmol ml^{-1} triethylamine in anhydrous dichloromethane (DCM) and stirring under argon overnight. The resulting solution was washed with 2M K_2CO_3 and separated into aqueous and DCM phases to remove HCl. The DCM phase was subsequently dried with anhydrous $MgSO_4$, and PEGDA was precipitated in diethyl ether, filtered, and dried under vacuum. The degree of acrylate functionalization was determined by ^{1}H-NMR to be 70%.

2.3.1.2. Synthesis of Acrylate-Derivatized

Cell Adhesion Peptide Cell adhesion peptide RGDS (American Peptide, Sunnyvale, CA) was reacted with acryloyl-PEG-N-hydroxysuccinimide (ACRL-PEG-NHS, 3.4 kDa, Nektar, San Carlos, CA) at a 1:1 molar ratio for 2 h in 50mM sodium bicarbonate buffer, pH 8.5 [71]. The product (ACRLPEG- RGDS) was purified by dialysis, lyophilized, and stored at -20°C until use.

2.3.1.3. Synthesis of Methacrylate-Derivatized High Molecular Weight HA and Alginate

Methacrylate-derivatized high M_w HA (HA_{HMW}-MA) and methacrylate-derivatized alginate (alginate-MA) were prepared according to standard methodologies [81]. HA (Streptococcus equi, M_w 1.65 x 10^3 kDa, Fluka) or alginate (Laminaria hyperborea, 300–350 kDa, 65–75% guluronate, FMC BioPolymer Philadelphia, PA) was dissolved at 1-wt% in dIH_2O and the pH of the resulting solution was adjusted to 8.0 using NaOH. A 10-fold molar excess of methacrylic anhydride (Polysciences, Warrington, PA) was added per disaccharide unit. Each reaction was allowed to proceed under constant stirring at 4°C, with the solution pH being maintained at 8.0 by periodic addition of 5M NaOH. The product of each reaction was precipitated twice into chilled ethanol 95%, dialyzed against dIH_2O for 48 h, and lyophilized. The extent of methacrylatederivatization of both HA and alginate was characterized by ^{1}H-NMR to be 3.2%.

2.3.1.4. Synthesis of Methacrylate-Derivatized

Intermediate Molecular Weight HA HA_{HMW}-MA was dissolved at 1 mg ml^{-1} in PBS containing 0.05% sodium azide and 5 U ml^{-1} hyaluronidase IV-S (H3884, Sigma). Following incubation at 37°C for 12 h, the enzyme was heat-inactivated. The digestion time and conditions were selected to yield a mean HA product size consistent with the HA M_w used in Hahn et al.[76]. The resulting digestion product (HA_{IMW}-MA) was dialyzed against dIH_2O for 48 h and lyophilized. The M_w of the isolated HA_{IMW}-MA was

determined to be ~600 kDa using gel permeation chromatography (Viscotek, Houston, TX).

2.3.1.5. Assessment of Alginate as a Control and of HA-MA Activity

The ability of alginate and HA_{HMW}-MA to interact with HA link protein (HABP) was evaluated relative to HA_{HMW} using an HA competitive ELISA assay (Echelon Biosciences, Salt Lake City, UT).

2.3.2. Cell Culture

Cryopreserved porcine VFFs at passage 3 from the same VFF explant culture employed in Hahn et al. [76] were obtained from Robert Langer, ScD (Massachusetts Institute of Technology (MIT), Cambridge, MA). These cells had been isolated from the mid-membranous LP of 6- to 12-month-old pigs, a common animal model for the human VF LP [82]. The discarded animal tissue was obtained via the MIT Division of Comparative Medicine and with the approval and according to the guidelines of the MIT animal care committee. The cryopreserved VFFs were thawed and expanded at 37°C/5% CO2 in Dulbecco's Modified Eagle's Media (DMEM, Hyclone, Logan, UT) supplemented with 10% fetal bovine serum (FBS), 2 ng ml^{-1} bFGF, 100 mU ml^{-1} penicillin, and 100 mg l^{-1} streptomycin (Hyclone).

2.3.3. Cell Encapsulation and Hydrogel

Maintenance Hydrogels were fabricated by preparing precursor solutions containing 100 mg $^{-1}$ ml (10 wt%) PEGDA, 5 mg ml^{-1} of methacrylate-derivatized polysaccharide (HA_{HMW}-MA, HA_{IMW}-MA, or alginate-MA), and 1 mmol ml^{-1} ACRLPEG- RGDS in HEPES buffered saline (HBS; 10mMHEPES, 150mM NaCl, pH 7.4). The concentrations of HA and alginate were selected to be consistent with Hahn et al. [76]. A 10-wt% 10 kDa PEGDA hydrogel was chosen for the base-scaffold due to a previous study of VFF responses to PEGDA gels [12]. In addition, the 100:5 weight ratio of PEGDA to polysaccharide was selected so that the degradation rate, modulus, and initial mesh structure of each hydrogel network would be dominated by PEGDA.

A 300 mg ml^{-1} solution of UV photoinitiator 2,2- dimethoxy-2-phenyl-acetophenone in N-vinylpyrrolidone was added at 1% (v/v) to each precursor solution. VFFs at passages 8–9 were harvested and resuspended in the filtersterilized precursor solutions at ~1 x 10^6 cells ml^{-1} (the seeding density employed in Hahn et al. [76]. The cell suspensions were then poured into molds composed of two glass plates separated by 1.1mm polycarbonate spacers and polymerized by 2 min exposure to longwave UV light (Spectroline, Westbury NY, ~6mW cm^{-2}, 365 nm). The hydrogel slabs were transferred to Omnitrays (Nunc, Rochester, NY) fitted with four sterile polycarbonate bars to simultaneously prevent gel flotation and prevent gel contact with the tray bottom. Hydrogels were immersed in DMEM supplemented with 10% FBS, 100 mU ml^{-1}

penicillin, and 100 mg l^{-1} streptomycin, and maintained at 37°C/5% CO2. Media was changed every 2 days.

2.3.4. Hydrogel Characterization

2.3.4.1. Initial Water Uptake

To compare the extent of initial water uptake by the various hydrogel formulations following polymerization, the initial weight (W_i) of each hydrogel was determined immediately following polymerization, after which the gels were submerged in media. Following 3 days of culture, the swollen weight (W_s) of each gel was determined. The equilibrium water uptake (S) was calculated as: $S = \frac{s}{i}$.

2.3.4.2. Hydrogel Mechanical Properties and Contraction

After 72 h swelling, three 8mmdiameter samples were cored from each hydrogel. The thickness of each disc was measured using a digital caliper. These thickness measures served both as gauge lengths for mechanical testing and as indicators of hydrogel degradation and/or VFF-mediated gel compaction. Following application of a 0.01N preload, each hydrogel was subjected to cyclic unconstrained compression (~1% cyclic strain) at 2.5 Hz using an Instron 3342 (Instron, Norwood, MA). During mechanical testing, samples were immersed in silicone oil to prevent hydrogel dehydration. The dynamic compressive modulus of each hydrogel formulation was extracted from the resulting stress–strain data.

2.3.5. Biochemical Analyses

At days 7 and 21 of culture, a series of 8mm diameter samples were collected from each hydrogel formulation for mechanical, biochemical, and histological analyses. Mechanical samples were tested as described above. Samples harvested for biochemical analyses were transferred to screw-cap vials, weighed, flash-frozen in liquid nitrogen, and stored at -80°C until time of analysis. The weight of each 8mm disc was used as a second indicator of gel degradation and/or compaction, since associated reductions in gel volume would be reflected in a mass loss. Hydrogel samples were digested for 72 h at 37°C in 1 ml of 0.12M NaOH per 0.2 g hydrogel wet weight [83, 84]. Digest aliquots were then analyzed for DNA, total collagen, elastin, and sulfated GAGs content per established protocols.

2.3.5.1. DNA Analysis

Aliquots of the hydrolyzed samples (n = 3–6 per formulation) were neutralized and their DNA content determined using the Invitrogen (Carlsbad, CA) PicoGreen assay [84]. DNA measures were translated to cell number using a conversion factor of 6.6 pg DNA per cell [85]. Calf thymus DNA (Sigma) served as a standard.

2.3.5.2. Sulfated GAG

Analysis GAGs production was measured using a modification of the Biocolor Blyscan assay (Accurate Chemical and Scientific Corp., Westbury, NY) [72]. In brief, 40 ml of each sample digest (n = 3–4 per formulation) was neutralized, mixed with 60 ml Blyscan dye reagent, and the absorbance at 525nm immediately measured relative to chondroitin sulfate B (Sigma).

2.3.5.3. Collagen Analysis

The amino acid hydroxyproline was quantified as an indirect measure of total collagen. In brief, aliquots (n = 3–7 per formulation) collected for collagen quantitation were hydrolyzed for 18 h at 110°C in 6 M HCl. Each sample was then dried on a Labconco Centrivap to remove HCl, resuspended in deionized water, and passed through a charcoal-packed centrifugal microcolumn (Nunc). The resultant samples were reacted with chloramine T and p-dimethylbenzaldehyde reagents [83, 84]. Sample absorbance was read at 550 nm relative to that of L-4-hydroxyproline (Sigma). Total collagen content was estimated from measured grams of hydroxyproline by dividing by 0.13.

2.3.5.4. Elastin Analysis

Elastin production was measured using direct ELISA [86]. NaOH digested samples (n = 4–11 per formulation) were neutralized and further digested with 0.25 M oxalic acid at 100 °C overnight. Oxalic acid was removed from the samples and exchanged for PBS using Microcon YM-3 centrifugal filters (Millipore, Billerica, MA).

One hundred microliters of the resulting samples were applied to a high binding multiwell plate for 3 h at room temperature. After blocking the plate with bovine serum albumin, adsorbed elastin fragments were detected by applying elastin antibody (BA-4, Santa Cruz Biotechnology, [SCBT], Santa Cruz, CA) followed by donkey anti-mouse HRP secondary antibody (SCBT) and 2,20-azino-bis(3- ethylbenzthiazoline-6-sulphonic acid). Absorbance was read at 410 nm, with bovine aortic elastin (Sigma) serving as a standard.

For each assay, the standards used were subjected to the same association with PEGDA and polysaccharide and to the same digestion conditions as the samples. Resulting collagen, elastin, and GAGs levels were normalized to cell number.

2.3.6. Histological

Analyses Days 7 and 21 samples harvested for histological analyses were fixed in 10% formalin for 30 min, embedded in Tissue- Tek freezing media, and frozen at -80°C. Thirty-five micrometer-thick sections were cut using a cryomicrotome. All immunostaining steps took place at room temperature unless otherwise noted.

2.3.6.1. ECM and Cell Phenotype

Analyses ECM deposition was analyzed in duplicate sections for each formulation using standard immunohistochemical technique. Rehydrated sections were

blocked with peroxidase for 10 min followed by 10 min exposure to Terminator (Biocare Medical, Concord, CA). Primary antibodies for elastin (BA-4, SCBT), collagen type I (Rockland Immunochemicals, Gilbertsville, PA), or collagen type III (Rockland Immunochemicals) diluted in HBS were then applied for 1 h. To identify VFFs displaying a myofibroblast-like phenotype, primary antibody for SM-α-actin (1A4, LabVision, Fremont, CA) was applied. HA cell surface receptors were also examined using antibodies to RHAMM (H-90, SCBT) and CD44 (F-4 SCBT). Bound primary antibody was detected by using AP-conjugated secondary antibody followed by application of the chromogen Ferangi Blue (Biocare Medical) or by using HRP-conjugated secondary antibody followed by application of the chromogen AEC (LabVision).

2.3.6.2. Cell Proliferation and Apoptosis and Signaling

To identify VFFs undergoing proliferation, sections were stained for Proliferating Cell Nuclear Antigen (PCNA; PC10, Invitrogen) per the above staining procedure, except that rehydrated sections were permeabilized (10 mM HEPES, pH 6.8, 100 mM NaCl, 3mM $MgCl_2$, 300 mM sucrose, 0.5% Triton X-100) for 30 min prior to Terminator application. Apoptotic cells were identified using a Terminal deoxynucleotidyl transferase dUTP nick end-labeling (TUNEL) assay (Roche, Indianapolis, IN) per manufacturer's protocol. Cell signaling was evaluated by staining permeabilized sections for PkC (C-15, SCBT) and active ERK1/2 (pERK1/2(Thr 202/Tyr 204), SCBT).

2.3.6.3. Semi-Quantitative Assessments

For intracellular markers of cell behavior (SM-α-actin, pERK1/2, PkC, PCNA, TUNEL), cell counts were carried out to semi-quantitatively evaluate immunostaining results. These assessments were conducted per established protocols [53, 87-89]. For each cell, i, in a given section, a staining intensity, d_i, was recorded on a scale of 0–3, 0 ‘‘no staining’’ and 3 ‘‘highest intensity among all treatment groups for that antibody.’’ The cumulative staining intensity, d, for a given antibody in a particular section was calculated using the following equation: $d \quad \frac{\sum d_i}{\text{total cell number}}$.

Since deposited ECM remained localized around the parent cells in each hydrogel formulation, as is characteristic for PEGDA gels [73, 90, 91], the relative levels of collagen and elastin among hydrogel formulations were also evaluated by cell counts per the above procedure. Each HA_{HMW} and HA_{IMW} cumulative staining intensity assessment was normalized to the corresponding intensity assessment for alginate hydrogels.

2.3.7. Statistical Analyses

Data are reported as mean ± standard error of the mean. Comparison of sample means was performed by one-way ANOVA and Tukey’s post hoc test (SPSS software, Chicago, IL), $P < 0.05$.

2.4. Results

The present study was designed to examine the impact of HA_{HMW} and HA_{IMW} relative to alginate on VFF ECM production and phenotype. Following 7 and 21 days of total culture, constructs were harvested and subjected to mechanical, histological, and biochemical analyses.

2.4.1. Alginate as a Control and HA-MA Activity

We first verified that alginate was an effective control for HA and that HA-MA retained similar biological function as pure HA. Alginate was intended to serve as a ‘‘scrambled’’ polysaccharide sequence which would impart similar viscoelasticity to the hydrogel network as HA but which would not have the associated cell-interactions. This is similar in concept to the use of the ‘‘scrambled’’ peptide sequence RGES as a control for the cell adhesion peptide RGDS [69]. Competitive ELISA results indicated that alginate was unable to effectively interact with HABP (Fig. 2B), despite the physiochemical similarities between alginate and HA (Fig. 2A). In contrast, HA-MA appeared to retain a similar level of affinity for HABP as unmodified HA (Fig. 2B). This was consistent with the work of Masters et al., which demonstrated that HA-MA and unmodified HA each resulted in similar valvular interstitial cell (VIC) ECM production at the HA methacrylation level used herein.

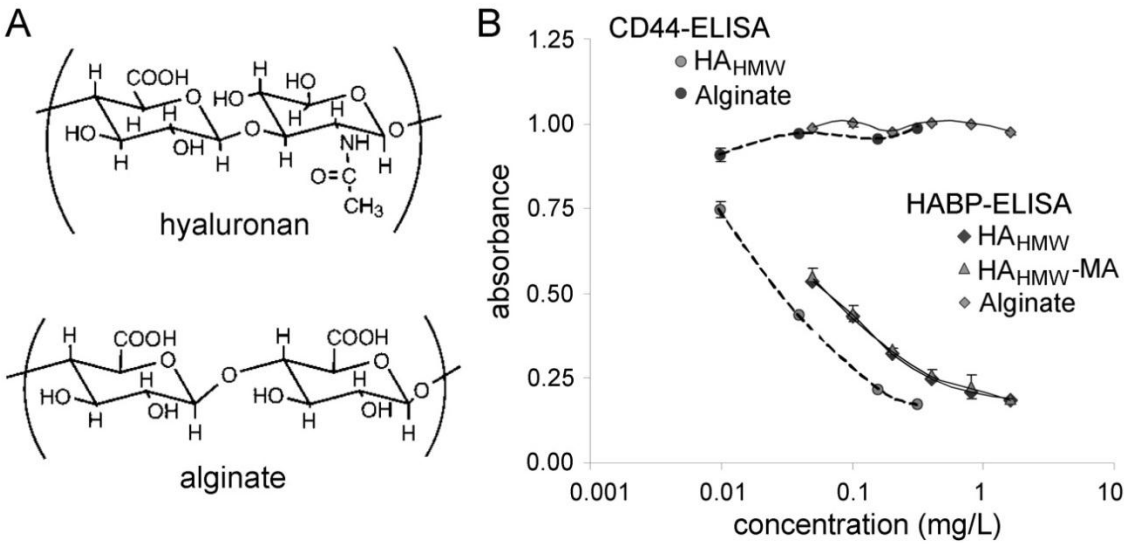

Fig. 2. (A) Structure of hyaluronan (HA) versus alginate disaccharide units. (B) Competitive ELISA results in which an increased absorbance signal corresponds to a decreased concentration of the test molecule and/or lower affinity of the test molecule for HA link protein (HABP). The ELISA results demonstrate that alginate does not effectively interact with HABP but that methacrylate-derivatized HA (HA-MA) has a similar affinity for HABP as unmodified HA.

2.4.2. Hydrogel Material Properties

The dense covalent crosslinking and chemical composition of pure PEGDA hydrogels result in gels that are essentially non-degradable and which permit limited cell-mediated remodeling [84, 90-92]. These features, although non-physiological, are desirable for studies focused on controlled evaluation of the impact of specific material properties (in the present work, bioactivity) on cell responses. To assess the degree to which the selected polysaccharide hydrogels retained the character of pure PEGDA hydrogels, the ‘‘bulk’’ material properties of each gel formulation were characterized.

Table 1. Hydrogel Modulus, Thickness, and Mass Assessments.

	Modulus (kPa)		**Thickness (mm)**		**Mass of 8 mm Discs (mg)**		
	Day 3	Day 21	Day 3	Day 21	Day 3	Day 7	Day 21
HA_{HWM}	58.1 ± 0.9	54.2 ± 6.5	1.12 ± 0.03	1.08 ± 0.03	58.3 ± 1.1	59.9 ± 1.2	57.7 ± 1.1
HA_{IMW}	55.0 ± 5.3	49.1 ± 2.7	1.12 ± 0.03	1.13 ± 0.03	59.7 ± 1.0	60.6 ± 0.9	59.7 ± 0.9
Alginate	60.5 ± 7.6	57.0 ± 6.1	1.12 ± 0.02	1.11 ± 0.02	58.1 ± 1.2	59.6 ± 0.8	59.1 ± 0.6
PEGDA	51.9 ± 2.6	46.1 ± 3.3	1.12 ± 0.03	1.13 ± 0.02	58.7 ± 1.0	61.6 ±0.5	59.5 ± 0.9

The initial water uptake, S, of each gel following polymerization was similar to that of a pure PEGDA gel (HA_{HMW}: 1.37 ± 0.06, HA_{IMW}: 1.43 ± 0.04, alginate: 1.43 ± 0.04, pure PEGDA: 1.40 ± 0.05). Furthermore, the initial (day 3) moduli of the HA_{HMW}, HA_{IMW}, and alginate cells were statistically indistinguishable, as were the day 21 moduli (Table 1). Comparison of the day 7 and day 21 moduli indicated that the reduction in modulus for each gel with time in culture was similar to that of pure PEGDA hydrogels (also containing encapsulated VFFs). To evaluate the potential contribution of gel degradation and VFF mediated compaction on the observed temporal changes in gel modulus, the thickness and mass of harvested gel discs were measured with time in culture (Table 1). These data correspond to a negligible reduction in gel volume with time. Collectively, the bulk modulus, thickness, water uptake, and gel mass assessments indicate that the material properties of the polysaccharide-containing gels were dominated by the presence of PEGDA rather than by the associated polysaccharides.

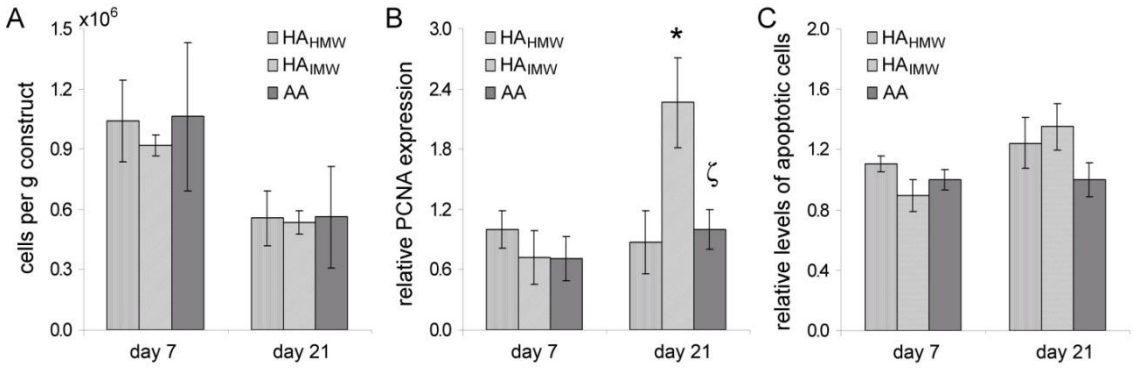

Fig. 3. Cell density, proliferation, and apoptosis. (A) The cell density within each hydrogel at days 7 and 21. (B) Relative levels of proliferation at days 7 and 21 based on PCNA immunostaining. (C) Relative levels of apoptotic cells at days 7 and 21 based on TUNEL assay results. *Significantly different from HA_{HMW} hydrogels, $P<0.05$. ζSignificantly different from HA_{IMW} hydrogels, $P < 0.05$.

2.4.3. Cell Density, Proliferation, and Apoptosis

The influence of scaffold composition on VFF proliferation and apoptosis was assessed via PCNA and TUNEL-based immunostaining, respectively. At day 7, no differences in cell proliferation or apoptosis across hydrogel formulations were noted (Fig. 3B and C). These day 7 PCNA and TUNEL results are reflected in the day 21 DNA measures, which indicate that net VFF proliferation and loss was similar across hydrogel formulations from day 7 to day 21 (Fig. 3A). Similar levels of cell apoptosis across hydrogel formulations continued to be observed through day 21 (Fig. 3C). However, PCNA expression was significantly elevated in HA_{IMW} hydrogels relative to HA_{HMW} ($P = 0.013$) and alginate gels ($P = 0.016$, Fig. 3B). These day-21 proliferation and apoptosis results suggest that, if cell densities had continued to be monitored past 21 days of

culture, differences in cell densities across formulations would have begun to be detected.

2.4.4. VFF ECM Deposition and Phenotype

VFF ECM production showed marked variations with hydrogel bioactivity (Fig. 4). The trends in elastin production at both days 7 and 21 indicated that elastin synthesis was greater in HA_{IMW} gels than in HA_{HMW} and alginate gels, with the differences at day 21 being statistically significant (HA_{HMW}, $P = 0.050$; alginate, $P < 0.001$). Although both days 7 and 21 data suggested an increasing trend for GAGs levels in alginate gels relative to both HA_{IMW} and HA_{HMW} hydrogels, these differences fell below statistical significance (Fig. 4B). Total collagen levels were significantly higher at day 7 in HA_{HMW} hydrogels than in HA_{IMW} ($P < 0.001$) and alginate ($P = 0.03$) gels. By day 21, this trend had shifted, with collagen levels in the alginate controls exceeding those in the HA_{HMW} hydrogels ($P = 0.025$, Fig. 4C). In contrast, the trend of lower total collagen production in HA_{IMW} hydrogels relative to alginate controls was stable from day 7 ($P = 0.015$) to day 21.

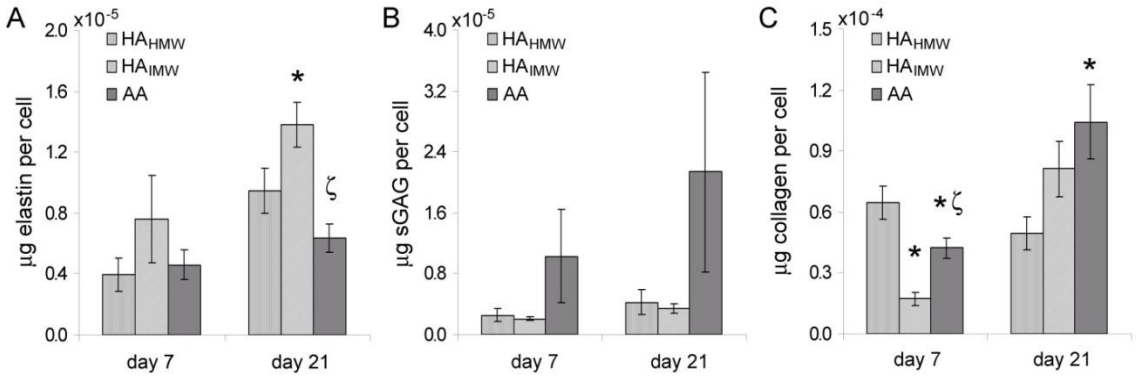

Fig. 4. Evaluation of VFF ECM deposition. (A) Elastin, (B) sGAG, and (C) total collagen production on a per cell basis at days 7 and 21. *Significantly different from HA_{HMW} hydrogels, $P<0.05$. ζSignificantly different from HA_{IMW} hydrogels, $P < 0.05$.

To gain further insight into effects of HA_{HMW} and HA_{IMW} on VFF ECM deposition, immunostaining for the two primary VF LP collagen types (collagen types I and III) [93] was conducted (Fig. 5A and B). Expression of both collagen type I and collagen type III displayed similar trends with hydrogel formulation at day 7, with collagen type I deposition being significantly higher in the HA_{HMW} gel relative to HA_{IMW} ($P < 0.001$) and alginate ($P = 0.001$) gels. By day 21, differences in collagen type I expression across hydrogels had flattened. However, collagen type III production was significantly higher in HA_{HMW} hydrogels relative to alginate controls ($P = 0.003$). As expected for PEGDA gels [73], staining for collagen types I and III (Fig. 6) and elastin (data not shown) was confined to the immediate pericellular space in each formulation.

To identify VFFs displaying a myofibroblast-like phenotype, expression of SM-α-actin was evaluated. The results for SM-α-actin were analogous to those for PCNA in that SM-α-actin levels were statistically indistinguishable across hydrogel formulations at day 7 (Fig. 5C). However, by day 21, VFFs in HA_{IMW} gels expressed higher levels of SM-α-actin relative to HA_{HMW} ($P = 0.004$) and alginate ($P < 0.001$) gels (Fig. 5D).

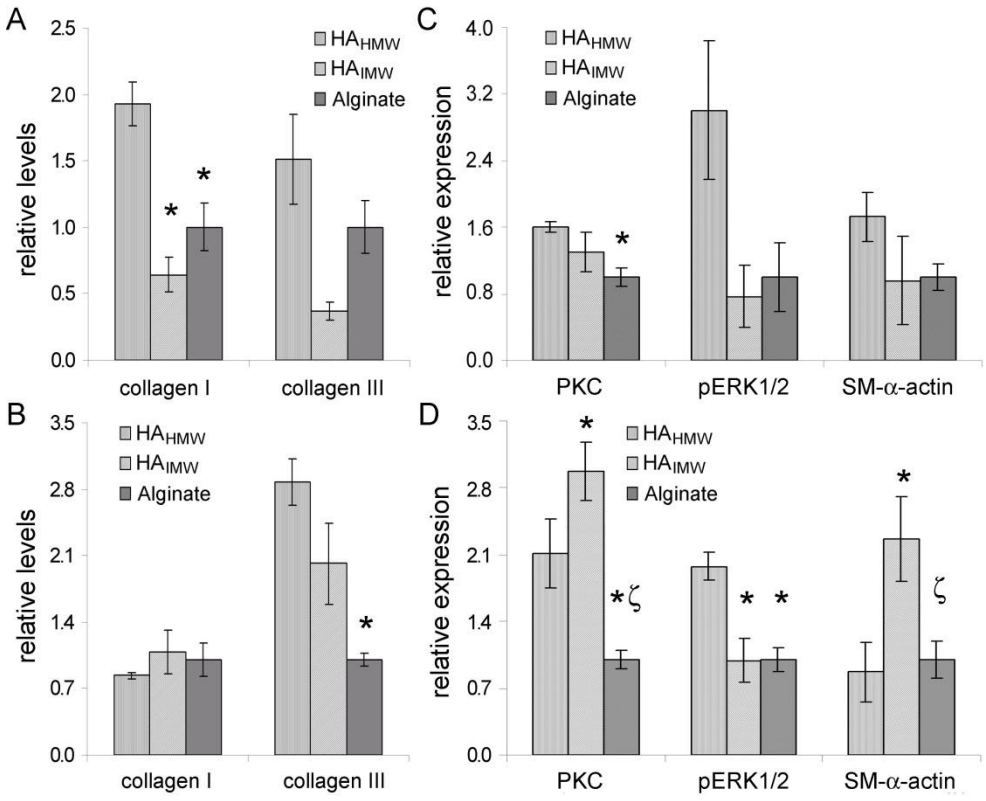

Fig. 5. Assessment of VFF collagen type production, phenotype, and signaling. Relative collagen type I and collagen type III expression across hydrogels at (A) day 7 and (B) day 21. Relative expression of PKC, pERK1/2, and SM-α-actin at (C) day 7 and (D) day 21. *Significantly different from HA_{HMW} hydrogels, $P < 0.05$. ζSignificantly different from HA_{IMW} hydrogels, $P < 0.05$.

2.4.5. Cellular Signaling

HA interactions with cell receptors, RHAMM and CD44, [78-80] trigger two primary signaling pathways, PkC and ERK, which then modulate cell gene expression. Therefore, the relative levels of RHAMM, CD44, PkC, and active ERK1/2 (pERK1/2) were semi-quantitatively assessed across hydrogel formulations. CD44 staining at both day 7 and day 21 was weak (<4 % of cells positively stained despite several antibody dilutions being assayed). In contrast, RHAMM staining was prominent at both time points and was significantly greater in HA_{HMW} and HA_{IMW} gels than in alginate gels ($P < 0.03$). Specifically, VFF expression of RHAMM at day 7 in HA_{HMW} and HA_{IMW} gels was 1.94 ± 0.05 and 2.89 ± 0.32 times greater, respectively, than in alginate gels. Relative RHAMM levels at day 21 followed a similar trend (data not shown). PkC expression was consistently higher in HA_{HMW} than in alginate gels ($P < 0.006$) at both days 7 and 21 (Fig. 4C and D). In addition, day 21 PkC levels were greater in HA_{IMW} hydrogels than in HA_{HMW} gels ($P = 0.038$) and alginate gels ($P < 0.001$). Relative pERK1/2 levels maintained a similar trend across formulations from day 7 to day 21, with day 21 pERK1/2 content being significantly higher in HA_{HMW} hydrogels relative to HA_{IMW} ($P = 0.029$) and alginate ($P = 0.013$) gels.

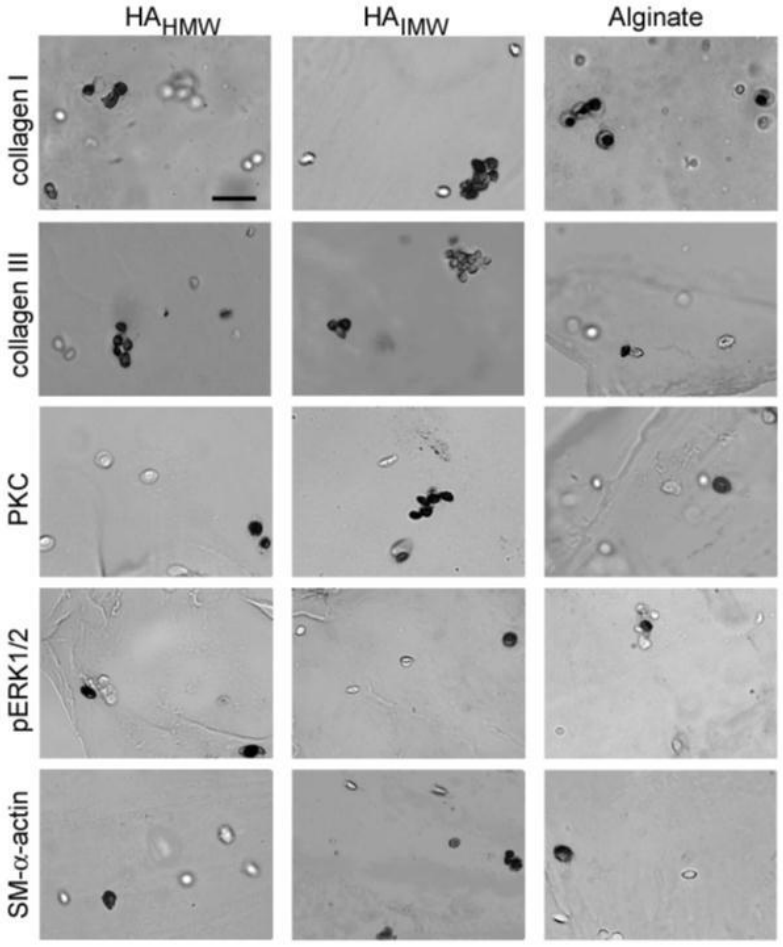

Fig. 6. Representative images of day 21 HA_{HMW}, HA_{IMW}, and alginate hydrogel sections immunostained for collagen type I, collagen type III, PKC, pERK1/2, or SM-α-actin. The scale bar in the upper-left image equals 40 mm and applies to all images.

2.5. Discussion

The aim of the present study was to validate PEGDA hydrogels as a model system to probe the effects of various bioactive moieties on VFF responses in 3D toward rational VF LP implant design. To accomplish this objective required that the current study be conducted so as to permit direct comparison with previous studies involving

more permissive scaffolds. Therefore, we chose to focus on HA, a polysaccharide that has been a particular focus in VF regeneration community. In the current work, porcine VFFs were encapsulated in PEGDA hydrogels containing consistent levels of HA_{HMW} (~1.65 x 10^3 kDa), HA_{IMW} (~600 kDa), or the control polysaccharide alginate. Modulus, water uptake, and gel mass assessments indicate that the bulk average microstructure, modulus, and degradation rate of the polysaccharide- containing gels were dominated by PEGDA. This enabled focus on the identity of the polysaccharide as the main source of variation in net cell responses. Although there were certainly local differences in gel properties at the microscale, our ECM and cell phenotypic measures represent averages over the bulk, as do our material property measures. Thus, since both the material property and cell response measures were made at the same length scales, the data represent an internally consistent set from which meaningful deductions can be made.

Regarding ECM production, VFF elastin deposition demonstrated an increasing trend with decreasing HA M_w by day 21 of culture. In comparing these results to literature, we are limited by the fact that most HA studies which permit the impact of HA M_w to be isolated from other experimental variables have been conducted in 2D with soluble, rather than matrix-bound, HA. Thus, the comparisons to follow must be interpreted with caution. That being said, the present results are in agreement with a recent 2D study of VICs by Masters et al.In that study, elastin synthesis at 20 days of culture was significantly higher in VICs exposed to ~400 kDa HA relative to ~800 kDa HA. However, a separate 2D study by Joddar and Ramamurthi [65], showed a decrease in vascular smooth muscle cell (SMC) elastin deposition at 21 days of culture with a

decrease in HA M_w from 2 x 10^3 kDa to ~200 kDa. Combined, these studies suggest that the influence of HA M_w on elastin synthesis may be cell-type dependent.

Examination of VFF GAGs deposition indicated no significant alteration in GAGs synthesis with increasing HA M_w, consistent with the results of Masters et al. Although, VFF total collagen production in HA_{IMW} hydrogels was significantly lower than that in HA_{HMW} gels at day 7, their day 21 total collagen content could not be statistically distinguished. As with elastin, literature shows conflicting results for the dependence of collagen deposition on HA M_w. Masters et al. found no significant difference in VIC total collagen production with increasing HA M_w at 20 days of culture. Joddar and Ramamurthi [65], however, observed an increase in vascular SMC collagen synthesis with decreasing HA M_w as HA dosages approached those used herein.

Regarding the synthesis of individual collagen types, VFF collagen type III deposition displayed an increasing trend with increasing HA M_w at both days 7 and 21. In contrast, although collagen type I expression at day 7 decreased with decreasing HA M_w, day 21 collagen type I levels did not vary significantly across formulations. This temporal alteration in collagen type I production may be linked to the corresponding shifts in PKC signaling with time in culture. The present collagen type III results agree with the effects of HA M_w on human dermal fibroblast collagen type III synthesis observed by David-Raoudi et al. Further comparison of the trends in collagen types I and III across hydrogels with that of total collagen suggests that collagen type I was the dominant collagen produced by the encapsulated VFFs, in each hydrogel formulation, at least by day 21. The ratios of the various collagen types secreted by VFFs are significant

because collagen type III tends to more abundant in highly elastic tissues, such as the VF LP [94]. Furthermore, the ratios of the various collagen types are frequently altered in aging and disease [94, 95].

Cell phenotype also appeared to be modulated by HA M_w. VFFs in HA_{IMW} hydrogels displayed a more proliferative phenotype at day 21 than cells in alginate or HA_{HMW} gel, as indicated by PCNA staining. A similar dependence of cell proliferation on HA M_w has been previously observed for VICs [81] and for vascular SMCs [65]. In addition, VFFs in HA_{IMW} hydrogels demonstrated increased SM-α-actin expression by day 21 relative to HA_{HMW} and alginate hydrogels. The increased levels of SM-α-actin and PCNA at day 21 in HA_{IMW} gels may be associated with the increased levels of PkC in the HA_{IMW} gels relative to alginate gels. Indeed, PkC signaling has previously been shown to increase the expression of SM-α-actin in lung fibroblasts [96]. Furthermore, the increased myofibroblastic phenotype of cells in the HA_{IMW} hydrogels at day 21 was associated with increased elastin deposition, consistent with the literature [97-101].

Cumulatively, the present results suggest that HA M_w must be carefully selected to achieve desired VFF responses. However, based on the current data, the HA_{HMW} gels would be the most appropriate for VF regeneration of the formulations examined. Specifically, the HA_{HMW} gel resulted in an elastin and collagen type composition most mimetic of normal superficial LP, which contains ~40% collagen type III [93] and a relatively low elastin to collagen ratio[102]. Furthermore, the lower induction of a myofibroblastic phenotype observed in the HA_{HMW} gels relative to HA_{IMW} gels with prolonged culture is desirable for inhibition of LP scar formation [103].

As previously mentioned, the effects of HA_{IMW} on VFF behavior relative to the control alginate have been examined in 3D using base-hydrogels of collagen type I [76]. However, it is difficult to extend upon that study to probe a broader HA concentration or Mw range due the interdependences among collagen gel bioactivity, modulus, and microstructure. In addition, collagen gels are prone to fibroblast-mediated contraction, making gel material properties difficult to control over time [76]. Although the material properties of PEGDA hydrogels are tunable and more readily controlled, cells encapsulated within PEGDA hydrogels take on rounded/stellate morphologies even in the presence of cell adhesion ligands such as RGDS (Fig. 6). This particular characteristic of PEGDA hydrogels, which results from their dense crosslinking and relatively slow degradation rates [84, 90-92] is not optimal for cells such as VFFs, which natively take on spindle-shaped morphologies. However, due to several of their unique properties, PEGDA hydrogels have been employed as a model scaffold by number of researchers focusing on fibroblast-like cells, in spite of this limitation [81, 84, 104-106]. To validate PEGDA hydrogels for the investigation of VFF responses to defined bioactivity in 3D, the day 21 setup for the present study was designed to be a direct analog of the previous collagen-based 3D study in which encapsulated VFFs were able to assume spindle-shaped morphologies [76].

Interestingly, each of the aspects of VFF behavior measured for HA_{IMW}-collagen relative to alginate-collagen control gels displayed similar trends in the HA_{IMW}-PEGDA gels relative to alginate-PEGDA gels (Table 2). Although elastin deposition was not measured in the alginate-collagen and HA_{IMW}-collagen study, the relative trends in day 21 total collagen synthesis, GAGs production, cell proliferation, and myofibroblastic phenotype between hydrogel formulations were maintained across the two studies [76]. This similarity in relative VFF response occurred despite the significant difference in cell morphologies in the PEG-based gels relative to the collagen gels. The good agreement between these two studies indicates that PEGDA hydrogels can serve as an effective model system for probing at least certain aspects of fibroblast-like cell responses to scaffold material properties despite the enforced non-native cell morphologies.

A limitation of the present study is the relatively restricted HA concentration and M_w range interrogated. Future experiments will explore a broader range of initial concentration and M_w. Furthermore, the present 3D model system can be readily extended to examining the influence of other biochemical moieties on VFF cell responses.

Table 2. Comparison of HA and Alginate Impact in PEGDA- Versus Collagen-Based Hydrogels.

	PEGDA hydrogels with RGDS functioning as the integrin adhesion ligand at day 21		**Collagen hydrogels with collagen type I functioning as the integrin adhesion ligand [107]**	
	HA_{HMW} relative to	HA_{IMW} relative to Alginate	HA_{HMW} relative to HA_{IMW}	HA_{IMW} relative to Alginate
Total collagen	↔	↓	–	↓
Collagen type I: type	↓	↓	–	–
Elastin	↓	↑	–	–
sGAG	↔	↓	–	↓
Proliferative cells	↓	↑	–	↑
Myofibroblast-like cells	↓	↑	–	↑

↔, indicates indeterminate, ↓ decrease, ↑ increase, – not measured. In Hahn et al. [76], the levels of proliferative cells were assessed via BrdU incorporation and the levels of myofibroblast-like cells were assessed by evaluating the degree of hydrogel compaction with time in culture. Collagen synthesis and sGAG production were evaluated histologically by reticular collagen stain and toluidine blue stain, respectively.

CHAPTER III

INFLUENCE OF GLYCOSAMINOGLYCAN IDENTITY ON VOCAL FOLD FIBROBLAST BEHAVIOR*

3.1. Overview

PEG hydrogels have recently begun to be studied for the treatment of scarred vocal fold lamina propria due, in part, to their tunable mechanical properties, resistance to fibroblastmediated contraction, and ability to be polymerized in situ. However, pure PEG gels lack intrinsic biochemical signals to guide cell behavior and generally fail to mimic the frequency-dependent viscoelastic response critical to normal superficial lamina propria function. Recent results suggest that incorporation of viscoelastic bioactive substances, such as GAGs, into PEG networks may allow these gels to more closely approach the mechanical responses of normal vocal fold lamina propria while also stimulating desired vocal fold fibroblast behaviors.

---

*Reprinted with permission from Influence of "glycosaminoglycan identity on vocal fold fibroblast behavior" by Andrea Carolina Jimenez-Vergara, Dany J. Munoz-Pinto, Silvia Becerra-Bayona, Bo Wang, Alexandra Iacob, Mariah S. Hahn, 2011, Acta Biomaterialia 7 (2011) 3964–3972, Copyright 2011, Acta Materialia Inc. Published by Elsevier Ltd.

Although a number of vocal fold studies have examined the influence of HA on implant mechanics and vocal fold fibroblast responses, the effects of other GAG types have been relatively unexplored. This is significant, since recent studies have suggested that CSC and HS are substantially altered in scarred lamina propria.

The present study was therefore designed to evaluate the effects of CSC and HS incorporation on the mechanical response of PEG gels and vocal fold fibroblast behavior relative to HA. As with PEG–HA, the viscoelasticity of PEG–CSC and PEG–HS gels more closely approached that of the normal vocal fold lamina propria than pure PEG hydrogels. In addition, collagen I deposition and fibronectin production were significantly higher in CSC than in HA gels, and levels of the myofibroblast marker SM-α-actin were greater in CSC and HS gels than in HA gels. Since collagen I, fibronectin, and SM-α-actin are generally elevated in scarred lamina propria these results suggest that CSC and HS may be undesirable for vocal fold implants relative to HA. Investigation of various signaling intermediates indicated that alterations in NFκB-p50, NFκB-p65, or pERK1/2 levels may underlie the observed differences among the PEG–GAG gels.

3.2. Introduction

Voice disorders resulting from scarring of the vocal fold lamina propria can be debilitating in terms of quality of life. The vocal folds are paired, multi-layered structures, each consisting of an underlying skeletal muscle layer, followed by the

lamina propria and overlying epithelium. The lamina propria is generally subdivided into the superficial lamina propria (commonly referred to as the SLP) and the vocal ligament [108]. During vocal fold vibration, the SLP is believed to move freely over the elastin- and collagen rich vocal ligament, undergoing the high frequency and strain excursions required for cyclic vocal fold closure. When SLP pliability and physical volume are reduced by the abnormal ECM deposition and fibroblast-mediated contracture associated with scarring, voice changes ranging from hoarseness to complete voice loss result, depending on the severity of the scar [60, 109].

Vocal fold scarring has proven difficult to treat with current surgical techniques and standard augmentation substances, such as collagen and fat [60, 61]. Researchers are therefore actively exploring alternative treatment routes, including the development of designer implants for functional SLP regeneration [4, 13, 14, 17, 18, 110-112]. PEG-based hydrogels have recently begun to be examined as vocal fold augmentation substances [9-14], due, in part, to their tailorable mechanical properties, resistance to fibroblast-mediated contraction, and ability to be polymerized in situ. However, pure PEG hydrogels lack intrinsic biochemical signals to guide cell behavior and generally fail to mimic the frequency- dependent viscoelastic response critical to normal SLP function [10-12, 14, 15].

Recent results suggest that conjugating viscoelastic bioactive substances, such as GAGs, into PEG networks may allow these hydrogels to more closely approach the mechanical responses of normal SLP while stimulating desired vocal fold fibroblast behaviors [10, 16]. GAGs are a family of charged polysaccharides which play key roles

in inflammation, cell migration, and cell phenotype modulation [113] and which include unsulfated forms (e.g. HA) as well as sulfated forms (e.g. HS, CSC, DS, and keratan sulfate (KS)). While a number of vocal fold studies have examined the impact of HA on implant mechanics and/or fibroblast behavior [10, 11, 13, 16-19], the influence of sulfated GAGs has been relatively unexplored. The present study was therefore designed to compare the effects of CSC and HS incorporation on PEG hydrogel biomechanical response and on associated vocal fold fibroblast behavior relative to HA. CSC and HS were selected for investigation over other sulfated GAGs for several reasons. First, although the DS-containing proteoglycan decorin has been a focus of several vocal fold studies [114, 115] due in part to its known role in dermal scar formation [116], recent quantitative measures suggest that expression of CSC, rather than DS, is substantially decreased in scarred lamina propria [20]. In addition, a separate study has shown that levels of specific HS proteoglycans are altered in scarred lamina propria [21].

3.3. Materials and Methods

3.3.1. Polymer Synthesis and Characterization

3.3.1.1. PEG-Diacrylate Synthesis

PEGDA was prepared as previously described by combining 0.1 mmol ml^{-1} dry PEG (10 kDa, Fluka), 0.4 mmol ml^{-1} acryloyl chloride, and 0.2 mmol ml^{-1} triethylamine in anhydrous dichloromethane and stirring under argon overnight [117]. The resulting

solution was washed with 2 M K_2CO_3 and separated into aqueous and dichloromethane phases to remove HCl. The dichloromethane phase was subsequently dried with anhydrous $MgSO_4$, and PEGDA was precipitated in diethyl ether, filtered, and dried under vacuum. The extent of PEG diacrylation was determined by ^{1}H NMR to be ~85%.

3.3.1.2. Synthesis of Methacrylate-Derivatized CSC and HS

In order to conjugate specific GAGs within the PEGDA-based hydrogel networks, each GAG type was methacrylate-derivatized according to standard protocols [81]. CSC (51 kDa, Sigma) and heparin (17 kDa, Sigma) were dissolved in deionized water to achieve a 1 wt.% final concentration, and the pH of each solution was adjusted to 8.0. A 10-fold molar excess of methacrylic anhydride (Polysciences) was added per disaccharide unit. Each reaction was allowed to proceed under constant stirring at 4 °C, with the solution pH being maintained at ~8.0 by periodic addition of 5 M NaOH. The reaction products (CSC-MA and HS-MA) were precipitated twice in chilled 95% ethanol, dialyzed against deionized water for 48 h, and lyophilized. The extent of methacrylate derivatization was characterized by ^{1}H NMR to be ~1–3% (per available–OH groups). These levels of methacrylate derivatization have previously been shown to negligibly alter the observed cell–GAG interactions [16, 74, 81, 118] yet are sufficient to avoid significant sol formation [119].

3.3.1.3. Synthesis of Methacrylate-Derivatized Intermediate Molecular Weight HA

Since the average molecular weight of HA in normal human vocal fold lamina propria is currently unknown, an intermediate molecular weight HA (~400 kDa) was selected for the present study [16]. To generate HA appropriate for the study, high molecular weight HA (~1.65 x 10^3 kDa from Streptococcus equi, Fluka) was first methacrylate-derivatized as above. The purified product was then dissolved at 1 mg ml^{-1} in phosphate-buffered saline (PBS) containing 0.05% sodium azide and 5 U ml^{-1} hyaluronidase IV-S (H3884, Sigma). Following incubation at 37 °C overnight, the enzyme was heat-inactivated. The resulting digestion product (HA-MA) was dialyzed against deionized water for 48 h and lyophilized. The average molecular weight of the isolated HA-MA was determined to be ~400 kDa with a polydispersity of ~1.25 using gel permeation chromatography (Viscotek).

3.3.1.4. Synthesis of Acrylate-Derivatized Cell Adhesion Peptide

Cell adhesion peptide RGDS (American Peptide) was reacted with acryloyl-PEG-N-hydroxysuccinimide (ACRL-PEG-NHS) (3.4 kDa, Nektar) at a 1:1 M ratio for 2 h in 50 mM sodium bicarbonate buffer, pH 8.5 [72]. The product (ACRL-PEG-RGDS) was purified by dialysis, lyophilized, and stored at ~20 °C until use.

3.3.2. Cell Culture

Cryopreserved porcine vocal fold fibroblasts at passage 3 were obtained from Robert Langer, ScD (Massachusetts Institute of Technology) [76]. These cells had been isolated by primary explant from the mid-membranous lamina propria of 6–12-month-old pigs, an accepted animal model for the human vocal fold lamina propria [109]. The discarded animal tissue was obtained from the MIT Division of Comparative Medicine and with the approval and according to the guidelines of the MIT animal care committee. The purity of the explant population was verified by positive staining for vimentin and negative staining for epithelial and endothelial cell-specific markers. The cryopreserved vocal fold fibroblasts were thawed and expanded at 37 °C/5% CO2 in DMEM (Hyclone) supplemented with 10% FBS, 2 ng ml^{-1} basic fibroblast growth factor (BD Biosciences), 100 U ml^{-1} penicillin and 100 mg l^{-1} streptomycin (Hyclone).

3.3.3. Hydrogel Fabrication and Maintenance

Hydrogels were fabricated by preparing precursor solutions containing 100 mg ml^{-1} 10 kDa PEGDA, 1.4 mg ml^{-1} methacrylate- derivatized GAG (CSC-MA, HS-MA, or HA-MA), and 1.4 lmol ml^{-1} ACRL-PEG-RGDS in HEPES-buffered saline (HBS) (10 mM HEPES, 150 mM NaCl, pH 7.4). The concentration of GAG was chosen to be consistent with GAG levels within the normal vocal fold lamina propria [20, 115]. In

addition, PEGDA molecular weight and concentration were selected to yield hydrogels with average dynamic elastic moduli appropriate to vocal fold applications [12, 14].

A 300 mg ml^{-1} solution of UV photoinitiator 2,2-dimethoxy-2- phenyl-acetophenone in N-vinylpyrrolidone was added at 1 vol.% to each precursor solution. The resulting solutions were then poured into molds composed of two glass plates separated by 1.1 mm polycarbonate spacers and polymerized by 3 min exposure to long wavelength UV light (Spectroline, ~6mWcm^{-2}, 365 nm). To generate cell-laden hydrogels, vocal fold fibroblasts at passages 5–6 were harvested and resuspended in the filter-sterilized precursor solutions at ~1 x 10^6 cells ml^{-1} prior to transfer to the hydrogel mold. Polymerized hydrogel slabs were transferred to Omnitrays (Nunc) fitted with four sterile polycarbonate bars to simultaneously prevent gel flotation and prevent gel contact with the tray bottom. Hydrogels were immersed in DMEM supplemented with 10% FBS, 100 U ml^{-1} penicillin, and 100 mg l^{-1} streptomycin and maintained at 37 °C/5% CO2. The medium was changed every 2 days.

3.3.4. Initial Hydrogel Characterization

3.3.4.1. Initial Water Uptake

To compare the extent of initial water uptake by the various hydrogel formulations following polymerization, the initial weight (W_i) of each gel (n = 8 per formulation) was determined immediately following polymerization, after which the gels were submerged in medium. After 24 h, the swollen weight (W_s) of each gel was

measured. The equilibrium water uptake (S) was calculated as $S = \frac{W_s}{W_i}$. These dates were used to compare the post-swelling GAG levels across gels.

3.3.4.2. Average Mesh Size

PEGDA hydrogel mesh size cannot be readily visualized using standard techniques such as scanning electron microscopy. In the present study, hydrogel mesh size was therefore characterized via a series of dextran diffusion experiments based on an adaptation of the methodology of Watkins and Anseth [120]. To avoid charge–charge interactions between the diffusing dextrans and the GAG chains in the hydrogel networks, fluorescently-labeled, charge-neutral dextrans were employed.

In brief, PEG–GAG hydrogels were prepared and allowed to swell overnight at 37 °C in PBS containing 0.05% azide (PBS–azide). One centimeter diameter discs were cored from each hydrogel formulation. Fluorescently-labeled, charge-neutral dextrans (40 and 70 kDa, Invitrogen) were dissolved at 0.05 mg ml^{-1} in PBS–azide and added at 1 ml per hydrogel disc (eight discs per formulation per dextran molecular weight). Dextran solutions were allowed to diffuse into the hydrogels for 24 h at 37 °C. Each gel disc was gently blotted and transferred to 1 ml of fresh PBS–azide. Dextran that had penetrated into the hydrogels was then permitted to diffuse out into the surrounding solution at 37 °C. After 24 h, the fluorescence of the PBS–azide solution surrounding each disc was measured at excitation and emission wavelengths of 530 and 590 nm. Dextran standard curves were used to convert each fluorescence signal to a concentration. For each hydrogel formulation, the measured concentration readings for each dextran molecular

weight were divided by gel weight and then plotted versus dextran hydrodynamic radius [121]. The area (A) under the resulting curve served as a quantitative indicator of the permissivity of each hydrogel (x) over the hydrodynamic radii range assayed. For the purposes of comparison, the calculated area values for CSC and HS gels were normalized to that of the HA gels to yield a relative mesh size value: $_{x}\ \left(\frac{A_x}{A_{HA}}\right)$.

3.3.4.3. Hydrogel Mechanical Properties

Following initial swelling, 8 mm diameter discs (n = 7–8 per formulation) were cored from each cell-laden hydrogel. The thickness of each disc was measured using a digital caliper. These thickness measures served both as gage lengths for mechanical testing as well as indicators of hydrogel degradation and/or cell-mediated gel compaction with time. Each hydrogel disc was mounted onto the compression platens of a DMA 800 (TA Instruments) and surrounded at the edges by silicone oil to prevent gel dehydration. Following application of a 0.01 N pre-load, each hydrogel disc was subjected to unconstrained compression at 1% cyclic strain at room temperature over the frequency range 1–100 Hz (100 Hz being the system maximum). The higher frequency testing conditions were selected to approach the frequencies of cyclic lamina propria loading experienced during phonation, with the onset of adult phonation occurring at ~150 Hz in males. Sample elastic compressive modulus (E′) and damping ratio ($\frac{E}{E}$, where E″ is the viscous compressive modulus) were extracted from the resulting stress strain data.

The fact that PEGDA hydrogels can be considered homogeneous and isotropic [122, 123] was used in comparing these compressive mechanical property data to literature values for the vocal fold lamina propria (which are generally obtained under shear). Specifically, the elastic compressive modulus of homogeneous, isotropic materials is related to the elastic shear modulus (G′) by the relationship $G = \frac{E}{(2 2)}$, where is the Poisson ratio. For polymeric hydrogels, ≈ 0.5, and thus, $G = \frac{E}{3}$ [36].

3.3.5. End-Point Hydrogel Analyses

After culture for 18 days, gels were harvested for mechanical, biochemical, and histological analyses. Mechanical samples (n = 3–5 per formulation) were tested as described above.

3.3.5.1. Biochemical Analyses

Samples harvested for biochemical analyses were transferred to screw cap vials, weighed, flash-frozen in liquid nitrogen, and stored at -80 °C until the time of analysis. The weight of each 8 mm disc was used as a second indicator of gel degradation and/or compaction, since the reduction in gel volume associated with both of these processes would be reflected in a mass loss, assuming lack of commensurate new matrix deposition [76]. Hydrogel samples were digested for 72 h at 37 °C in 1 ml of 0.12 M NaOH per 0.2 g hydrogel wet weight [16, 83]. DNA, total collagen, and elastin were

then analyzed by established protocols. For each assay, the standards used were subjected to the same association with PEGDA and GAG and to the same digestion conditions as the samples. The resulting collagen and elastin data were normalized to cell number, as determined from the DNA measurements.

3.3.5.2. DNA Analysis

Aliquots of the hydrolyzed samples (n = 3–6 per formulation) were neutralized and their DNA contents determined using the Invitrogen PicoGreen assay [84]. DNA measures were translated to cell numbers using a conversion factor of 6.6 pg DNA per cell [85]. NaOH-treated calf thymus DNA (Sigma) served as a standard.

3.3.5.3. Collagen Analysis

The amino acid hydroxyproline was quantified as an indirect measure of total collagen. In brief, aliquots (n = 4–6 per formulation) collected for collagen quantitation were hydrolyzed for 18 h at 110 °C in 6 M HCl. Each sample was then dried in a Labconco Centrivap to remove HCl, resuspended in deionized water, and passed through a centrifugal microcolumn (Nunc) packed with charcoal to remove caramelized sugars. The resultant samples were reacted with the reagents chloramine T and p-dimethylbenzaldehyde [83]. Sample absorbance was read at 550 nm relative to that of L-4-hydroxyproline (Sigma). Total collagen content was estimated from measured grams of hydroxyproline by dividing by 0.13 [124].

3.3.5.4. Elastin Analysis

Elastin production was measured using indirect ELISA [86]. NaOH-digested samples (n = 3–4 per formulation) were neutralized and further digested with 0.25 M oxalic acid at 100 °C overnight. Oxalic acid was removed from the samples and exchanged for PBS using Microcon YM-3 centrifugal filters (Millipore). One hundred microliters of the resulting samples were applied to a high binding multiwell plate for 3 h at room temperature. After blocking the plate with bovine serum albumin, adsorbed elastin fragments were detected by applying elastin antibody (BA-4, SCBT) followed by donkey anti-mouse HRP-conjugated secondary antibody (Jackson Immunochemicals) and 2,20-azino-bis(3-ethylbenzthiazoline 6-sulphonic acid). Absorbance was read at 410 nm, with bovine aortic elastin (exposed to both NaOH and oxalic acid treatment) serving as a standard.

3.3.6. Histological Analyses

Day 18 samples harvested for histological analyses were fixed in 10% formalin for 30 min, embedded in Tissue-Tek freezing medium, and frozen at -80 °C. Thirty-five micron sections were cut using a cryomicrotome. All immunostaining steps took place at room temperature unless otherwise noted.

3.3.6.1. Immunostaining

ECM deposition was analyzed for each formulation using standard immunohistochemical techniques. Rehydrated sections were blocked with peroxidase for 10 min, followed by 30 min exposure to Terminator blocking agent (Biocare Medical). Primary antibodies for collagen I (Rockland Immunochemicals), collagen III (Rockland Immunochemicals), elastin (BA-4, Santa Cruz Biotechnology), fibrillin-1 (C-19, Santa Cruz Biotechnology), or fibronectin (C-20, Santa Cruz Biotechnology) diluted in HBS were then applied for 1 h. To identify vocal fold fibroblasts displaying a myofibroblastlike phenotype, a primary antibody for SM-α-actin (1A4, LabVision) was applied. Bound primary antibody was detected using alkaline phosphatase-conjugated secondary antibody (Jackson Immunochemicals) followed by application of the chromogen Ferangi Blue (Biocare Medical) or using HRP-conjugated secondary antibody (Jackson Immunochemicals) followed by application of the chromogen AEC (LabVision). For cell signaling studies involving antibodies for pERK1/2 (Thr 202/Tyr 204, Santa Cruz Biotechnology), pPLC-γ1 (Tyr 1253, Santa Cruz Biotechnology), NFκB-p50 (C-19, Santa Cruz Biotechnology), and NFκB-p65 (C-20, Santa Cruz Biotechnology), rehydrated sections were permeabilized (10 mM HEPES, pH 6.8, 100 mM NaCl, 3 mM $MgCl_2$, 300 mM sucrose, 0.5% Triton X-100) for 30 min prior to Terminator application.

3.3.6.2. Semi-Quantitative Assessments

For intracellular markers (SM-α-actin, pERK1/2, pPLC-γ1, NFjBp50, NFjB-p65), cell counts were carried out to semi-quantitatively evaluate the immunostaining results. These counts were conducted according to established methods [53, 88, 89] on sections from at least three different discs (a total of ~1500 vocal fold fibroblasts) for each formulation. For each cell i in a given section, a staining intensity d_i was recorded on a scale of 0–3 (0 = no staining; 3 = highest intensity among all formulations for that antibody) by a single observer blinded to outcome. The cumulative staining intensity d for a given antibody in a particular section was calculated using the equation: $d \quad \frac{\sum d_i}{\text{total cell number}}$. In addition, since deposited ECM remained localized around the parent cells in each hydrogel formulation, as is characteristic for PEGDA gels [15], the relative levels of collagen I, collagen III, fibrillin-1, and fibronectin among hydrogel formulations were also evaluated by cell count using the above procedure.

Counts for all stainings for which statistically significant differences were observed among PEG–GAG formulations were repeated by two additional observers blinded to both sample identity and outcome. Each of these recounting assessments demonstrated at least 95% correlation with the original counts. The resulting average cumulative staining intensities for each antibody were regarded as vectors with CSC, HS, and HA components: $[d_{CSC}\ d_{HS}\ d_{HA}]$. For the purposes of comparison, these vectors were normalized to unit magnitude by standard methods: $\frac{[d_{CSC}\ d_{HS}\ d_{HA}]}{\sqrt{d_{CSC}^2\ \ d_{HS}^2\ \ d_{HA}^2}}$.

3.3.6.3. Comparison of Collagen I and Collagen III

Although the collagen I counting assessments do not give the absolute amounts of collagen I in each formulation, they do bind the ratios between the collagen I levels among formulations. Similarly, the collagen III counting assessments bind the ratios between the collagen III levels among formulations. Given the predominance of collagen I and collagen III (>90% of total collagen) in the vocal fold lamina propria [93], weighting factors for the collagen I and collagen III staining intensity vectors should exist for which the sum of the weighted vectors approximates the total collagen vector:

$$\left(\alpha_1 \begin{bmatrix} \text{Col I}_{CSC} \\ \text{Col I}_{HS} \\ \text{Col I}_{HA} \end{bmatrix} \quad \alpha_3 \begin{bmatrix} \text{Col III}_{CSC} \\ \text{Col III}_{HS} \\ \text{Col III}_{HA} \end{bmatrix} \quad \begin{bmatrix} \text{total collagen}_{CSC} \\ \text{total collagen}_{HS} \\ \text{total collagen}_{HA} \end{bmatrix} \right) \quad (1)$$

i.e. α_1 and α_3 which minimize the error between the left- and righthand sides of Eq. (1) can be determined. When the collagen I and collagen III vectors are first normalized to unit magnitude prior to the determination of α_1 and α_3, the ratio of the resultant α_1 and α_3 can be interpreted as the relative contribution of the collagen I and collagen III vectors to the overall total collagen vector. Thus, the ratio $\frac{(\alpha_1 x \text{Col I}_x)}{\alpha_3 x \text{Col III}_x}$ can be interpreted as the relative amount of collagen I versus collagen III in formulation x. In the present study, α_1 and α_3 were determined to be 3.0×10^{-5} and 1.5×10^{-5}, respectively, using the Solver function of the Excel Analysis Toolbox, with the sum of the mean square error utilized as the error function to be minimized.

3.3.7. Statistical Analyses

Data are reported as means ± standard deviation. Comparison of sample means was performed by ANOVA. When readings for various measures could be attributed to the same sample group (e.g. 24 h elastic compressive modulus values at each sampled frequency), a single two-way ANOVA was performed for sample comparison. In the case of immunostaining, the sections used for two different antibodies were not be considered as representing the same sample, even if arising from the same gel disc. Therefore, statistical comparisons for each antibody were performed separately using one-way ANOVA.

When the P value associated with the independent variable main effect fell below 0.05, pair-wise comparisons between specific formulations were conducted using Tukey's post hoc test (two-tailed, SPSS software). The significance values associated with subsequent pair-wise comparisons are given in the main text.

3.4. Results

3.4.1. Hydrogel Material Properties

In order to attribute differences in vocal fold fibroblast behavior across hydrogel formulations specifically to initial differences in gel GAG composition, it was important that the remaining hydrogel material properties could be considered consistent across

gels. The ‘‘bulk’’ material properties of each gel formulation were therefore characterized and compared. The initial water uptake S of each gel type following polymerization was similar (Table 3), indicating that the post-swelling concentration of GAG in each gel type was similar at (0.14/1.38) or ~0.1 wt.% [119]. Similarly, comparison of the equilibrium diffusion of charge-neutral dextrans indicated that the bulk average mesh size of the swollen gel networks could be considered consistent across formulations (Table 3). Mechanical property data for the PEG–GAG hydrogels over the frequency range 1–40 Hz are summarized in Fig. 7 and Table 4. Although mechanical measures were collected up to 100 Hz (approaching the onset of phonation at ~150 Hz), values above 40 Hz were neglected due to data quality limitations associated with testing device inertia. The average elastic compressive modulus values of both pure PEG and the PEG–GAG gels were ~16 kPa at 1 Hz. As loading frequency increased, the average elastic compressive modulus values of both the pure PEG and PEG–GAG hydrogels increased to ~25 kPa (40 Hz, Fig. 7). Given the homogeneous and isotropic nature of PEG-based gels [122, 123], these average elastic compressive modulus values can be assumed to correspond to an elastic shear modulus of ~8 kPa for both the pure PEG and PEG– GAG gels.

Table 3. Hydrogel Water Uptake and Relative Mesh Size.

	Water Uptake (S) [a]	Relative Mesh Size[a,b]
CSC	1.38 ± 0.02	1.01 ± 0.03
HS	1.38 ± 0.01	1.00 ± 0.01
HA	1.39 ± 0.01	1.00 ± 0.04

[a]Eight specimens were tested for both water uptake and relative mesh size assessments.
[b]A relative mesh size of 1.00 corresponds to an average mesh size of ~18 nm [123].

As the loading frequency increased, the differences in damping ratios between the GAG-containing and non-GAG-containing gels increased, with the damping ratios of the PEG–CSC, PEG–HS, and PEG–HA gels being significantly greater than that of the PEG gels at 40 Hz ($P = 0.0129$, $P = 0.046$, and $P = 0.013$, respectively). Specifically, the damping ratios of the PEG–GAG hydrogels were ~0.8 at 40 Hz, whereas pure PEG gels displayed a damping ratio of ~0.55 at 40 Hz. Elastic shear modulus and damping ratio ranges for the vocal fold lamina propria at similar strains and loading frequencies are 0.1–7 kPa and 0.6–2, respectively [125, 126]. Thus, conjugation of GAG into PEG networks allowed the hydrogels to more closely approach ‘‘average’’ lamina propria mechanical properties, at least in terms of observed damping ratios.

Mechanical property assessments at the study end-point indicated that the initial mechanical properties were maintained over 18 days of culture (Table 4). Similarly, the 24 h and 18 day thickness and mass data corresponded to negligible alterations in gel volume with time (Table 4). Thus, the bulk modulus, thickness, and gel mass assessments indicated that the PEG–GAG gels retained the slow degradation rate and resistance to cell-mediated contraction characteristic of pure PEG hydrogels [16].

Table 4. Hydrogel Modulus, Thickness, and Mass Assessments[a].

	Elastic Compressive Modulus (kPa) at 1 Hz		Thickness (mm)		Mass of 8 mm Discs (mg)	
	24 h	18 days	24 h	18 days	24 h	18 days
CSC	16.4 ± 2.7	19.1 ± 1.3	1.15 ± 0.04	1.16 ± 0.04	57.6 ± 0.9	59.5 ± 3.0
HS	17.4 ± 2.1	18.3 ± 2.5	1.15 ± 0.05	1.14 ± 0.07	57.6 ± 0.4	59.4 ± 3.4
HA	16.7 ± 2.0	17.5 ± 1.7	1.16 ± 0.03	1.17 ± 0.02	58.1 ± 0.2	58.7 ± 5.3

[a]Data were collected on the following numbers of cell-laden samples per formulation: Elastic compressive modulus, n = 7-8 (24 h) and n = 3-5 (18 days); thickness, n = 7-8 (24 h) and n=3-5 (18 days); mass of discs, n = 8 (24 h) and n = 8-11 (18 days).

3.4.2. Cell Density and ECM Deposition

Scarring is characterized by altered cell densities as well as altered deposition and contraction of ECM constituents. For instance, increases in collagen I, collagen III, and fibronectin expression have been associated with vocal fold scar formation [109]. In addition, the density of the elastic microfibril, fibrillin-1, has been observed to be significantly reduced in normal and hypertrophic dermal scars relative to normal skin [127]. In the present study, end-point cell densities within each hydrogel formulation were 65–70% of the initial seeding density, as is typical for cells photo-encapsulated within PEGDA hydrogels [128]. Similarly, hydroxyproline assessments indicated that total collagen production was consistent across hydrogel formulations (Fig. 8A).

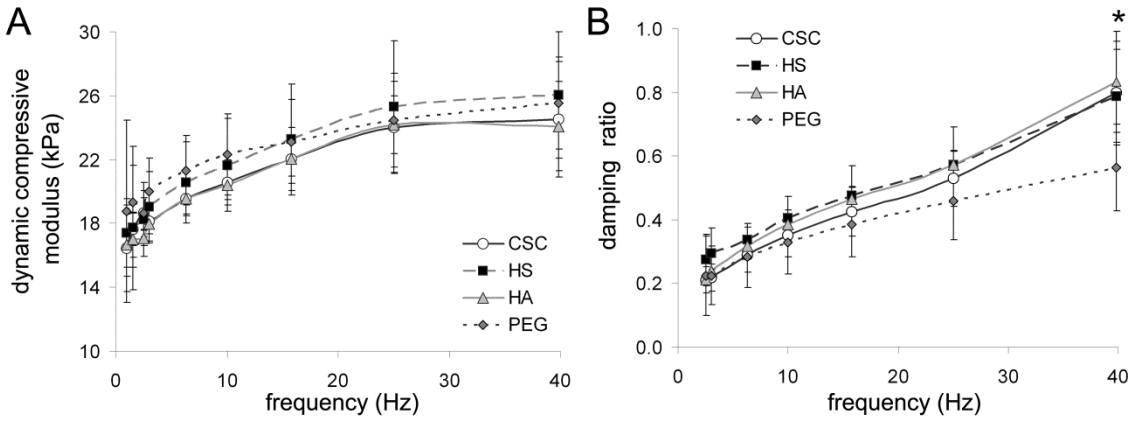

Fig. 7. (A) The elastic compressive modulus and (B) damping ratio of the various PEG–GAG formulations compared with pure PEG gels. For each formulation, 7–8 cell-laden gels were tested. *P < 0.05, significant difference for each PEG–GAG gel compared with the PEG hydrogel controls at 40 Hz.

Biochemical and histological assays also suggested that elastin deposition per cell could not be distinguished among gel types (Fig. 8A and B). However, fibrillin-1 levels were significantly greater in HS ($P = 0.001$) and HA ($P = 0.034$) hydrogels than in CSC gels (Fig. 8B), and fibronectin synthesis was higher in CSC than in HA gels ($P = 0.044$, Fig. 9). Similarly, collagen I expression was significantly greater in CSC gels relative to HA ($P = 0.002$) and HS ($P = 0.021$) hydrogels, whereas collagen III expression was higher in HA gels than in CSC ($P < 0.001$) and HS ($P = 0.001$) hydrogels. Quantitative comparison of the present collagen I and collagen III unit magnitude intensity vectors (Fig. 9) with the total collagen vector (Fig. 8) indicated collagen I: collagen III ratios of approximately 13, 3, and 0.7 in the CSC, HS, and HA formulations, respectively. Representative images for collagen III staining are given in Fig. 10 and display the pericellular localization observed for each of the examined ECM proteins [12, 16].

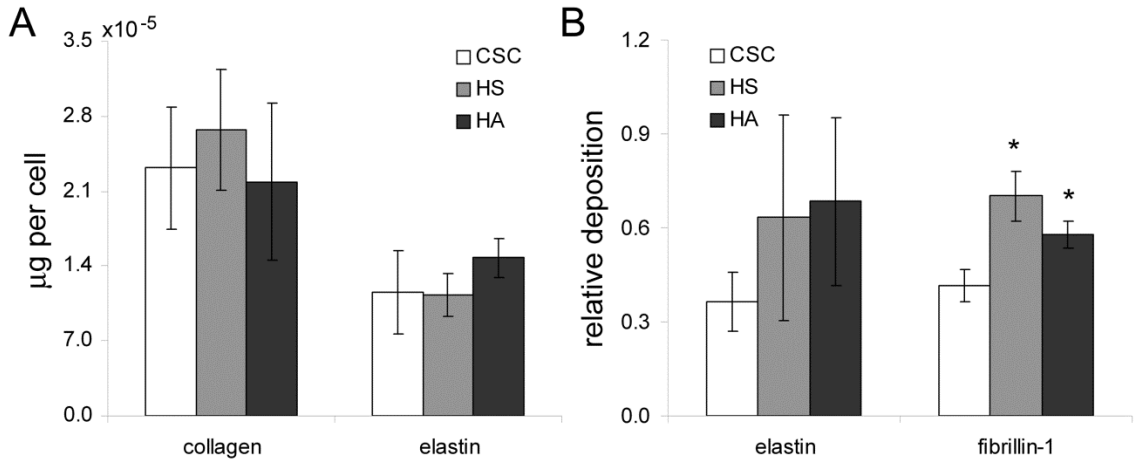

Fig. 8. Total collagen and elastic fiber production across hydrogel formulations. (A) Average total collagen (based on hydroxyproline measures) and elastin (based on ELISA assessments) per cell. (B) Semi-quantitative histological assessments of elastin and fibrillin-1. For the purposes of comparison, the elastin and fibrillin-1 cumulative staining intensity vectors were normalized to unit magnitude. *Significantly different from CSC hydrogels, $P < 0.05$.

3.4.3. Cell Phenotype and Signaling

Scarring and contracture are often promoted by resident fibroblasts taking on contractile, myofibroblast-like phenotypes [129]. Therefore, vocal fold fibroblast expression of the myofibroblast marker SM-α-actin was evaluated across hydrogel formulations (Fig. 11). Levels of SM-α-actin were lower in HA hydrogels relative to CSC ($P < 0.001$) and HS ($P < 0.001$) gels. To gain an insight into the intracellular signaling underlying observed vocal fold fibroblast phenotype and ECM production, signaling molecules activated by GAG interactions with cell surface receptors CD44 and RHAMM were investigated. As shown schematically in Fig. 12, GAG interactions with these receptors activate a number of signaling molecules, including NFκB, ERK1/2, and PLC-c1, which in turn modulate cell gene expression [78-80]. In the present study, no

significant differences in pPLC-γ1 levels were observed among formulations (Figs. 10 and 11). However, NFκB-p50 levels were significantly higher in HS gels relative to HA ($P < 0.001$) and CSC ($P < 0.001$) gels (Fig. 11), and NFκB-p65 levels were greater in CSC hydrogels than in HA gels ($P = 0.041$). In addition, pERK1/2 levels were lower in HS gels relative to CSC hydrogels ($P = 0.036$).

3.5. Discussion

The present study examined the impact of CSC and HS relative to HA on vocal fold fibroblast ECM production and phenotype with the aim of improving the design of implants for the treatment of SLP scarring. For an implant to restore scarred vocal fold SLP and/or to inhibit further SLP fibrosis, it is critical that the scaffold not trigger fibrotic vocal fold fibroblast behaviors, such as the increased deposition of total collagen [21]. In the current work, vocal fold fibroblasts in hydrogels containing CSC and HS displayed similar levels of total collagen relative to vocal fold fibroblasts in gels containing HA. Given that HA has previously been associated with a reduction in fibrotic response for a range of tissue types [13, 112, 130], the similarity in total collagen production between CSC, HS, and HA gels may be advantageous in terms of SLP restoration. That said, marked differences in the relative production of collagens I and III were observed among hydrogel formulations, with CSC having the highest collagen I: collagen III ratio and HA having the lowest collagen I: collagen III ratio. As previously discussed, comparison of the present total collagen and collagen type data indicated that

the collagen I: collagen III ratio varied with formulation, from ~12 in the CSC gels to ~0.7 in the HA gels. Since the ratio of collagen I to collagen III in the vocal fold SLP is estimated to be less than 1.5 [93, 131], the current results suggest that the HA formulation resulted in collagen compositions most mimetic of normal SLP.

In normal human vocal fold lamina propria, fibrillin-1 tends to be enriched in the pliable SLP, whereas elastin is essentially absent in this layer [102]. Fibrillin-1 has therefore been hypothesized to play a key role in SLP elasticity during phonation [20]. Although elastin deposition was similar across the PEG–GAG gel formulations, the HS hydrogels appeared to support the highest fibrillin- 1: elastin ratio, a feature which may be desirable for lamina propria regeneration. However, in the absence of quantitative measures of fibrillin-1, definitive statements regarding which PEG–GAG formulation supports a more appropriate fibrillin-1: elastin ratio cannot be made. In contrast to elastin, fibronectin was moderately increased in CSC hydrogels relative to HA gels. Since fibronectin expression has been consistently observed to be heightened in scarred vocal fold lamina propria [109], the increased fibronectin levels associated with CSC gels may be unfavorable for vocal fold scar treatment.

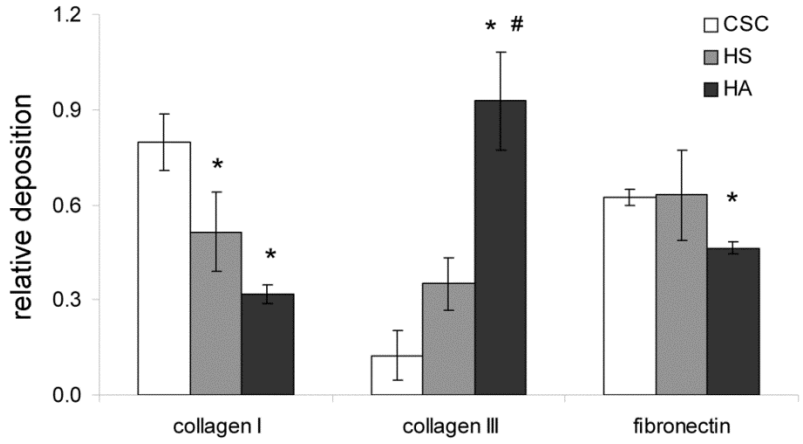

Fig. 9. Semi-quantitative histological assessments of collagen type and fibronectin production across hydrogel formulations. For the purposes of comparison, the cumulative staining intensity vectors for each antibody were normalized to unit magnitude. *Significantly different from CSC hydrogels, $P < 0.05$; #significantly different from HS hydrogels, $P < 0.05$.

Expression of the myofibroblast marker SM-α-actin decreased significantly from CSC to HS and from HS to HA hydrogels. Given the role of myofibroblasts in scar contraction and abnormal ECM synthesis [129], these results indicate that CSC and HS hydrogels may stimulate undesirable vocal fold fibroblast phenotypes. To gain an insight into the internal cellular signaling underlying the observed vocal fold fibroblast phenotype and ECM production, signaling molecules activated by GAG interactions with the cell surface receptors CD44 and RHAMM were investigated. Although the signaling cascades initiated by GAGs and/or GAG-associated molecules (such as growth factors) [132] are complex, CD44- and RHAMM-activated intermediates were selected for investigation due to the fact that each GAG under investigation directly interacts with one or both of these receptors. Specifically, both HA and HS actively bind RHAMM [133], whereas both HA and CSC interact with CD44 [133, 134] (although HS and CSC

have over 10-fold lower affinities for RHAMM and CD44, respectively, than HA [134, 135]).

Comparison of the SM-α-actin and signaling data suggests that the increased levels of SM-α-actin in CSC gels may be correlated with increased NFκB-p65- and/or pERK1/2-related signaling. Previous research has shown that expression of SM-α-actin by dermal fibroblasts is regulated in part by activation of the ERK1/2 pathway [136]. Similarly, ERK1/2 activation has been associated with increased fibronectin expression by kidney myofibroblasts [137]. For HS hydrogels, the higher SM-α-actin levels relative to HA gels may also be correlated with an increase in NFκB-p50, a transcription factor which plays important roles in inflammatory and immune responses. This would be consistent with a previous study of myofibroblasts which found that suppressing NFκB-p50 activation reduced expression of SM-α-actin as well as of collagen I [138].

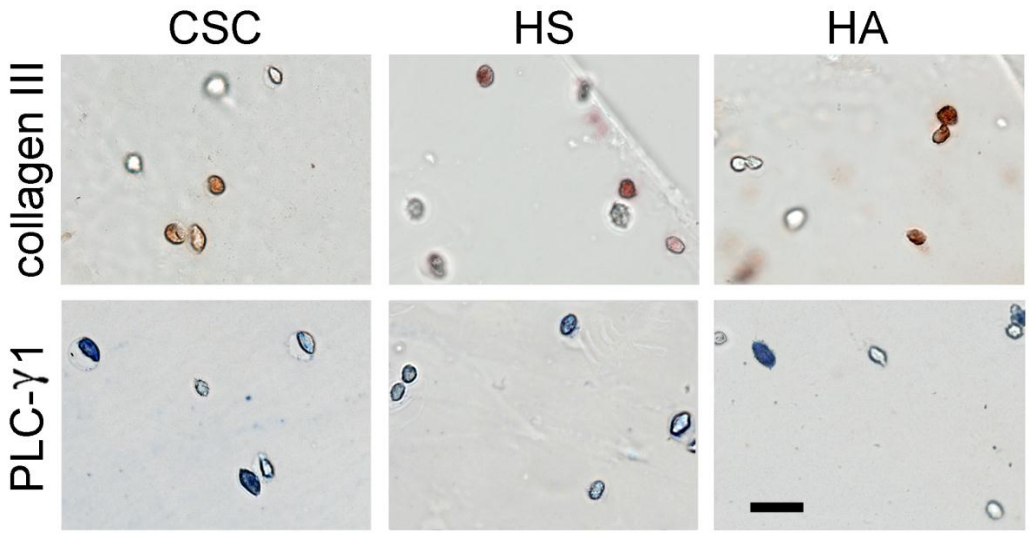

Fig. 10. Representative images of CSC, HS, and HA hydrogel sections immunostained for collagen III and PLC-γ1. The scale bar in the lower right-hand image equals 40 lm and applies to all images.

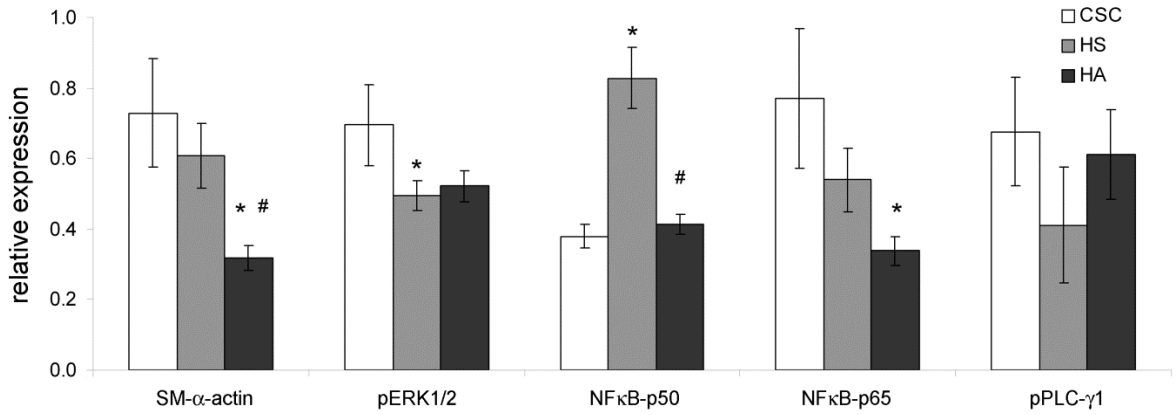

Fig. 11. Semi-quantitative histological assessments of SM-α-actin, pERK1/2, NFκB-p50, NFκB-p65, and pPLC-γ1 expression across hydrogel formulations. For the purposes of comparison, the cumulative staining intensity vectors for each antibody were normalized to unit magnitude. *Significantly different from CSC hydrogels, $P < 0.05$; #significantly different from HS hydrogels, $P < 0.05$.

Several limitations of the present study merit comment. The tight cross-link density and slow degradation rate of PEGDA gels induced the associated cells to take on oval/stellate morphologies, despite the presence of the cell adhesion ligand RGDS [12, 16]. These morphologies are non-native for vocal fold fibroblasts, which are normally elongated. However, a previous study has demonstrated that vocal fold fibroblasts encapsulated within PEGDA gels responded to matrix-mediated stimuli with similar trends (at least in terms of relative collagen, elastic fiber, and SM-α-actin expression) as vocal fold fibroblasts encapsulated in hydrogels permissive of more elongated cell morphologies [16]. An additional limitation of the present work results from the analysis of only a single concentration of each GAG type. Furthermore, the potential impact of the proteoglycan core protein or varying GAG chain length in modulating cellular interpretation of the applied GAG signals was not accounted for. Similarly, CSC and HS interact with a range of growth factors [139-143], and the potential effects of these

factors on observed cell behavior were not assessed. In terms of analysis methods, many of the present conclusions are based on semiquantitative immunostaining analyses and thus the results should be interpreted with caution. This is particularly true for the activated transcription factors examined, since the immunostaining assessments did not distinguish between nuclear and cytoplasmic proteins.

That said, the cumulative ECM and phenotypic data indicate that the PEG–HA gels may be the most appropriate for vocal fold SLP regeneration of the formulations examined, at least for the GAG molecular weights investigated. Future studies will therefore focus on PEG–HA hydrogels and will explore a broader range of PEGDA molecular weights and concentrations in order to further improve the correspondence between the dynamic mechanical response of PEG–HA gels and that of the vocal fold lamina propria.

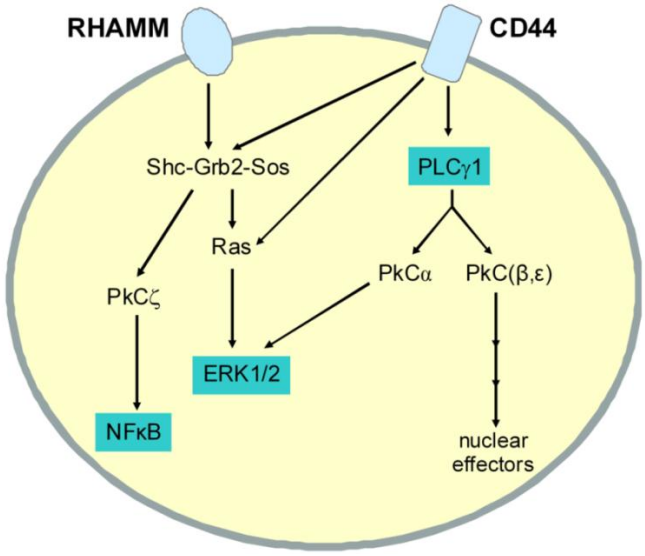

Fig. 12. Schematic of RHAMM and CD44 signaling and associated signaling intermediates, adapted from Turley et al. [80].

CHAPTER IV

REGULATION OF SMOOTH MUSCLE CELL PHENOTYPE BY GLYCOSAMINOGLYCAN IDENTITY*

4.1. Overview

The retention of lipoproteins in the arterial intima is an initial event in early atherosclerosis and occurs, in part, through interactions between negatively charged GAGs and the positively charged residues of apolipoproteins. Smooth muscle cells (SMCs) which infiltrate into the lipoproteinenriched intima have been observed to transform into lipid-laden foam cells. This phenotypic switch is associated with SMC acquisition of a macrophage-like capacity to phagocytose lipoproteins and/or of an adipocyte-like capacity to synthesize fatty acids de novo. The aim of the present work was to explore the impact of GAG identity on SMC foam cell formation using a scaffold environment intended to be mimetic of early atherosclerosis.

*Reprinted with permission from Influence of "Regulation of smooth muscle cell phenotype by glycosaminoglycan identity" by Xin Qu, Andrea Carolina Jimenez-Vergara, Dany J. Munoz-Pinto, Diana Ortiz, Rebecca E. McMahon, Deissy Cristancho, Silvia Becerra-Bayona, Viviana Guiza-Arguello, K. Jane Grande-Allen, Mariah S. Hahn, 2010, Acta Biomaterialia 7 (2011) 1031–1039, Copyright 2010, Acta Materialia Inc. Published by Elsevier Ltd.

In these studies, we focused on CSC, DS, and an intermediate molecular weight hyaluronan (HA_{IMW}, ~400 kDa), the levels and/or distribution of each of which are significantly altered in atherosclerosis. DS hydrogels were associated with greater SMC phagocytosis of apolipoprotein B than HAIMW gels. Similarly, only SMCs in DS constructs maintained increased expression of the adipocyte marker A-FABP relative to HA_{IMW} gels over 35 days of culture.

The increased SMC foam cell phenotype in DS hydrogels was reflected in a corresponding decrease in SMC myosin heavy chain expression in these constructs relative to HA_{IMW} gels at day 35. In addition, this DS-associated increase in foam cell formation was mirrored in an increased SMC synthetic phenotype, as evidenced by greater levels of collagen type I and glucose 6-phosphate dehydrogenase in DS gels than in HAIMW gels. Combined, these results support the increasing body of literature that suggests a critical role for DS-bearing proteoglycans in early atherosclerosis.

4.2. Introduction

Coronary artery disease is a leading cause of death in the USA [144] and develops when excess cellular and ECM components build up in the coronary arteries through the process of atherosclerosis [22-24]. Until recently it was generally believed that the extracellular lipids associated with early atherosclerosis originated from dead foam cells derived from invading macrophages. However, it is now recognized that this early accumulation of lipids precedes macrophage infiltration and instead arises

primarily from enhanced lipoprotein retention by the ECM of the arterial intima [22-24]. In fact, recent studies indicate that ionic interactions between the negatively charged GAG side-chains of intimal proteoglycans (PGs) and the positively charged apolipoprotein residues of low density lipoproteins (LDL) are critical to early atherosclerotic lipid retention [25-27]. As arterial LDL loading increases in atherogenesis, macrophages and SMCs increasingly infiltrate into the intima, followed by the appearance of foam cells [22]. Although foam cells were long considered to arise exclusively from macrophages, it is now known that SMCs form a significant portion of the foam cell population [145, 146]. The transition of SMCs to foam cells is marked by the acquisition of macrophage-like behaviors, such as scavenger– receptor uptake of LDL [147, 148], and/or by the acquisition of adipocyte-like properties, including expression of adipocyte fatty acid binding protein (A-FABP) [146]. Although it is recognized that GAG retention of lipoproteins is a key event in SMC foam cell formation [22], the extent to which specific GAG types contribute to this process is relatively poorly understood. Thus, the present work was designed to explore the impact of GAG identity on SMC phenotype using a scaffold environment intended to be mimetic of early atherosclerosis. Specifically, the effects of CSC, DS, and an intermediate molecular weight hyaluronan (HA_{IMW}, ~400 kDa) were examined, as the levels and/or distribution of each of these GAG types are altered in early atherosclerosis [22, 149-154].

To generate culture conditions mimetic of early atherosclerosis, PEGDA hydrogel was selected as the base scaffold into which the desired GAG signals were

conjugated. PEGDA gels have several properties which make them appropriate for the present studies. First, pure PEGDA hydrogels function as biological ‘‘blank slates’’ in that they are intrinsically resistant to protein adsorption and cell adhesion [70]. Thus, hybrid PEGDA–GAG gels permit the defined investigation of GAG identity on SMC behavior. In addition, the slow degradation rate and high cross-link density of PEGDA gels force encapsulated cells to take on rounded/stellate morphologies with limited cell–cell interactions [16, 72]. These particular characteristics of PEGDA hydrogels are generally considered undesirable for the study of normal SMC function. However, they are appropriate for atherosclerotic mimetic environments, since atherosclerosis-induced changes are associated with SMCs taking on rounded/stellate morphologies [155-157] with limited intercellular gap junctions [158]. Finally, the dense cross-linking and slow degradation rate of PEGDA gels prevent cell-mediated hydrogel contraction and the associated changes in scaffold material properties which can confound interpretation of cell responses [16].

In the present work, porcine SMCs were encapsulated in PEGDA hydrogels containing 0.1 wt.% GAG, a concentration selected to be consistent with GAG levels in arterial tissue [150, 159]. A 10 wt.% 10 kDa PEGDA hydrogel was chosen for the base scaffold in order to mimic the modulus of lipid-rich regions of grade II atherosclerotic plaque [160]. Following 14 and 35 days of culture, SMC phenotype in each formulation was assessed biochemically and histologically.

4.3. Materials and Methods

4.3.1. Polymer Synthesis and Characterization

4.3.1.1. PEGDA Synthesis

PEGDA was prepared as previously described [117] by combining 0.1 mmol ml^{-1} dry PEG (10 kDa, Fluka), 0.4 mmol ml^{-1} acryloyl chloride, and 0.2 mmol ml^{-1} triethylamine in anhydrous DCM and stirring under argon overnight. The resulting solution was washed with 2 M K_2CO_3 and separated into aqueous and DCM phases to remove HCl. The DCM phase was subsequently dried with anhydrous $MgSO_4$, and PEGDA was precipitated in diethyl ether, filtered, and dried under vacuum. The extent of PEG diacrylation was determined by ^1H NMR to be ~75%.

4.3.1.2. Synthesis of Methacrylate-Derivatized CSC and DS

In order to conjugate specific GAGs into the PEGDA-based hydrogel networks, each GAG type was methacrylate-derivatized according to standard protocols [81]. CSC (~50 kDa, 6.4 wt.% sulfur, Sigma) and DS (~41.5 kDa, 6.1 wt.% sulfur, Sigma) were selected to have molecular weights (MWs) consistent with those observed in atherosclerotic tissue [149, 159]. The respective sulfur contents of these GAG chains indicated that, on average, the CSC and DS disaccharide units had a charge density consistent with mono-sulfation. The GAGs were dissolved in deionized dIH_2O to achieve a 1 wt.% final concentration, and the pH of each solution was adjusted to 8.0. A

10-fold molar excess of methacrylic anhydride (Polysciences) was added per disaccharide unit. Each reaction was allowed to proceed under constant stirring at 4 °C, with the solution pH being maintained at ~8.0 by periodic addition of 5 M NaOH. The product of each reaction was precipitated twice using chilled 95% ethanol, dialyzed against dIH_2O for 48 h, and lyophilized. The extent of methacrylate-derivatization was characterized by ^1H NMR to be ~1.0–1.6%. These levels of methacrylate-derivatization have been previously shown to negligibly alter observed cell-GAG interactions [16, 81, 118, 161-163].

4.3.1.3. Synthesis of Methacrylate-Derivatized Intermediate Molecular Weight HA

Recent studies indicate that atherosclerotic vessels contain two primary HA populations, one with $M_W > 1 \times 10^3$ kDa, which is also present within normal tissue, and a second with M_W 340 kDa, which appears to be specific to atherosclerotic tissue [149, 154]. To generate HA appropriate for the examination of atherosclerotic conditions, high M_W HA (HA_{HMW}, Streptococcus equi, M_W ~1.65 x 10^3 kDa, Fluka) was first methacrylate derivatized as above. The purified product was then dissolved at 1 mg ml^{-1} in phosphate- buffered saline (PBS) containing 0.05% sodium azide and 5U ml^{-1} hyaluronidase IV-S (H3884, Sigma). Following incubation at 37 °C overnight, the enzyme was heat inactivated. The resulting digestion product (HA_{IMW}-MA) was dialyzed against dIH_2O for 48 h and lyophilized. The mean M_W of the isolated HA_{IMW}-MA was determined to be ~400 kDa, with a polydispersity of ~1.3, using gel permeation chromatography (Viscotek).

4.3.1.4. Synthesis of Acrylate-Derivatized Cell Adhesion Peptide

Cell adhesion peptide RGDS (American Peptide) was reacted with acryloyl-PEG-N-hydroxysuccinimide (ACRL-PEG-NHS, 3.4 kDa, Nektar) at a 1:1 M ratio for 2 h in 50mM sodium bicarbonate buffer, pH 8.5 [20]. The product (ACRL-PEG-RGDS) was purified by dialysis, lyophilized, and stored at -20 °C until use.

4.3.2. Characterization of Hydrogel Properties

4.3.2.1. Hydrogel Initial Water Uptake

To compare initial hydrogel water uptake across formulations, the initial weight (W_i) of each gel was determined immediately following polymerization, after which the gels were submerged in media. After 24 h, the swollen weight (W_s) of each gel was measured. The equilibrium water uptake (S) was calculated as: $S = \frac{s}{i}$. This information was used to estimate the increase in hydrogel volume due to swelling, data which were then used to compare post-swelling GAG levels across gels.

4.3.2.2. Average Mesh Size

PEGDA hydrogel mesh size cannot be visualized using standard techniques such as conventional SEM [164]. In the present study, hydrogel mesh size was characterized via a series of dextran diffusion experiments based on an adaptation of the methodology of Watkins et al. [120]. To avoid charge–charge interactions between the diffusing dextrans and the GAG chains tethered to the hydrogel network, fluorescently labeled,

charge-neutral dextrans were employed. In brief, PEGDA-GAG hydrogels were prepared and allowed to swell overnight at 37 °C in PBS containing 0.05% azide (PBS–azide). 1 cm diameter discs were cored from each hydrogel formulation. Fluorescently labeled, charge-neutral dextrans (40 and 70 kDa, Invitrogen) were dissolved at 0.05 mg ml^{-1} in HEPES-buffered saline (HBS) (10 mM HEPES, 150 mM NaCl, pH 7.4) containing 0.05% azide and added at 1 ml per hydrogel disc (3 discs per dextran MW). Dextran solutions were allowed to diffuse into the hydrogels for 24 h at 37 °C. Each gel disc was subsequently gently blotted and transferred to 1 ml of fresh PBS–azide. Dextran that had penetrated into the hydrogels was then permitted to diffuse out into the surrounding solution at 37 °C. After 24 h, the fluorescence of the PBS– azide solution surrounding each disc was measured at excitation/ emission wavelengths of 530/590 nm. Dextran standard curves were used to convert each fluorescence signal to a concentration. For each hydrogel formulation, the measured concentration readings for each dextran MW were divided by the gel thickness and then plotted versus dextran hydrodynamic radius [121]. The area (A) under the resulting curve served as a quantitative indicator of hydrogel permissivity over the hydrodynamic radii range assayed. For the purposes of comparison, the calculated area values for CSC and DS gels were normalized to that of the HA_{IMW} gels to yield relative mesh size values.

4.3.2.3. Hydrogel Permissivity to LDL

To confirm the ability of LDL molecules to diffuse into the hydrogel networks, three gels from each formulation were exposed overnight at room temperature to 50 lg ml^{-1} of fluorescently labeled LDL (Invitrogen) in PBS. After 24 h, the levels of LDL which had diffused into the hydrogel networks were examined using confocal microscopy (Leica). The resulting confocal image series were volume-rendered using Osirix freeware and compared against control gels which had not been exposed to LDL.

4.3.2.4. Comparison of GAG LDL Retention

To assess differences in the LDL-binding capacity of the various GAG-laden hydrogels, samples which had been exposed overnight to fluorescently labeled LDL were transferred to fresh PBS–azide. Over a period of 24 h, the PBS solution surrounding each gel was exchanged twice, after which the hydrogels were transferred to fresh PBS for fluorescence imaging.

4.3.3. Cell Culture

Cryopreserved aortic SMCs (Cell Applications) isolated from pigs, a common animal model for vascular SMC physiology [165, 166], were thawed and expanded in monolayer culture between passages 4–8. Prior to encapsulation, cells were maintained at 37 °C in 5% CO2 in DMEM (Hyclone) supplemented with 10% FBS (Hyclone), 1 ng

ml^{-1} basic fibroblast growth factor (BD Biosciences), 100 mU ml^{-1} penicillin and 100 mg l^{-1} streptomycin (Hyclone).

4.3.4. Cell Encapsulation and Hydrogel Maintenance

Hydrogels were fabricated by preparing precursor solutions containing 100 mg ml^{-1} 10 kDa PEGDA, 1 mg ml^{-1} methacrylatederivatized GAG, and 1 lmol ml^{-1} ACRL-PEG-RGDS in HBS. The 100:1 weight ratio of PEGDA to GAG was chosen to ensure that the degradation rate, modulus, and initial mesh structure of each hydrogel network would be dominated by PEGDA [19]. A 300 mg ml^{-1} solution of UV photoinitiator 2,2-dimethoxy-2-phenyl acetophenone in N-vinylpyrrolidone was added at 1% to each precursor solution. SMCs were harvested and resuspended in the filter-sterilized precursor solutions at ~1 x 10^6 cells ml^{-1}. The cell suspensions were then poured into molds composed of two glass plates separated by 0.5 mm polycarbonate spacers and polymerized by 2 min exposure to longwave UV light (Spectroline, ~6 m Wcm^{-2}, 365 nm). The hydrogel slabs were transferred to Omnitrays (Nunc) fitted with four sterile polycarbonate bars to simultaneously prevent gel flotation and prevent gel contact with the tray bottom. Hydrogels were immersed in DMEM supplemented with 10% FBS, 100 U ml^{-1} penicillin, and 100 mg l^{-1} streptomycin and maintained at 37 °C in 5% CO2. The FBS lot used for the present studies contained ~50 mg dl^{-1} LDL according to the manufacturer's quality control assays.

4.3.4.1. Hydrogel Mechanical Properties and Contraction

Following initial swelling, three 8 mm diameter samples were cored from each hydrogel. The thickness of each disc was measured using a digital caliper. These thickness measures served both as gage lengths for mechanical testing as well as indicators of hydrogel degradation and/or SMC-mediated gel compaction with time. Following application of a 0.01 N preload, each hydrogel was subjected to cyclic unconstrained compression (~10% cyclic strain) at 1 Hz using an Instron 3342. The dynamic compressive modulus of each hydrogel formulation was extracted from the resulting stress–strain data.

4.3.5. End-Point Hydrogel Analyses

On days 14 and 35 of culture, a series of 8 mm diameter samples were collected from each hydrogel formulation for mechanical, biochemical, and histological analyses. Mechanical samples were tested as described above.

4.3.5.1. Collagen and Elastin Analyses

Samples harvested for biochemical analyses were transferred to screw cap vials, weighed, flash frozen in liquid nitrogen, and stored at -80 °C until time of analysis. The weight of each 8 mm disc was used as a second indicator of gel degradation and/or compaction, since the reduction in gel volume associated with both of these processes would be reflected in a mass loss, assuming lack of commensurate new matrix

deposition [16]. Hydrogel samples were digested for 72 h at 37 °C in 1 ml of 0.12 M NaOH per 0.2 g hydrogel wet weight [83, 84]. DNA, total collagen, and elastin were then analyzed using established protocols. For each assay, the standards used were subjected to the same association with PEGDA and GAG and to the same digestion conditions as the samples. The resulting collagen and elastin data were normalized to cell number.

DNA Analysis. Aliquots of the hydrolyzed samples (n = 12 per formulation) were neutralized and their DNA content determined using the Invitrogen PicoGreen assay [84]. DNA measures were translated to cell number using a conversion factor of 6.6 pg DNA per cell [85]. Calf thymus DNA (Sigma) served as a standard.

Collagen Analysis. The amino acid hydroxyproline was quantified as an indirect measure of total collagen. In brief, aliquots (n = 4–6 per formulation) collected for collagen quantitation were hydrolyzed for 18 h at 110 °C in 6 M HCl. Each sample was then dried on a Labconco Centrivap to remove HCl, resuspended in dIH_2O, and passed through a charcoal-packed centrifugal microcolumn (Nunc) to remove caramelized sugars. The resultant samples were reacted with chloramine T and p-dimethylbenzaldehyde reagents [83, 84]. Sample absorbance was read at 550 nm relative to that of L-4-hydroxyproline (Sigma). Total collagen content was estimated from measured grams of hydroxyproline by dividing by 0.13 [124].

Elastin Analysis. Elastin production was measured using indirect ELISA [86]. NaOH digested samples (n = 9–14 per formulation) were neutralized and further digested with 0.25 M oxalic acid at 100 °C overnight. Oxalic acid was removed from the samples and exchanged for PBS using Microcon YM-3 centrifugal filters (Millipore). 100 μl of the resulting samples were applied to a high binding multiwell plate for 3 h at room temperature. After blocking the plate with bovine serum albumin (BSA), adsorbed elastin fragments were detected by applying elastin antibody (BA-4, Santa Cruz Biotechnology, [SCBT]) followed by donkey anti-mouse HRP secondary antibody (SCBT) and 2,2'-azino-bis(3-ethylbenzthiazo-line-6-sulphonic acid). Absorbance was read at 410 nm, with bovine aortic elastin (Sigma) serving as a standard.

4.2.5.2. GAG Analyses

Quantification of individual GAG types as well as changes in these GAG types requires specialized techniques, which generally rely on identifying specific GAG classes based on their characteristic component disaccharides. Given the anticipated levels of new GAG synthesis (~5 μg $(g\ gel)^{-1}$ = ~50 lg $(g\ PEG)^{-1}$) [72], the high sensitivity technique known as fluorescence assisted carbohydrate electrophoresis (FACE) was employed and GAG type assessments were limited to HA, DS, and CSC disaccharide units.

To separate newly synthesized GAGs from the GAG chains covalently linked to the PEGDA hydrogel networks, a two step degradation process was employed. The first phase of this process was intended to release newly deposited GAGs, while the second

step was intended to release GAGs conjugated to the hydrogel network. In brief, harvested hydrogel samples were sliced into a series of 35 lm sections using a cryomicrotome, after which these sections were exposed to 1 mg ml^{-1} proteinase K (Worthington Biochemical) in PBS at 37 °C. Sectioning increased the surface area for enzymatic action, allowing the proteinase K to release GAGs bound to either proteoglycan core proteins or to cell receptors. However, since the covalent bonds linking the methacrylate-derivatized GAGs to the PEGDA chains are not labile by proteinase K, the GAGs tethered to the hydrogel networks were not released by this treatment. Following 24 h of digestion, the samples were heated to inactivate the proteinase K, after which they were centrifuged and the supernatant collected. The gel sections were subsequently rinsed with PBS, and the wash solution was combined with the initial proteinase K supernatant. The gels sections were then immersed in 0.1 M NaOH for 24 h at 37 °C to induce hydrolysis of the hydrogel structure and the release of conjugated GAG chains.

Each proteinase K supernatant and NaOH-treated sample was exposed to 0.3 mU μl^{-1} chondroitinase ABC (Proteus vulgaris, Sigma) for 3 h at 37 °C, followed by exposure to 0.3 mU μl^{-1} chondroitinase ACII (Flavobacterium heparinum, Seikagaku America) overnight at 37 °C [43,44]. This enzymatic treatment digested chains of HA, CSC, and DS into their component disaccharides, which can be considered to be primarily ΔDi-HA, ΔDi-6S, and ΔDi-4S, respectively. The chondroitinase ABC/ACII treated samples were then dried, fluorotagged with 2-aminoacridone HCl (AMAC, Invitrogen) [167], and mixed with glycerol. These samples were subsequently

electrophoresed on monosaccharide gels prepared as previously described [167]. Negative control samples of pure AMAC were run on each gel, and enzyme digestion products were identified by correspondence to bands in disaccharide standard lanes. The gel bands were imaged using a Kodak GelLogic station and analyzed using Image J software. The quantity of each disaccharide was determined from the integrated optical density of the appropriate band, internal maltriose standards, and sample volume information [20]. The measured disaccharide values were then normalized to sample PEG content, which was quantified by iodine staining of the electrophoresed, NaOH-treated samples as per Suggs et al. [168].

4.3.5.2. Histological Analyses

Samples harvested for histological analyses were fixed in 10% formalin for 30 min, embedded in Tissue-Tek freezing medium, and frozen at -80 °C. 35 μm sections were cut using a cryomicrotome.

Immunostaining. SMC ECM production and phenotype were analyzed for each gel sample using standard immunohistochemical techniques. All immunostaining steps took place at room temperature unless otherwise noted. Rehydrated sections were blocked with peroxidase for 10 min, followed by 10 min exposure to Terminator block (Biocare Medical). Primary antibodies for elastin (BA-4, SCBT), collagen type I (Rockland Immunochemicals), or collagen type III (Rockland Immunochemicals), which had been diluted in PBS containing 0.05% Tween 20 and 3% BSA, were then applied for

1 h. Primary antibodies for smooth muscle myosin heavy chain (MHC) (G-4, SCBT), calponin h1 (CALP, SCBT), A-FABP (C-15, SCBT), and apolipoprotein B (apoB) (ab20737, Abcam) were similarly applied to construct sections for 1 h, except that rehydrated sections were permeabilized with PBS containing 0.5% Triton X-100 for 10 min prior to Terminator application. Bound primary antibody was detected using alkaline phosphatase-conjugated secondary antibody (Jackson Immunochemicals) followed by application of the chromogen Ferangi Blue (Biocare Medical) or using horseradish peroxidase-conjugated secondary antibody followed by application of the chromogen AEC (LabVision). Based on observed differences in SMC behavior in HA_{IMW} and DS gels, day 14 hydrogel samples were also immunostained for the metabolic marker glucose 6-phosphate dehydrogenase (G6PD) (ab61704, Abcam) and ECM protein osteocalcin (M-15, SCBT) as per the above procedure.

Semi-quantitative Assessments. For intracellular markers (calponin h1, MHC, A-FABP, apoB, and G6PD), cell counts were carried out as semi-quantitative analyses of the immunostaining results. These counting assessments were conducted by two independent observers on two or three sections per sample of each PEGDA-GAG formulation (~500–3000 cells) according to established methods [53, 87-89]. For each cell i in a given section, a staining intensity d_i was recorded on a scale of 0–3, 0 representing no staining and 3 representing the highest intensity observed among all gel formulations for that antibody. The cumulative staining intensity d for a given antibody in a particular section was calculated using the equation: $d \frac{d_i}{\text{total cell number}}$. In addition,

since deposited ECM tended to remain localized around the parent cells in each hydrogel formulation, as is characteristic for PEGDA gels [73, 90, 169], the relative levels of osteocalcin, collagen type I, collagen type III, and elastin among hydrogel formulations were also evaluated by cell counts as per the above procedure. For the purposes of comparison, the resulting average cumulative staining intensities for CSC and DS gels at a given time point were normalized to the corresponding HA_{IMW} average cumulative staining intensity.

4.3.6. Statistical Analyses

Data are reported as means ± standard error of the mean. Comparison of sample means was performed by one-way ANOVA and Tukey's post-hoc test (SPSS software), $P < 0.05$.

4.4. Results

4.4.1. Hydrogel Material Properties

4.4.1.1. Hydrogel Swelling, LDL Permissivity, and Binding Affinity

In order to specifically attribute differences in SMC behavior across hydrogel formulations to initial differences in gel GAG composition, it was important that the remaining hydrogel material properties could be considered consistent across gels. The

‘‘bulk’’ material properties of each gel formulation were therefore characterized and compared. The initial water uptake S of each gel following polymerization was similar (CSC, 1.42 ± 0.02; DS, 1.38 ± 0.03; HA_{IMW}, 1.43 ± 0.02), indicating that gel equilibrium hydration could be considered consistent across formulations. The ability of LDL to diffuse through and bind to the GAG-laden hydrogel networks was also characterized by exposing the swollen gels fluorescently labeled LDL, examining the equilibrium levels of LDL diffusion, and then assessing LDL retention when the external LDL solution was removed. Fig. 13 demonstrates the ability of LDL to partition into and diffuse evenly throughout the GAG-laden hydrogels. When the observed LDL fluorescence intensities within the hydrogel networks were quantified against known LDL standards, each hydrogel demonstrated similar permissivity to LDL (Table 5). This result was anticipated based on the similarity in bulk average mesh size across hydrogel formulations, as determined by the equilibrium diffusion of a set of neutral dextrans (Table 5), and based on previous reports indicating that the average mesh size of 10% 10 kDa PEGDA hydrogels could be considered to be roughly twice the average hydrodynamic radius of LDL [12, 72]. Comparison of LDL retention by the GAG-containing hydrogels following the exchange of the external LDL solution with PBS indicated that each GAG-laden gel had a similar average capacity to bind LDL (Table 5).

Table 5. Hydrogel Relative Mesh Size, LDL Permissivity, and LDL Retention.

Gel Type	Relative Mesh Size	LDL Diffusion into Network (μg/g)	LDL Retained (μg/g)
CSC	1.01 ± 0.01	7.52 ± 0.20	0.052 ± 0.028
DS	1.02 ± 0.01	7.37 ± 0.40	0.043 ± 0.013
HA_{IMW}	1.00 ± 0.01	7.52 ± 0.16	0.046 ± 0.019

4.4.1.2. Assessments of Alterations in GAG Levels and Gel Material Properties

Comparison of the initial and end-point mechanical data (Table 6) suggested that the bulk gel modulus could be considered indistinguishable across formulations at each time point. Similarly, the initial and end-point gel thickness and mass data corresponded to a negligible reduction in gel volume with time (Table 6). FACE analysis of the GAGs within hydrolyzed day 0 gels indicated ~100% conjugation of methacrylate-derivatized GAG to the hydrogel networks at the time of polymerization (~11 mg GAG (g PEG)$^{-1}$ = ~1.1 mg ml^{-1} precursor solution = ~ 0.79 mg g^{-1} swollen gel, Table 7). Furthermore, the levels of GAGs conjugated to the gel networks at day 14 were not substantially altered from day 0 values. Although the levels of network-conjugated GAGs appeared to have decreased by day 35 relative to time 0 values, these differences were not statistically significant (Table 7). Cumulatively, the bulk modulus, thickness, gel mass, and conjugated GAG assessments indicated that the PEGDA–GAG gels retained the slow degradation rate and resistance to cell-mediated contraction characteristic of pure PEGDA hydrogels [84, 90-92].

To assess potential alterations in the GAG types experienced by encapsulated cells due to newly synthesized GAGs, FACE analyses were performed on GAGs

released from thin hydrogel sections following exposure to proteinase K. These newly synthesized GAGs were primarily comprised of ΔDi-6S disaccharides (a primary component of CSC) (data not shown) in each hydrogel type, and were measured at between 0.012 and 0.052 mg (g PEG)$^{-1}$, which is equivalent to ~0.0008–0.0038 mg GAG per g swollen gel (Table 7).

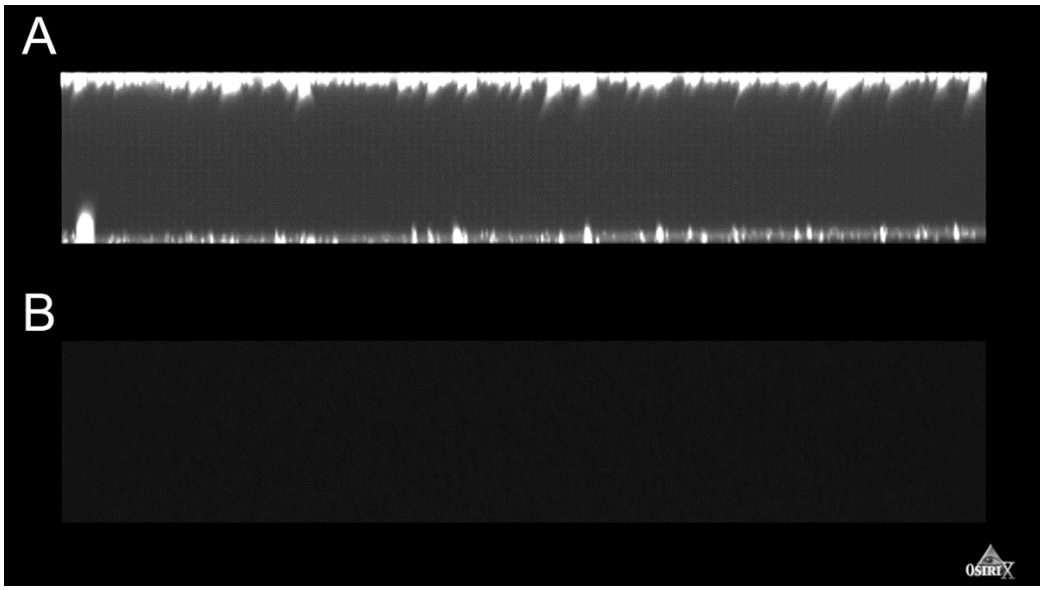

Fig. 13. Representative side views of 3D renderings of two, confocal image series taken of PEGDA–GAG hydrogels. The upper image is of a hydrogel that had been immersed in a fluorescently labeled LDL solution for 24 h prior to imaging. The external LDL solution is apparent at the upper and lower borders of the gel. The lower image is of a control hydrogel immersed in PBS, rather than LDL, for 24 h prior to imaging. The upper and lower images were generated and rendered using the same microscope and software settings to ensure that the grayscale intensities of the hydrogel side views could be compared.

Table 6. Hydrogel Modulus, Thickness, and Mass Assessments.

Gel Type	Modulus (kPa)		Thickness (mm)		Mass of 8 mm Discs (mg)	
	initial	final	initial	final	initial	final
CSC	81.6 ± 3.4	86.6 ± 1.7	0.56 ± 0.01	0.59 ± 0.01	28.4 ± 0.3	29.4 ± 0.3
DS	79.1 ± 2.3	83.0 ± 12.2	0.55 ± 0.01	0.55 ± 0.01	27.6 ± 0.5	27.8 ± 0.4
HA_{IMW}	80.4 ± 3.6	81.5 ± 12.0	0.57 ± 0.01	0.56 ± 0.01	28.7 ± 0.4	28.1 ± 0.5

4.4.2. SMC Collagen and Elastin Deposition

To gage the extent to which encapsulated SMCs were taking on a synthetic phenotype, elastin and collagen production was analyzed biochemically and histologically at days 14 and 35. As expected for PEGDA gels [73], staining for elastin and individual collagen types was confined to the immediate pericellular space in each formulation (Fig. 14), enabling reliable semi-quantitative histological analyses of these ECM proteins. Day 14 histological and biochemical data suggested that DS may enhance elastin production relative to HA_{IMW} and CSC (Fig. 15A). However, for both assessment methods, no statistical differences between elastin levels among hydrogel types were observed. In contrast, day 14 hydroxyproline measures indicated that total collagen levels were significantly higher in DS gels relative to HA_{IMW} gels ($P = 0.014$, Fig. 3B). Analysis of individual collagen types demonstrated that collagen type I deposition was significantly greater in DS gels than in CSC gels ($P = 0.036$), whereas collagen type III was significantly greater in HA_{IMW} gels relative to CSC hydrogels ($P = 0.020$) (Fig. 3B). Comparison of the collagen type I and type III trends with that of total collagen suggested that collagen type I was the dominant collagen being produced by the

encapsulated SMCs. By day 35, differences in elastin production among formulations were no longer apparent (Fig. 15C), although the day 14 trends in collagen type I were maintained at this time point (Fig. 15D). In particular, collagen type I deposition on day 35 was greater in DS gels than HA_{IMW} gels (P = 0.050). As shown in the notations associated with Fig. 15, total collagen and total elastin levels per cell remained essentially unaltered from day 14 to day 35, indicating that the cells had reached a steady-state betweenthe productionand degradation of these molecules.

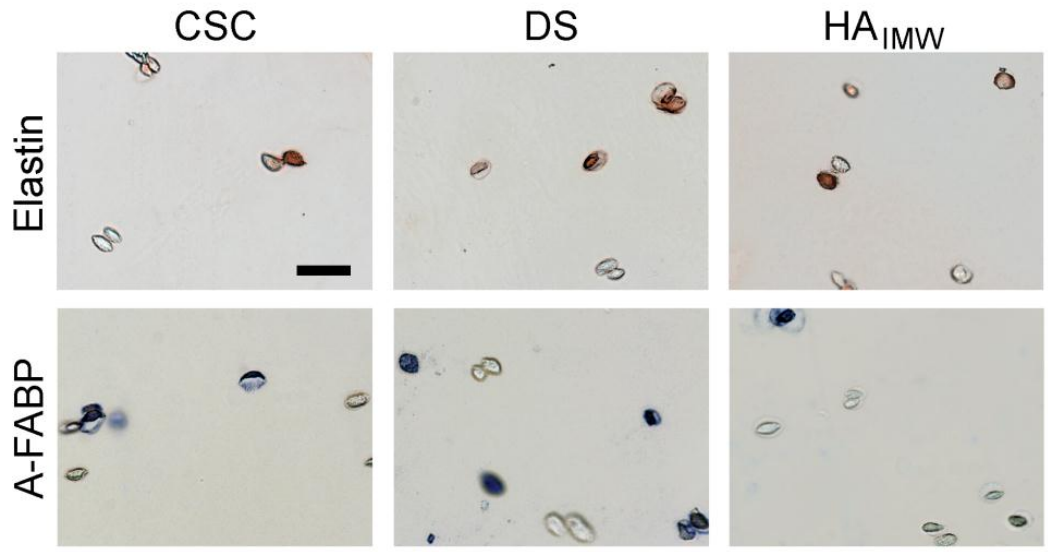

Fig. 14. Representative images of day 14 CSC, DS, and HA_{IMW} hydrogel sections immunostained for elastin and A-FABP. The scale bar in the upper left image represents 40 μm and applies to all images.The noted values for the immunostaining assessments are unitless, but represent both average intensity (on a scale of 1–3) as well as the cell fraction positively stained.

Table 7. Results from FACE-Based GAG Analyses.

GAG Source	Gel Type	Initial (mg/g PEG)	Day 14 (mg/g PEG)	Day 35 (mg/g PEG)
Conjugated	**CSC, DS, HA_{IMW}**	11.7 ± 3.0	10.7 ± 3.6	7.0 ± 1.2
	CSC		0.015 ± 0.003	0.012 ± 0.008
Synthesized	**DS**		0.051 ± 0.023	0.018 ± 0.006
	HA_{IMW}		0.052 ± 0.027	0.013 ± 0.006

4.4.3. SMC Phenotype

SMC acquisition of adipocyte-like or macrophage-like characteristics was similarly examined (Fig. 16). On day 14, SMC uptake of LDL (as evidenced by intracellular apoB) was higher in DS gels relative to HA_{IMW} gels ($P = 0.026$) (Fig. 16A). In addition, expression of the late-term adipogenic marker A-FABP was significantly greater in CSC ($P = 0.034$) and DS ($P = 0.018$) gels than in HA_{IMW} gels (Figs. 14 and 16A). Similarly, day 35 apoB uptake ($P = 0.05$) and A-FABP expression ($P = 0.015$) continued to be greater in DS gels relative to HA_{IMW} gels (Fig. 16C). The degree to which encapsulated cells displayed markers associated with a mature, contractile SMC phenotype was also investigated through analysis of calponin h1 and MHC expression. On day 14, calponin h1 levels were greater in DS gels relative to both CSC ($P = 0.021$) and HA_{IMW} ($P = 0.011$) constructs (Fig. 16B). In contrast, MHC measures indicated that both DS ($P = 0.011$) and HA_{IMW} ($P = 0.039$) better supported a contractile phenotype than CSC.

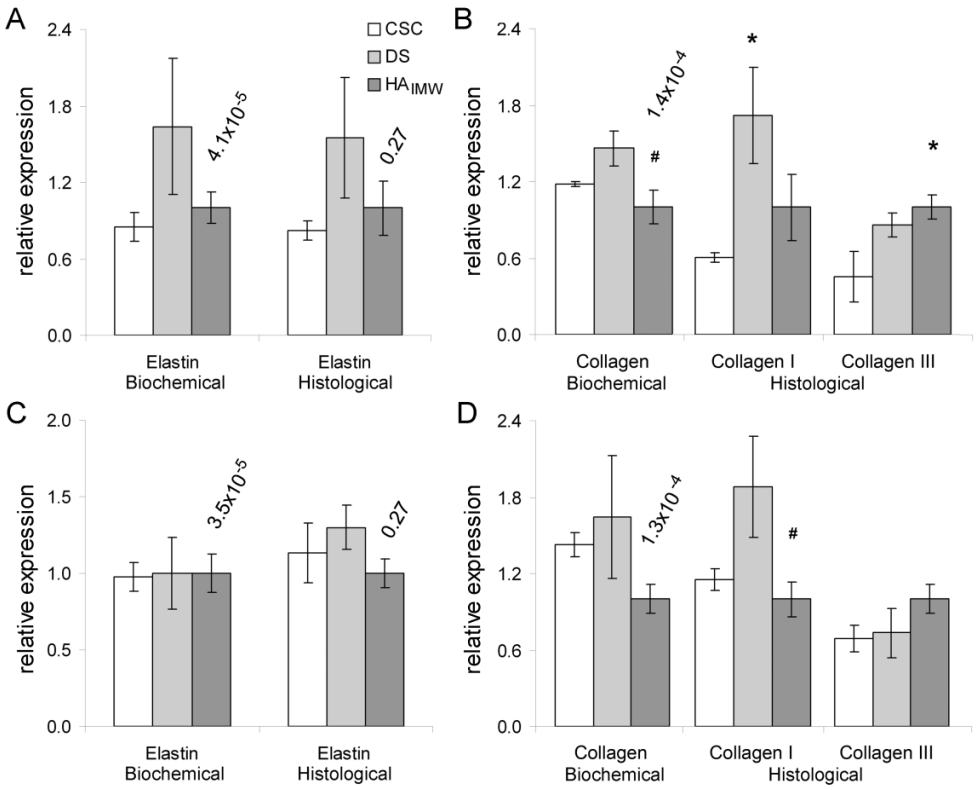

Fig. 15. ECM deposition across formulations. (A and C) Relative elastin production by both biochemical and histological assessments on days 14 and 35, respectively. (B and D) Relative total collagen, collagen type I and collagen type III production on days 14 and 35, respectively. *Significantly different from CSC hydrogels, $P < 0.05$. #Significantly different from DS hydrogels, $P < 0.05$. CSC and DS data at each time point have been normalized to the corresponding HA_{IMW} data, the average values for which are noted above the HA_{IMW} formulation where applicable. For the elastin and collagen biochemical data, the units of the noted values are in micrograms per cell.

By day 35, calponin h1 expression had leveled out among formulations, and the MHC trends had shifted, with HA_{IMW} gels supporting greater MHC expression than either DS ($P = 0.050$) or CSC ($P = 0.048$) gels (Fig. 16D). Due to the observed differences between the apoB and A-FABP profiles of HA_{IMW} and DS gels, day 14 hydrogel samples were also immunostained for G6PD and osteocalcin in order to gain further insight into the cell responses within these gels. G6PD is a key metabolic enzyme

associated with a primarily anabolic pathway essential in the regulation of oxidative stress [170, 171], one of the stressors in atherosclerosis. In addition, osteocalcin is an ECM protein produced by foam cells in calcific plaques. As shown in Fig. 17, both G6PD ($P < 0.001$) and osteocalcin ($P = 0.010$) were elevated in DS gels relative to HA_{IMW} hydrogels.

4.5. Discussion

The aim of the present study was to examine the impact of GAG type on SMC acquisition of adipocyte-like or macrophage-like characteristics within an environment mimetic of early atherosclerosis. The results from the aforementioned apoB and A-FABP analyses suggest that DS gels support greater foam cell formation than HA_{IMW} hydrogels.

To assess the extent to which SMC acquisition of foam cell characteristics was correlated with a transition towards a synthetic phenotype, SMC collagen and elastin production were evaluated. No significant differences in SMC elastin deposition were observed over the course of the present study. This result is in agreement with the literature, which indicates that, although changes in elastin levels are at times observed in atherosclerotic lesions, these alterations are generally not consistent in their directionality [172]. Instead, changes in elastic fiber structure characterize atherosclerotic vessels [172]. Regarding collagen, DS gels displayed greater deposition of collagen type I than CSC and HA_{IMW} gels on day 14 and day 35, respectively. The

literature indicates that SMC synthesis of total collagen in general, and of collagen type I in particular, is up-regulated in early atherosclerotic lesions [145, 173, 174]. In addition, levels of the anabolic enzyme G6PD were elevated in DS gels relative to CSC and HA_{IMW} hydrogels, at least at day 14. Thus the present data suggest that DS induces a more synthetic SMC phenotype than CSC or HA_{IMW}, in agreement with the increased foam cell transition observed for DS relative to HA_{IMW}.

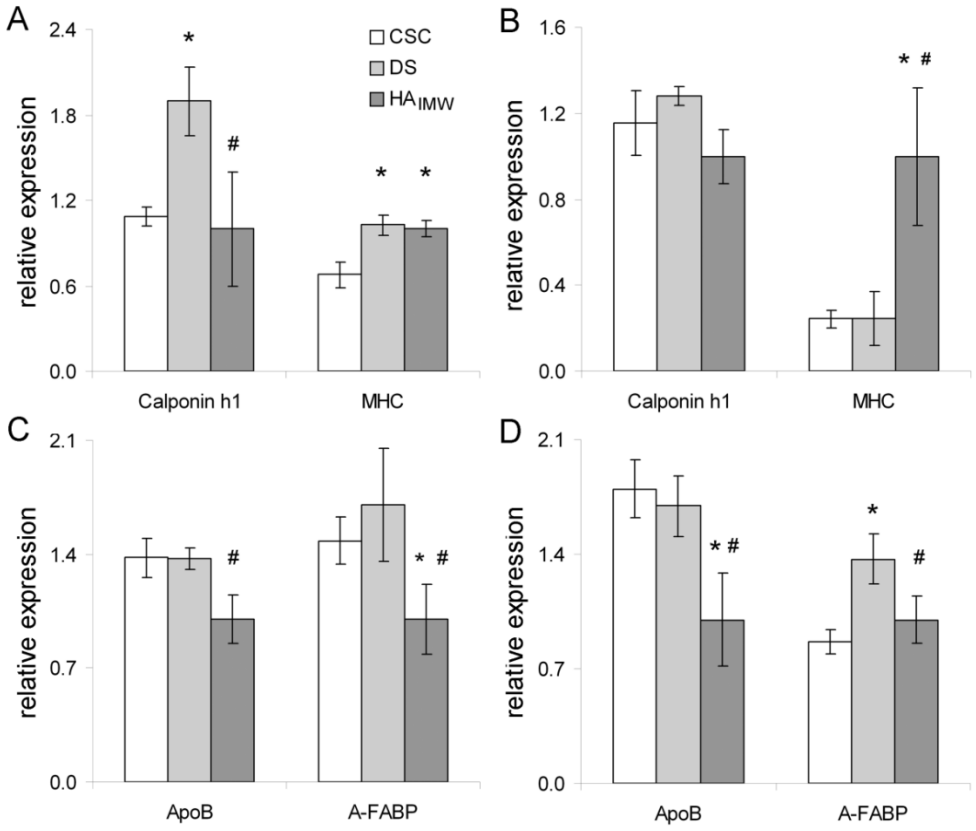

Fig. 16. Evaluation of SMC foam cell versus contractile phenotypes. (A and B) Relative expression of markers of a SMC contractile apparatus on days 14 and 35, respectively. (C and D) Relative apoB uptake and A-FABP expression on days 14 and 35, respectively. *Significantly different from CSC hydrogels, $P < 0.05$. #Significantly different from DS hydrogels, $P < 0.05$. CSC and DS data at each time point have been normalized to the corresponding HA_{IMW} data, the average values for which are noted above the HA_{IMW} formulation, where applicable. The noted values for the immunostaining assessments are unitless but represent both average intensity (on a scale of 1–3) as well as the cell fraction positively stained.

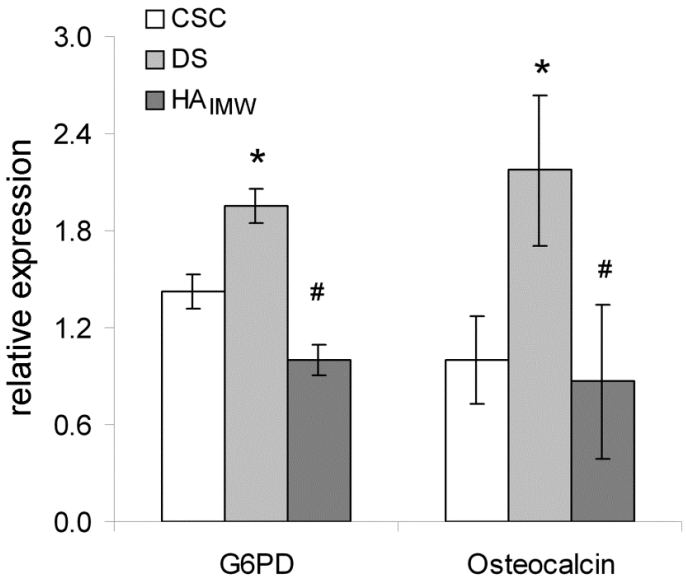

Fig. 17. Relative G6PD and osteocalcin expression on day 14. *Significantly different from CSC hydrogels, $P < 0.05$. #Significantly different from DS hydrogels, $P < 0.05$.

The increase in SMC acquisition of synthetic and foam cell phenotypes in DS gels was not, at least initially, marked by a corresponding decrease in SMC contractile marker expression. Specifically, day 14 calponin h1 levels were greater in DS gels relative to HA_{IMW} gels. Only day 35 MHC measures suggested that the increased foam cell phenotype associated with SMCs in DS gels was being mirrored in decreased expression of a contractile phenotype. An increase in SMC contractile marker expression in early atherogenesis followed by a down-regulation of these markers in later atherosclerotic stages has previously been documented. For instance, a recent study of SMCs in the aortic arch of LDL receptor knockout mice revealed increased MHC expression in high cholesterol mice by day 28, coincident with the SMC proliferation

and ECM remodeling associated with early atherosclerosis [175]. However, by day 98 SMC MHC expression in the advancing atherosclerotic lesions had decreased [175].

The apparent link between DS and SMC foam cell formation suggested by the present results is in agreement with the current literature. Specifically, biglycan (a CS/DS-containing small leucine- rich proteoglycan) has been the focus of several recent studies of proteoglycan involvement in early atherosclerotic lipid deposition [22, 23, 25, 176-178]. However, the above comparisons with in vivo data must be interpreted with caution due to the simplified in vitro system used here.

Several limitations of the present manuscript merit comment. Although we mimicked the cell morphology and limited intercellular junctions associated with SMCs within atherosclerotic lesions, we did not reproduce several other aspects of early atherogenesis. Specifically, the proliferation and migration associated with SMC responses to arterial wall injury were not mirrored. Indeed, SMC proliferation and migration were essentially prevented by the same PEGDA hydrogel properties which allowed us to induce rounded/stellate SMC phenotypes. Furthermore, the origins of SMC rounding in atherosclerotic environments, which are linked to changes in ECM composition and SMC integrin profiles, were not recapitulated [156]. The present work also did not fully replicate the complex cascade of events/interactions between several cell types, growth factors, cytokines, and ECM molecules which ultimately lead to the formation of atheromatous plaques [27, 179]. Similarly, the role of the proteoglycan core protein in modulating SMC responses to CSC or DS signals was not accounted for.

Finally, as previously discussed, the interaction of LDL with GAG chains is ionic in nature [177]. Thus, GAG chain length and charge densities are determining factors in the levels of bound lipid per chain [177, 178]. Although we have attempted to mimic the GAG chain lengths associated with atherosclerotic vessels in the present work, the CSC and DS chains conjugated to the hydrogel networks may not have charge densities appropriate to the atherogenic environment [180]. That said, we have reported the sulfur levels within the DS and CSC chains employed here, which should allow appropriate comparison with future work.

CHAPTER V

APPROACH FOR FABRICATING TISSUE ENGINEERED VASCULAR GRAFTS WITH STABLE ENDOTHELIALIZATION*

5.1. Overview

A major roadblock in the development of TEVGs is achieving construct endothelialization that is stable under physiological stresses. The aim of the current study was to validate an approach for generating a mechanically stable layer of ECs in the lumen of TEVGs. To accomplish this goal, a unique method was developed to fabricate a thin EC layer using PEGDA as an intercellular ‘‘cementing’’ agent. This EC layer was subsequently bonded to the lumen of a tubular scaffold to generate a bi-layered construct. The viability of bovine aortic endothelial cells (BAECs) through the ‘‘cementing’’ process was assessed. ‘‘Cemented’’ EC layer expression of desired phenotypic markers (AcLDL uptake, VE-cadherin, eNOS, PECAM-1) as well as of injury-associated markers (E-selectin, SM22α) was also examined.

---

*Reprinted with permission from Influence of “Approach for Fabricating Tissue Engineered Vascular Grafts with Stable Endothelialization” by Andrea Carolina Jimenez-Vergara, Viviana Guiza-Arguello, Silvia Becerra-Bayona, Dany J. Munoz-Pinto, Rebecca E. Mcmahon, Anabel Morales, Lynnette Cubero-Ponce, and Mariah S. Hahn, 2010, Annals of Biomedical Engineering, Vol. 38, No. 9, September 2010, Copyright 2010, 2010 Biomedical Engineering Society.

These studies indicated that the ‘‘cementing’’ process allowed ECs to maintain high viability and expression of mature EC markers while not significantly stimulating primary injury pathways.

The stability of the ‘‘cemented’’ EC layers under abrupt application of high shear pulsatile flow (~11 dyn cm^{-2}, Pavg ~ 95 mmHg, ΔP ~ 20 mmHg) was evaluated and compared to that of conventionally ‘‘seeded’’ EC layers. hereas the ‘‘cemented’’ ECs remained fully intact following 48 h of pulsatile flow, the ‘‘seeded’’ EC layers delaminated after less than 1 h of flow.

Furthermore, the ability to extend this approach to degradable PEGDA ‘‘cements’’ permissive of cell elongation was demonstrated. Combined, these results validate an approach for fabricating bi-layered TEVGs with stable endothelialization.

5.2. Introduction

In 2006, ~448,000 coronary artery bypass procedures were performed in the US alone [181]. Autologous saphenous veins and mammary arteries are currently the preferred graft materials for these small-caliber vessels (<6 mm ID), but many patients lack usable autologous tissue [182]. Prostheses formed from synthetic materials, such as polytetrafluoroethylene or polyethylene terephthalate, which are suitable as peripheral vessel grafts, fail as small-caliber vessel replacements due to their thrombogenicity, relatively poor elasticity, and low compliance [183]. Tissue engineering represents a potential alternate source of functional coronary artery grafts [184-186].

Coronary arteries consist of three layers: the intima—coated on the luminal surface by an endothelial cell (EC) monolayer; the media—composed of SMCs in a collagen and elastin-rich ECM; and the adventitia—a loosely organized layer maintained by fibroblasts. The medial layer is considered to be primarily responsible for vascular tone and for vessel elasticity under physiological loading conditions [187]. Furthermore, an intact endothelial layer is considered to be critical to the long-term inhibition of thrombosis and hyperplasia [188]. Arterial TEVGs will therefore likely require both functional medial and intimal layers [183].

Achieving TEVG endothelialization that is stable under physiological loading conditions is challenging, and engineered EC layers frequently delaminate upon exposure to high shear pulsatile flow [28, 29]. A range of methods have been employed to enhance stable vascular graft endothelialization, including specialized EC seeding methods [29] and luminal coatings (e.g., fibronectin, collagen) [30]. However, only moderate long-term success has been attained with these approaches. Another recent study achieved stable EC presence under prolonged (14 day) TEVG mechanical conditioning by encapsulating ECs within ~1 mm thick hydrogel layers [117]. Although this experimental design prevented EC loss due to physiological conditioning, the 3D arrangement of ECs likely induced non-physiological behaviors.

The aim of the current study was to validate an approach for generating a thin, mechanically stable layer of ECs in the lumen of TEVGs. To accomplish this goal, a unique method was developed to fabricate bonded EC layers using PEGDA as a ‘‘cementing’’ agent between adjacent ECs. PEGDA was selected for use since its

photoactivity not only enabled the bonding of ECs into a continuous layer but also facilitated the generation of bi-layered TEVGs. In addition, the non-thrombogenic nature [189] and broadly tunable material properties (including modulus [92] and degradation rate [189, 190]) of PEGDA gels are well-established, giving the resulting constructs potential utility in both the in vitro and in vivo scenarios.

In the present study, we examined the viability of bovine aortic endothelial cells (BAECs) through the ‘‘cementing’’ process. ‘‘Cemented’’ EC layer expression of quiescent phenotypic markers and of inflammatory/damage-associated markers was also investigated. Finally, the stability of the ‘‘cemented’’ EC layers under abrupt application of high shear pulsatile flow (~11 dyn cm^{-2}, Pavg ~ 95 mmHg, ΔP ~ 20 mmHg) was evaluated and compared to that of conventionally ‘‘seeded’’ EC layers.

5.3. Materials and Methods

5.3.1. Polymer Synthesis

PEGDA was prepared as previously described [191] by combining 0.1 mmol ml^{-1} dry PEG (6 kDa, Sigma), 0.4 mmol ml^{-1} acryloyl chloride, and 0.2 mmol ml^{-1} triethylamine in anhydrous DCM and stirring under argon overnight at 4 °C. The resulting solution was washed with 2 M K_2CO_3 and separated into aqueous and DCM phases to remove HCl. The DCM phase was subsequently dried with anhydrous $MgSO_4$, and PEGDA was precipitated in diethyl ether, filtered, and dried under vacuum.

Cell adhesion peptide RGDS (American Peptide) was conjugated to acryloyl-PEG-N-hydroxysuccinimide (ACRL-PEG-NHS, 3.4 kDa, JenkemUSA) at a 1:1 molar ratio for 2 h in 50 mM sodium bicarbonate buffer, pH 8.5.9 The product (ACRL-PEG-RGDS) was purified by dialysis, lyophilized, and stored at 220 °C until use.

5.3.2. Cell Culture

Cryopreserved bovine aortic ECs (BAECs, Cell Applications) at passage 4 were thawed and expanded at 37 °C and 5% CO2. During expansion, cells were cultured in Dulbecco's Modified Eagle's Media (DMEM, Hyclone) containing 10% iron-supplemented bovine calf serum (BCS, Hyclone), 100 mU ml^{-1} penicillin, and 100 mg l^{-1} streptomycin (Hyclone).

5.3.3. Fabrication of Bi-layered Tubular Hydrogel Constructs

5.3.3.1. Fabrication of Conventionally ''Seeded'' Control

Hydrogels RGDS-containing PEGDA hydrogels with a ''seeded'' EC luminal layer were prepared by conventional methods. In brief, a precursor solution containing 0.1 g ml^{-1} PEGDA and 2 mM ACRL-PEG-RGDS was prepared in HBS-TEOA (10 mM HEPES, 150 mM NaCl, 115 mM triethanolamine, pH 7.4). Ten microliters of photoinitiator solution (300 mg ml^{-1} of UV photoinitiator 2,2-dimethoxy-2-phenyl-acetophenone (Sigma) in N-vinylpyrrolidone (Sigma)) were then added per mL of

mixture. The resulting solution was sterilized using a 0.22 ml PES filter, pipetted into tubular molds (3 mm ID, 5 mm OD), and polymerized by 6 min exposure to longwave UV light (365 nm, ~10 mW cm^{-2}, UVP model B-100SP).

Following overnight immersion in media, the polypropylene joints that would be used to mount the constructs onto the pulsatile flow bioreactor system were inserted into each gel end. BAECs at passage [84, 187] were seeded onto the luminal surface of the gels in four sequential steps. At each step, BAECs were resuspended in DMEM containing 10% BCS and injected into the lumen of each construct at 120,000 cells per cm^2. Following 1 h incubation at 37 °C, the gel was rotated 90° and the seeding process was repeated. The ‘‘seeded’’ constructs were maintained in DMEM containing 10% BCS and 1% PSA (PSA: 10 U ml penicillin, 10 g l streptomycin, and 25 mg l^{-1} amphotericin; Mediatech).

5.3.3.2. Fabrication of ‘‘Cemented’’ Hydrogels

Constructs with ‘‘cemented’’ EC layers were prepared by a unique sequential polymerization process. In brief, a precursor solution containing 0.1 g ml^{-1} PEGDA and 2 mM ACRL-PEG-RGDS in HBS-TEOA was first prepared. Ten microliters of photoinitiator solution were then added per mL of mixture, and the resulting solution was sterilized by filtration.

BAECs at passage [84, 187] were harvested and resuspended at high density (125 x 10^6 cells ml^{-1}) in the PEGDA precursor solution. Fifty microliters of the resulting mixture were spread evenly onto a 3 mm OD glass rod over a 5.5 cm length. This EC-

PEGDA coating was then dried as a thin layer by 8 min application of a sterile airstream. During airstream application, the rod was held horizontally and constantly rotated to facilitate the fabrication of an even coating (Fig. 18).

Each EC-coated rod was inserted as the inner mandrel of a double-walled cylindrical mold, the outer wall of which was composed of a hollow UV transparent plastic cylinder (5 mm ID). PEGDA precursor solution was gently pipetted into the cylindrical molds and polymerized by exposure to UV light (365 nm, ~10 mW cm^{-2}, UVP model B-100SP) for 6 min. The resulting bi-layered hydrogels were then removed from their molds and transferred to DMEM containing 10% BCS and 1% PSA.

‘‘Seeded’’ and ‘‘cemented’’ controls fabricated using enzyme-degradable hydrogels were prepared as described above, except that PEGDA containing the collagenase-labile peptide sequence APQGIAGQK was used for the ‘‘cementing’’ solution rather than pure PEGDA.

5.3.3.3. Fabrication of ‘‘Encapsulated’’ Hydrogel

Controls PEGDA hydrogels containing ECs encapsulated per conventional methods were also fabricated. A precursor solution containing 0.1 g ml^{-1} PEGDA and 2 mM ACRL-PEG-RGDS in HBS-TEOA was prepared. Ten microliters of photoinitiator solution were then added per mL of mixture, and the resulting solution was sterilized by filtration. Harvested ECs were then added directly to the precursor solution to achieve a cell number per total gel volume equivalent to that employed for the ‘‘cemented’’ layer

gels. The resulting EC suspension was pipetted into a set of molds and polymerized by 6 min exposure to UV light.

5.3.4. Analyses Conducted within 24 h of Endothelial Layer Fabrication

5.3.4.1. Analyses of Cell Death and Metabolic Activity

The cytotoxicity of the ‘‘cementing’’ process was assessed by measuring lactate dehydrogenase (LDH) levels released by ‘‘cemented’’ ECs at 1 and 24 h postpolymerization. Immediately following polymerization, hydrogels with ‘‘cemented’’ EC layers (n = 9) were cut into a series of 4-mm long ring segments. Each segment was then rapidly transferred to fresh cell culture media. After 1 h, LDH levels in the media surrounding each segment were measured using the LDH Cytotoxicity kit (Roche). Since the construct segments were transferred to media immediately following polymerization and without pre-rinsing, any LDH released due to cell membrane damage incurred during the ‘‘cementing’’ process would be represented in this initial 1 h measure.

Following the 1 h LDH time point, the media in each construct was exchanged with fresh media. At 24 h, 6 of the 9 ‘‘cemented’’ construct segments were allocated for LDH cytotoxicity assays, and the remaining three gels were allocated for mitochondrial activity analyses. For the LDH samples, the media surrounding each gel segment was collected and analyzed as above. Mitochondrial activity was assessed using the Vybrant Metabolic Assay (Invitrogen) per manufacturer protocol. For both the LDH and Vybrant

Assays, cells exposed to encapsulation within PEGDA gels but not to pre-drying were used as controls.

5.3.4.2. Mechanical Assessment

Mechanical analyses were conducted using a modification of the circumferential property testing technique validated in Johnson et al.[192] and Hiles et al.[193] In brief, the dimensions of ring segments 2–4 cm in width were measured using digital calipers. These measures served as dimension inputs for subsequent stress and strain calculations and as swelling indicators. Each ring was mounted onto an Instron 3342 by threading opposing stainless steel hooks through the segment lumen. The hooks were then uniaxially separated at a rate of 6 mm min^{-1} until construct failure. As hook separation increased, the mounted ring was drawn into an increasingly oblong oval conformation. Johnson et al. confirmed that the force applied by the hooks to this oblong oval could be approximated as being equally distributed between two parallel rectangles, each with sides equal to the width and wall thickness, h_v, of the ring. The gauge length, lg, was taken to be the inner diameter, D_v, of the unstretched ring plus h_v, and the elastic modulus, E, of each sample was defined as the slope of the resulting stress–strain curve at a reference stress of 20 kPa [84]. Samples remained immersed in PBS until immediately prior to mechanical analyses, and testing was completed rapidly to avoid sample dehydration.

5.3.5. Analyses Conducted 3 Days Following Endothelial Layer Fabrication

Three days following endothelial layer fabrication, a set of ‘‘seeded’’ EC layer constructs and a set of ‘‘cemented’’ EC constructs were harvested. Acetylated low density lipoprotein (AcLDL) uptake analyses as well as antibody-based assessments of various functional and injury-associated EC markers were then performed.

5.3.5.1. AcLDL Uptake

To assess the ability of ‘‘cemented’’ ECs to uptake AcLDL, harvested constructs (n = 6 per treatment group) were rinsed three times with PBS. All segments were exposed to 5 μg ml^{-1} AcLDL-AlexaFluor 488 (Invitrogen) in DMEM containing 1 mM Ca^{2+} and 1 mM Mg^{2+} for 4 h at 37 °C. Negative control segments were immersed in formalin to induce cell death prior to AcLDL exposure. Following AcLDL application, segments were rinsed extensively in PBS and imaged using a fluorescence microscope (Zeiss Axiovert).

5.3.5.2. Competitive ELISA

Analyses Competitive ELISA assays were conducted to quantitatively compare the expression of various indicators of EC functionality or EC damage across treatment groups.

Protein Isolation. Proteins from ‘‘seeded’’ and ‘‘cemented’’ EC samples (n 3–6 per treatment group) were isolated using a modification of a procedure validated by Hummon et al. [194]. In brief, each construct segment was homogenized in Trizol (Invitrogen), after which chloroform was added per manufacturer protocol. The associated phenol-chloroform phase was mixed with ethanol to precipitate DNA. The resulting phenol–ethanol phase was then transferred to 3.4 kDa SnakeSkin dialysis membranes (Pierce, Rockford). The solutions were dialyzed for ~60 h at 4 °C against an aqueous solution of 0.1% sodium dodecyl sulfate (SDS), with buffer exchange every ~18–20 h. The resultant protein mass [194] was collected and resuspended in PBS containing 0.5% SDS and 1% Triton X-100.

ELISA Technique. Primary antibodies and their corresponding peptide antigens were purchased from SCBT. High binding EIA 96 well plates (Costar) were coated overnight at 4 °C with 2 ng per well of peptide for endothelial nitric oxide synthase (eNOS, C-20), vascular endothelial (VE)-cadherin (C-19), platelet/endothelial cell adhesion molecule-1 (PECAM-1, M-20), smooth muscle 22α (SM22α, P-15), or E-selectin (C-20). The coated wells were then blocked with bovine serum albumin (BSA). Peptide standards and resuspended protein samples were diluted in PBS containing 3% BSA and 0.05%Tween 20 and incubated with primary antibody for 1 h at room temperature prior to transfer to the coated wells. The plate was then incubated for 1 h at room temperature with continuous gentle mixing, after which HRP-conjugated secondary antibody (Jackson Immunochemicals) was applied to each well. Levels of

antigen in each sample were evaluated indirectly via measuring the amount of secondary antibody bound to each well. This was quantified by the addition of 2,2'-azino-bis(3-ethylbenzthiazoline-6-sulphonic acid) and subsequent absorbance measurements at 410 nm. ELISA results were normalized to sample total protein as determined using the CBQCA assay (Invitrogen) per manufacturer protocol. Samples were measured in duplicate.

5.3.5.3. Histological Analyses

Construct segments reserved for immunostaining were fixed in formalin for 30 min. Each sample was then transferred to Tissue-Tek freezing media, snap frozen, and cut into 20 μm sections using a cryotome. Rehydrated sections were blocked with peroxidase (Biocare Medical) for 10 min followed by 10 min exposure to Terminator block (Biocare Medical). Primary antibodies diluted in HBS (10 mM HEPES, 150 NaCl, pH 7.4) containing 3% BSA and 0.05% Tween 20 were then applied to the sections for 1 h. Bound primary antibody was detected using AP-conjugated secondary antibody (Jackson Immunochemicals) diluted in HBS containing 3% BSA and 0.05% Tween 20 followed by application of the chromogen Ferangi Blue (Biocare Medical). Stained sections were imaged using a Zeiss Axiovert 200 microscope.

5.3.6. Stability Under Physiological Stress Application

Three days following endothelial layer fabrication, remaining ‘‘seeded’’ constructs (n 3) and BAEC ‘‘cemented’’ constructs (n 3) were mounted onto the inner ports of a custom pulsatile flow bioreactor graft chamber [117].

5.3.6.1. Bioreactor Flow Loop

EC layer stability under pulsatile flow conditions was evaluated using a modification of the bioreactor system described in Bulick et al. [117]. In brief, a peristaltic pump drew media from a reservoir, generating the desired flow rate of media through the system. The media flow was then passed through a compliance chamber, and a CellMax pump (Spectrum Labs) was used to overlay the desired pulsatile waveform. The flow was then passed through the constructs. Pressure profiles were monitored immediately upstream and downstream of each construct using sterile transducers (Merit Medical) equipped with inlet and outlet valves. After exiting the constructs, the media was passed back to the media reservoir, completing the flow circuit. Both the graft chamber and the media reservoir were fitted with vent ports to maintain both chambers at atmospheric pressure and to allow for gas exchange. The elasticity of the hydrogels themselves acted to maintain the constructs on the graft chamber fittings during pulsation, preventing media leakage from the higher pressure construct lumens into the surrounding, lower pressure graft chamber bath.

5.3.6.2. Mechanical Stimulation Regimen

The graft chambers into which the constructs had been mounted were connected to the flow loops described above. The graft chamber bath was filled with DMEM supplemented with 10% BCS and 1% PSA. The inner flow loop was filled with DMEM containing 10% BCS and 1% PSA as well as 1.75% dextran 70 (Pharmacosmos) to increase media viscosity. Flow was initiated at 22 ml min^{-1} per construct. After 2 min, the flow was increased to 75 ml min^{-1} per construct. Following an additional 5 min, flow through each construct was ramped to 180 mL/min, and the mean pressure (P_{avg}) in each construct lumen was adjusted to ~95 mmHg using the pressure transducer valves.

Visual inspection indicated that the EC layers on the ‘‘seeded’’ constructs were no longer present following 1 h of full flow. Flow was therefore slowly ramped down in both the ‘‘seeded’’ and ‘‘cemented’’ construct chambers at this time point. Grafts were gently dismounted and images were taken of each construct lumen, after which the grafts were remounted and flow reinitiated as described above. Following 1 h of stable application of full flow conditions, pulsation (120 beats per minute [bmp], DP ~ 20 mmHg) was initiated. Continuous pulsatile flow was applied for 48 h, after which each flow loop was dismantled and constructs were harvested for imaging and histological analyses. Samples collected for immunostaining were processed as described above.

5.3.6.3. Shear Stress Estimates and Viscosity

Measures Rigorous estimates of the wall shear stress, τ_w, experienced by the ECs under the above pulsatile flow conditions can be obtained from the mathematical descriptions of pulsatile flow in rigid pipes developed by Womersley [195, 196] and the associated dimensionless Womersley number, $\alpha = R\sqrt{\frac{}{\mu}}$; where R = vessel inner radius, = frequency of oscillation, q media density, and μ = media viscosity. The magnitude of a is a indicator of the impact of pulsatile flow frequency relative to viscous effects. To calculate the Womersley number for the present system, the extent to which dextran 70 increased the media viscosity had to be evaluated.

The viscosity of DMEM containing 10% BCS, 1% PSA, and 1.75% dextran 70 was determined using a Physica MCR 300 Modular Compact Rheometer fitted with a CP50-1 cone plate [197]. During testing, the temperature was held constant at 37 °C using a Peltier temperature controller. The change in media shear stress with increasing shear rate from 0.5 to 200 s^{-1} was monitored by the device and was used to calculate media viscosity. Through this technique, the viscosities of both dIH_2O and of DMEM containing 10% BCS but no dextran were determined to be ~0.65 cP at 37 °C, in good agreement with previous literature [198]. In contrast, the viscosity of media containing 1.75% dextran 70 was measured at 1.18 ± 0.17 cP.

Thus, for R 0.16 cm and $4\pi s^{-1}$, α was approximately 5.2. This α value was mimetic of coronary and carotid arteries for which α = 3–10. In this a range, the Hagen–Poiseuille equation can be assumed to provide a useful estimate of wall shear stress

[199]. Specifically, the Hagen–Poiseuille equation predicts that $\tau_{w} \sim \frac{4\mu Q}{\pi R^3}$; where Q = volumetric flow rate. In this case, $\tau_w \sim 11$ dyn cm^{-2}, which is within the physiological range for coronary arteries [200].

5.3.6.4. Circumferential Strain

Estimates To estimate the circumferential strain experienced by the constructs, the measured elastic moduli and vessel dimensions were input into the Bernoulli equation $\sim \frac{(P)R}{h_v E}$; where R = inner vessel radius, h_v = wall thickness, and E = construct modulus [201]. This equation has previously been shown to be in good agreement with actual strains experienced by PEGDA constructs in the current bioreactor setup [84]. For the present hydrogel formulations (E ~ 67.0 kPa, $h_v \sim 0.1$ cm, R ~ 0.16 cm) and pulsatile conditions ($\Delta P \sim 20$ mmHg), $\Delta \sim 0.064$.

5.3.7. Statistical Analyses

All data are reported as mean ± standard error of the mean. Comparisons among hydrogel treatment groups were conducted using ANOVA and Tukey's post-hoc test (SPSS software), $p \leq 0.05$.

5.4. Results and Discussion

The aim of the current study was to develop an approach for fabricating TEVGs with thin, mechanically stable endothelial linings. To achieve this objective, a unique method was developed to fabricate luminal EC layers using PEGDA as an intercellular ‘‘cementing agent.’’ In this approach, ECs are suspended in an aqueous PEGDA solution which is dried as a thin coating onto the surface of a glass rod. The dried, PEGDA-EC layer is then simultaneously partially rehydrated, polymerized, and bonded to an outer hydrogel layer by the rapid addition of a second PEGDA precursor solution to the construct mold followed by immediate UV exposure. The resulting bi-layered hydrogel contains a dense luminal EC layer which is mechanically stable and which permits direct exposure of EC surfaces to the luminal environment. This ‘‘cementing’’ process is illustrated in detail in Fig. 18 and its associated legend.

Due to the drying step associated with the fabrication of ‘‘cemented’’ EC layers, it was important to first assess the viability of ‘‘cemented’’ ECs. The cytotoxicity of the ‘‘cementing’’ process was therefore assessed by measuring the levels of LDH released by ‘‘cemented’’ ECs at 1 and 24 h post-polymerization. Due to the method of construct handling and preparation, the 1 h LDH readings could be taken to represent the extent of immediate cell death induced by the ‘‘cementing’’ process. Interestingly, the levels of LDH released at 1 h from ‘‘cemented’’ ECs were statistically indistinguishable from the amount of LDH released from an equivalent number of cells encapsulated in PEGDA gels without a drying step. The 24 h LDH assay detected LDH released from the gels

between 1 and 24 h postpolymerization and served as a measure of apoptosis induced by the ‘‘cementing’’ process. As with the 1 h LDH assay, no statistically significant differences were observed between the LDH released at 24 h by ‘‘cemented’’ ECs relative to encapsulated ECs (Fig. 19).

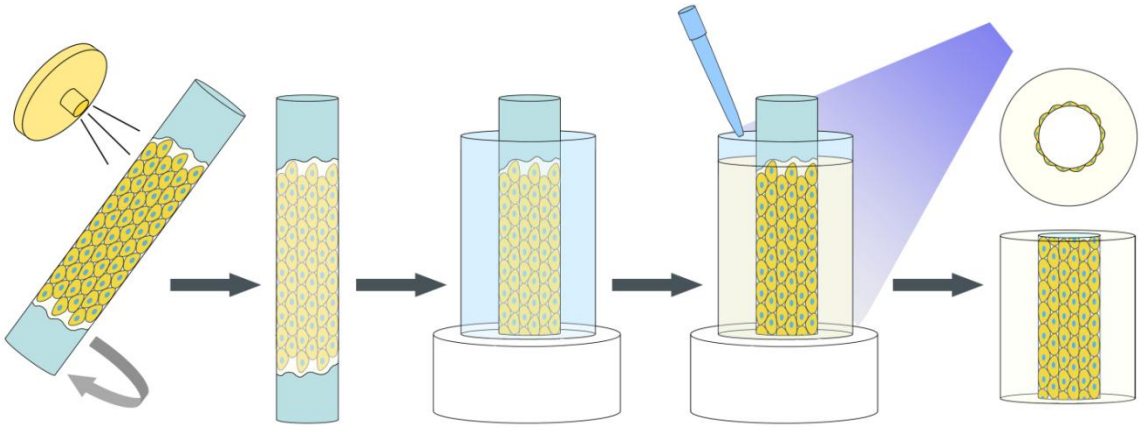

Fig. 18. A schematic of the ‘‘cemented’’ EC layer fabrication process. ECs suspended at high density in a PEGDA precursor solution are spread evenly over the length of a glass rod, and a sterile air-stream is applied under constant rod rotation to generate a dried EC-containing film. Each EC-coated rod is inserted as the inner mandrel of a tubular mold. A PEGDA precursor solution is rapidly, but gently, pipetted into the mold and polymerized immediately by exposure to longwave UV light. The brief time delay (seconds) between the addition of the outer PEGDA solution and the onset of UV-induced photopolymerization is sufficient to permit at least partial rehydration of the EC-containing film (as indicated by the loss of film opacity) but not to permit significant motion of associated ECs. The harvested gel contains a dense layer of ECs that are directly exposed to the luminal environment. Currently, the mechanism by which this process forces ECs to the rod surface to the exclusion of PEGDA is unclear. However, since EC surfaces are charged, it can be speculated that each cell in the coating solution can induce a local, opposing charge on the glass insulator surface if the cell and rod are brought into sufficiently close proximity. The drying process may induce this proximity. The resulting electrostatic interactions would encourage heightened contact between the cells and the glass rod, which may thereby force residual PEGDA solution between the cell and rod out into neighboring intercellular spaces. In contrast, cell surfaces facing the airstream remain covered in PEGDA, which may result in the formation of a protective film preventing cell dehydration as drying proceeds. This process can readily be expanded to include a second cell type (such as SMCs) in the outer PEGDA precursor solution.

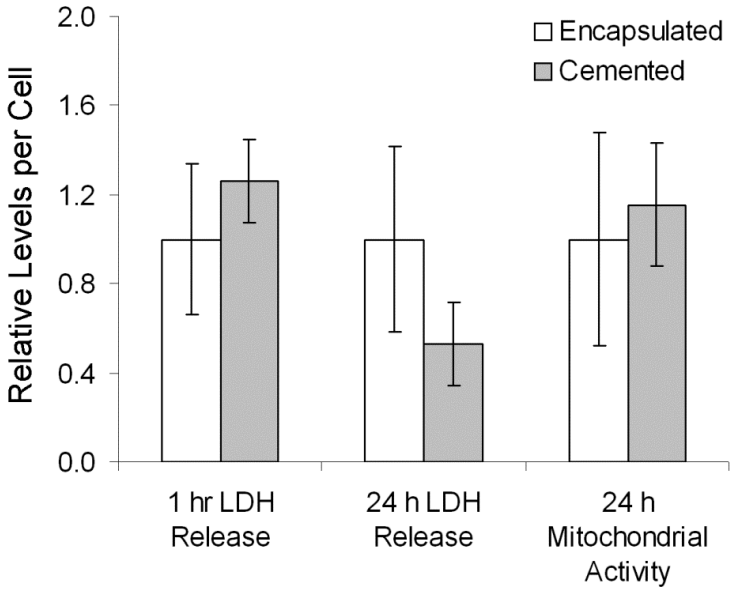

Fig. 19. LDH release and mitochondrial activity assays intended to assess the cytocompatibility of the ‘‘cementing’’ process relative to conventional encapsulation. The 1 and 24 h LDH release assays served as quantitative indicators of ‘‘cementing’’-induced necrosis and apoptosis, respectively. The 24 h mitochondrial activity assay assessed the retention of mitochondrial integrity following the ‘‘cementing’’ process.

Similarly, cell mitochondrial activity assessments indicated no loss in viability due to the ‘‘cementing’’ process relative to cells exposed to standard PEGDA encapsulation conditions (Fig. 19). Combined, the LDH and mitochondrial activity results indicate that the PEGDA ‘‘cementing’’ process is of similar cytocompatibility as the conventional PEGDA ‘‘encapsulation’’ process, a method regarded as essentially non-cytotoxic. The mechanism underlying the relatively low cell death observed in the ‘‘cemented’’ layers is currently unclear, although the presence of PEGDA in the ‘‘drying’’ solution may underlie this result. It can be speculated that the PEGDA solution forms a film on the surface of the cells facing the airstream, thereby protecting the cells from desiccation during the drying process.

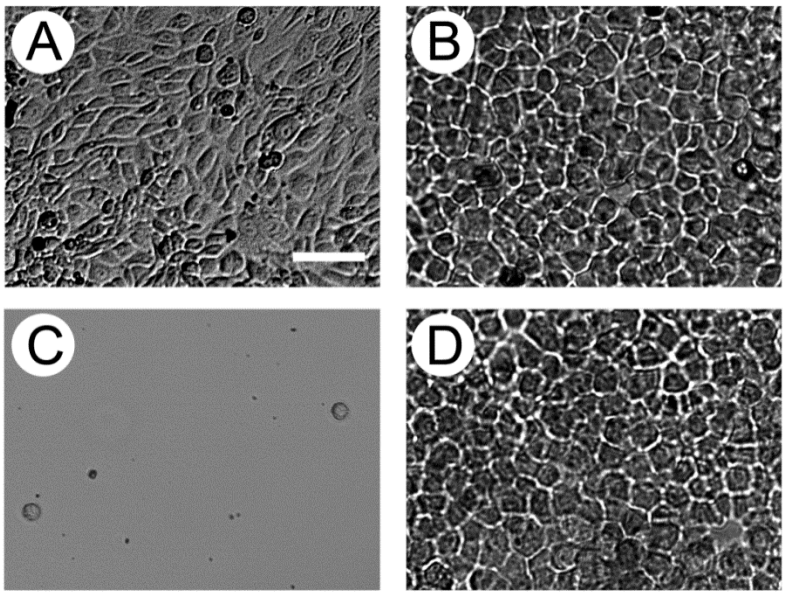

Fig. 20. Stability of ‘‘cemented’’ BAEC layers relative to ‘‘seeded’’ BAEC layers. Representative images of (a) ‘‘seeded’’ BAEC layers and (b) ‘‘cemented’’ BAEC layers 72 h post-fabrication and before the onset of flow. Representative images of (c) ‘‘seeded’’ BAEC layers following 1 h of 11 dyn/cm2 flow and (d) ‘‘cemented’’ BAEC layers following 48 h of continuous 11 dyn cm^{-2} flow and 6.4% cyclic circumferential strain. The scale bar in (a) applies to all images and equals 40 μm.

The EC-layer drying process also required that the resulting bi-layered grafts be examined for tears that could potentially be induced by the significant postpolymerization swelling associated with PEGDA hydrogels. The ‘‘cemented’’ constructs were therefore carefully examined under DIC microscopy at high magnification (2009) for surface tears or fractures. As expected for 10 wt.% hydrogels prepared from 6 kDa PEGDA, the inner diameter of both the ‘‘seeded’’ and ‘‘cemented’’ constructs increased from the initial diameter set by the mandrel (3 mm) to ~3.2 mm on swelling [202]. However, no tears were observed in any of the ‘‘cemented’’ grafts either before or after flow, as illustrated in the rightmost column of Fig. 20**.** In fact, the gel swelling proved beneficial in that it aided the gentle and rapid detachment of

the polymerized gel and associated EC layer from the glass mandrel. Thus, the ‘‘cementing’’ process permitted the generation of intact bi-layered hydrogels.

The stability of the ‘‘cemented’’ EC layers through 48 h of continuous application of pulsatile flow was also evaluated and compared to that of ‘‘seeded’’ EC layers. Constructs with ‘‘seeded’’ EC layers delaminated in less than 1 h at full flow (~180 ml min^{-1}, P_{avg} ~ 95 mmHg), prior to initiation of pulsation (Figs. 20a and 20c). This rapid delamination occurred despite the relatively high levels of RGDS (2 mM) conjugated to the PEGDA gels to enhance ‘‘seeded’’ EC adhesion. In contrast, ‘‘cemented’’ EC layers remained intact through the initiation of pulsation and a subsequent 48 h of full pulsatile flow (~180 ml min^{-1}, ΔP ~ 20 mmHg; Figs. 26b and 26d). Given the average ‘‘cemented’’ construct modulus of 67.0 ± 3.4 kPa and the applied DP, the cyclic circumferential strain experienced by the dynamic constructs was estimated to be ~6.4% by the Bernoulli equation. Similarly, the mean construct wall shear stress at full flow conditions was calculated to be ~11 dyn cm^{-2} using the Poiseuille assumption, as justified in ‘‘Materials and Methods’’. Thus, the ‘‘cemented’’ EC layers remained intact through extended application of physiological cyclic strains and shear stresses.

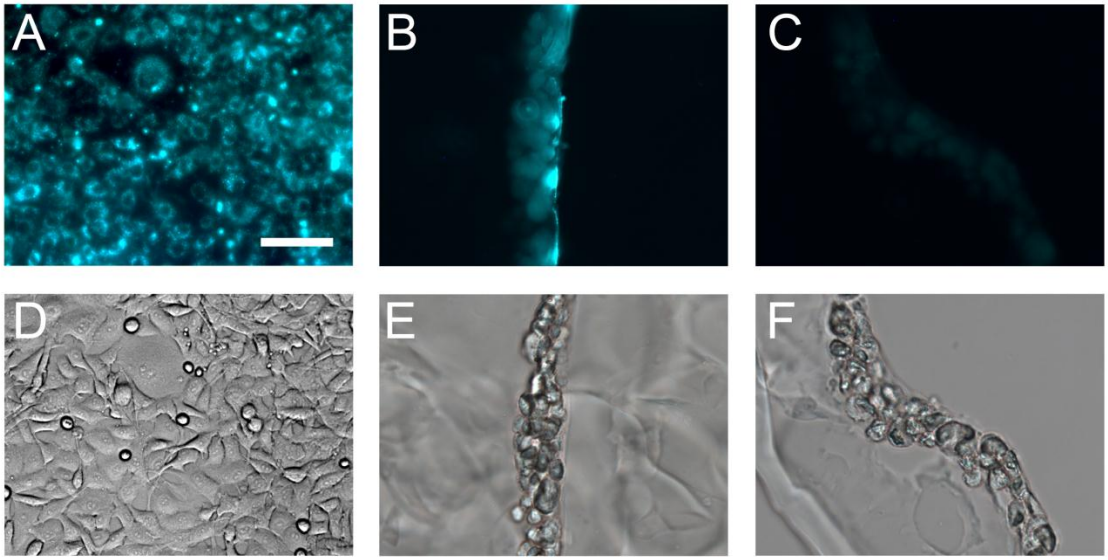

Fig. 21. Assessment of ‘‘cemented’’ BAEC layer uptake of AcLDL. Representative fluorescence images of (a) a conventional EC layer exposed to AlexaFluor 488-labeled AcLDL, (b) a ‘‘cemented’’ EC layer exposed to AlexaFluor 488-labeled AcLDL, and (c) a ‘‘cemented EC layer immersed in formalin to induce cell death prior to AcLDL application. (d, e, f) The brightfield images corresponding to (a), (b), and (c), respectively. The scale bar in (a) applies to all images and equals 40 μm.

‘‘Cemented’’ and ‘‘seeded’’ BAEC constructs were further compared for expression of several functional and damage-associated EC markers. Uptake studies demonstrated that the ability of ‘‘cemented’’ ECs to internalize AcLDL was retained for at least 72 h post-‘‘cementing’’ (Fig. 21). Since only live ECs are capable of AcLDL endocytosis (Figs. 21b vs. 21c), these results also supported the high viability of ‘‘cemented’’ ECs indicated by the LDH release and metabolic activity assays. Furthermore, competitive ELISA and immunostaining assays were used to evaluate the phenotype of the ‘‘cemented’’ ECs. Consistent with AcLDL uptake results, levels of eNOS (NOS3), an enzyme involved in the maintenance of vascular homeostasis [203], were similar in ‘‘cemented’’ ECs relative to ‘‘seeded’’ ECs at 72 h of culture (prior to

initiation of flow, Figs. 22, 23a, and 23b). These levels of eNOS were maintained by the ‘‘cemented’’ ECs following 48 h of pulsatile flow (Figs. 22 and 23c). Expression of PECAM-1 and VE-cadherin, molecules associated with EC cell–cell adhesion or junction formation, followed more complicated trends (Figs. 22, 23d–23f, and 23g–23i**,** respectively). Specifically, levels of both markers appeared to be lower in the statically-cultured, ‘‘cemented’’ EC layers relative to ‘‘seeded’’ layers, although these differences fell below statistical significance. However, ‘‘cemented’’ EC VE-cadherin levels significantly increased following exposure to pulsatile flow ($p = 0.02$), recovering to ‘‘seeded’’ EC levels.

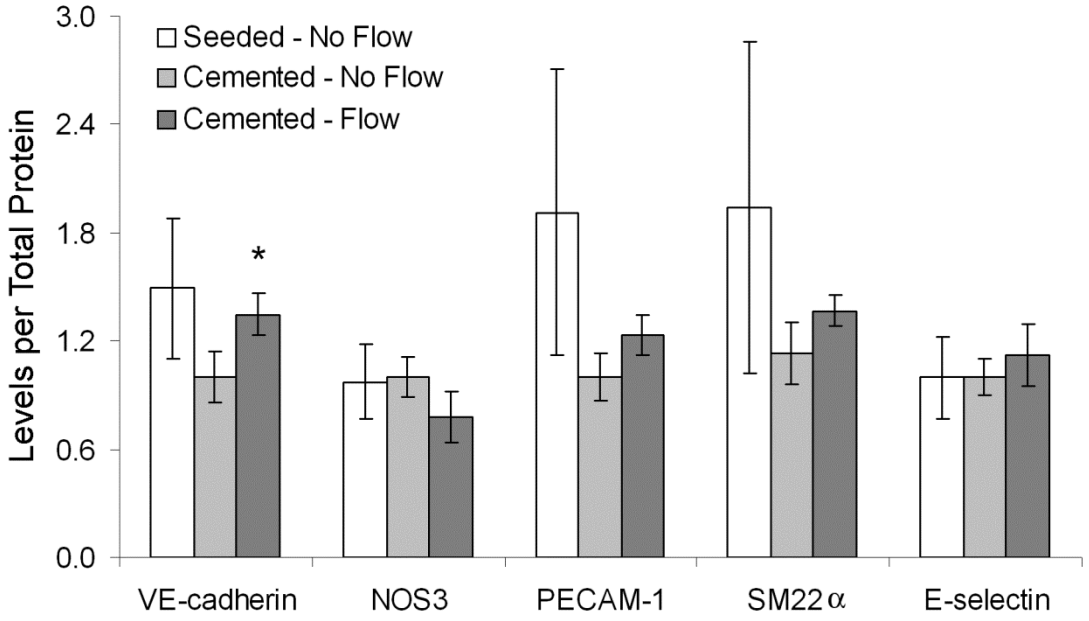

Fig. 22. Quantitative comparison of the expression of functional and damage-associated markers by ‘‘cemented’’ ECs relative to conventionally ‘‘seeded’’ ECs. ‘‘Cemented’’ EC phenotype was analyzed for both static and dynamic constructs. *indicates a significant difference with the corresponding measures for ‘‘cemented’’ EC—no flow constructs, $p < 0.05$.

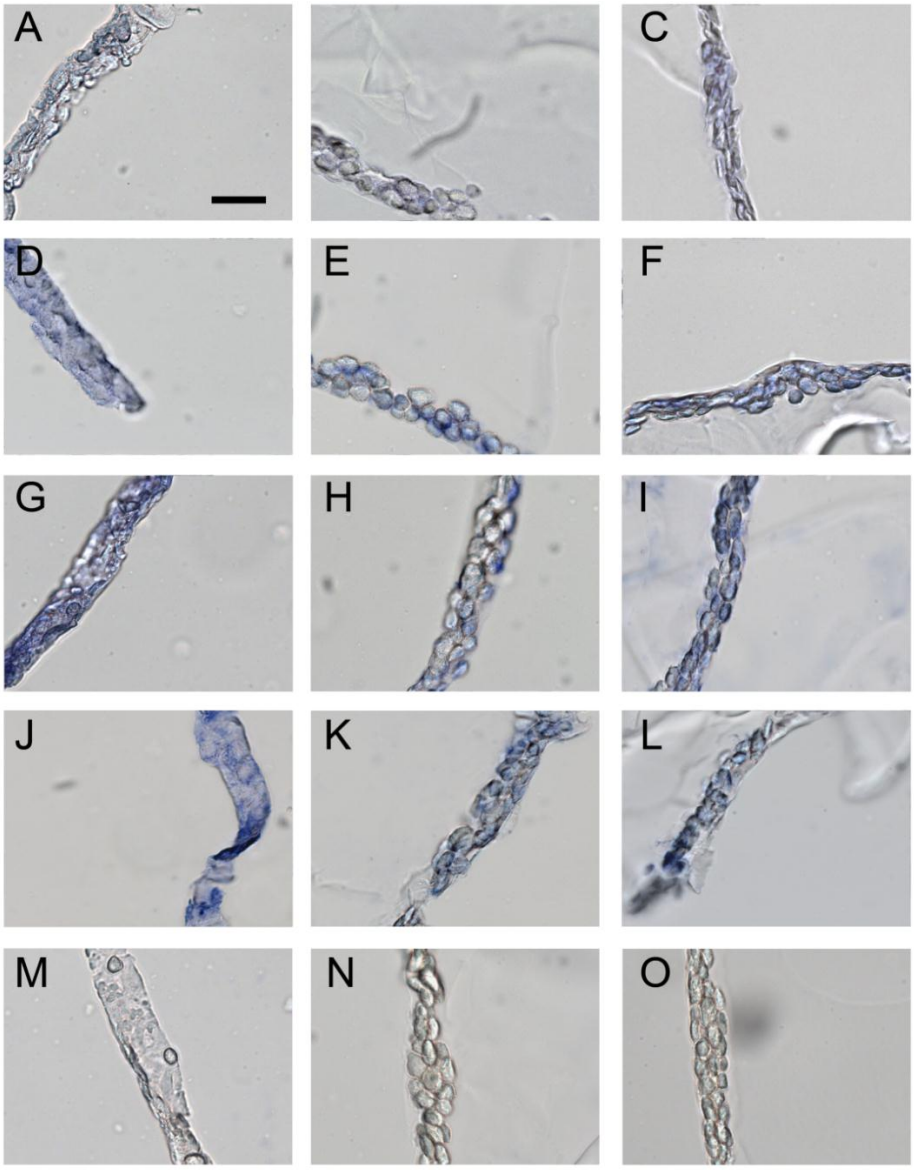

Fig. 23. Expression of mature- and injury-associated EC markers. Representative images of eNOS-stained sections from (a) ‘‘seeded’’ EC layers (72 h post-fabrication), (b) ‘‘cemented’’ EC layers (72 h post-fabrication), and (c) ‘‘cemented’’ EC layers (after 48 h of pulsatile flow). Representative images of PECAM-1-stained sections from (d) ‘‘seeded’’ EC layers (72 h post-fabrication), (e) ‘‘cemented’’ EC layers (72 h post-fabrication), and (f) ‘‘cemented’’ EC layers (after 48 h of pulsatile flow). Representative images of VE-cadherin-stained sections from (g) ‘‘seeded’’ EC layers (72 h post-fabrication), (h) ‘‘cemented’’ EC layers (72 h postfabrication), and (i) ‘‘cemented’’ EC layers (after 48 h of pulsatile flow). Representative images of SM22α-stained sections from (j) ‘‘seeded’’ EC layers (72 h post-fabrication), (k) ‘‘cemented’’ EC layers (72 h post-fabrication), and (l) ‘‘cemented’’ EC layers (after 48 h of pulsatile flow). Representative images of E-selectin-stained sections from (m) ‘‘seeded’’ EC layers (72 h post-fabrication), (n) ‘‘cemented’’ EC layers (72 h post-fabrication), and (o) ‘‘cemented’’ EC layers (after 48 h of pulsatile flow). The scale bar in (a) applies to all images and equals 40 μm.

Combined, the ELISA results suggest that the ‘‘cementing’’ process allows ECs to retain their ability to express mature EC markers and to respond to mechanical conditioning while not significantly stimulating primary injury pathways. However, despite the presence of adhesion peptide RGDS in the coating solution, ECs took on rounded or elliptical morphologies in the pure PEGDA ‘‘cemented’’ layers (Figs. 20, 21, and 23). These cell morphologies, which result from the dense crosslinking (~15–20 nm average mesh size)1 and relatively slow degradation rate of pure PEGDA hydrogels (1–2 years for ~95% degradation) [84, 90-92] are non-optimal for ECs, which natively take on elongated morphologies. We therefore extended the present method to utilize an enzyme-degradable PEGDA ‘‘cement’’ in place of pure PEGDA. As illustrated in Fig. 24, the degradable ‘‘cement’’ permitted cells to take on more natural cell shapes via local, cell-based cleavage of the ‘‘cement’’ network [204].

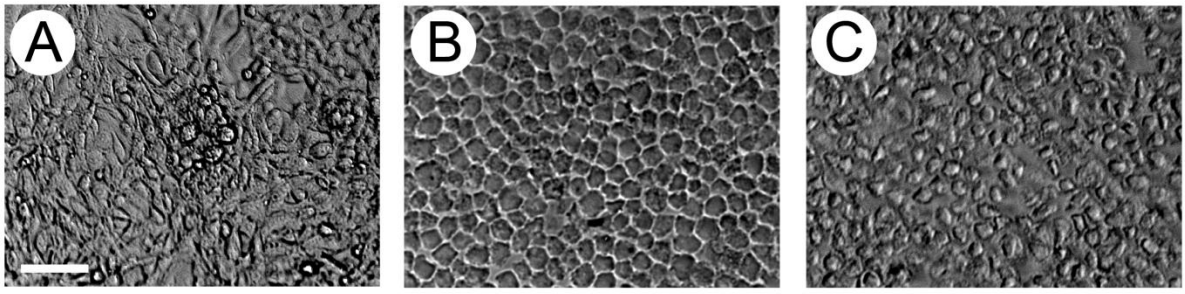

Fig 24. Evaluation of the ability of ECs ‘‘cemented’’ using an enzyme-degradable PEGDA to alter their shape with time in culture. Representative images of (a) ECs ‘‘seeded’’ on the surface of an enzyme-degradable PEGDA gel following 4 days of culture; (b) ECs ‘‘cemented’’ using degradable PEGDA following 1 day of culture; and (c) ECs ‘‘cemented’’ using degradable PEGDA following 4 days of culture. The scale bar in (a) applies to all images and equals 40 μm.

Collectively, the present results establish an approach for fabricating TEVGs with mechanically stable, physiologically relevant endothelialization. In addition, although a PEGDA hydrogel was used as the scaffold to which the ‘‘cemented’’ EC layer was bonded during construct fabrication, the EC- PEGDA coating can be conjugated to any protein-based scaffold containing sufficient levels of free cysteines (e.g., fibrin gels) [205, 206]. Therefore, the present method can be extended to generating stable, luminal EC layers on a range of TEVG scaffolds.

CHAPTER VI

OSTEOGENIC POTENTIAL OF POLY(ETHYLENE GLYCOL)-POLY(DIMETHYLSILOXANE) HYBRID HYDROGELS*

6.1. Overview

Growth factors have been shown to be potent mediators of osteogenesis. However, their use in tissue engineered scaffolds not only can be costly but also can induce undesired responses in surrounding tissues. Thus, the ability to specifically induce osteogenic differentiation in the absence of growth factors through manipulation of scaffold material properties would be desirable for bone regeneration. Previous research indicates that addition of inorganic or hydrophobic components to organic, hydrophilic scaffolds can enhance MSC osteogenesis. However, the combined impact of scaffold inorganic content and hydrophobicity on MSC behavior has not been systematically explored, particularly in 3D culture systems.

---

*Reprinted with permission from Influence of "Osteogenic potential of poly(ethylene glycol)-poly(dimethylsiloxane) hybrid hydrogels" by 7. D.J. Munoz-Pinto, A.C. Jimenez-Vergara, Y. Hou, H.N. Hayenga, M. Grunlan, M.S. Hahn, 2012, Tissue Engineering Part A , In press, Copyright 2012, Mary Ann Liebert, Inc.

The aim of the present study was therefore to examine the effects of simultaneous increases in scaffold hydrophobicity and inorganic content on MSC osteogenic fate decisions in a 3D culture environment toward the development of intrinsically osteoinductive scaffolds. Mouse 10T½ MSCs were encapsulated in a series of novel scaffolds composed of varying levels of hydrophobic, inorganic poly(dimethylsiloxane) (PDMS) and hydrophilic, organic PEG. Following 21 days of culture, increased levels of osteoblast markers, runx2 and osteocalcin, were observed in scaffolds with increased PDMS content. Bone ECM molecules, collagen I and calcium phosphate, were also elevated in formulations with higher PDMS:PEG ratios. Importantly, this osteogenic response appeared to be specific in that markers for chondrocytic, smooth muscle cell, and adipocytic lineages were not similarly affected by variations in scaffold PDMS content. As anticipated, the increase in scaffold hydrophobicity accompanying increasing PDMS levels was associated with elevated scaffold serum protein adsorption. Thus, scaffold inorganic content combined with alterations in adsorbed serum proteins may underlie observed cell behavior.

6.2. Introduction

MSC differentiation is known to be influenced by a range of environmental stimuli, among the most potent of which are growth factors. However, the use of growth factors in tissue engineering scaffolds not only can be costly but also can induce undesired responses in surrounding tissues. Thus, MSC-based bone regeneration

strategies would be benefited by the identification of scaffold material properties which intrinsically promote osteoblast lineage progression in the absence of growth factors.

A number of studies have shown that the addition of inorganic components to organic scaffolds can enhance both their osteoconductivity and osteoinductivity [31-36, 53, 207-209]. These inorganic additives have included not only hydroxy atite, but also a range of silicon-containing compounds, such as silica, silane, and siloxane [33-36, 207-209]. In addition, scaffold hydrophobicity has been demonstrated to influence osteogenic differentiation [37, 39, 210]. However, the combined effects of scaffold inorganic content and hydrophobicity have not been systematically explored. Furthermore, most of the aforementioned studies were performed in two-dimensional (2D) culture, and, thus, may not be indicative of the effects of the same scaffold variables in more biomimetic, three-dimensional (3D) culture systems. The aim of the present study was therefore to examine the impact of simultaneous increases in scaffold hydrophobicity and inorganic content on MSC osteogenic lineage progression in a 3D culture environment.

Toward this goal, we developed a novel series of scaffolds comprised of varying levels of hydrophobic, inorganic PDMS and hydrophilic, organic PEG. PEG was selected for the hydrophilic, organic component due to its established biocompatibility and its previous use in bone regeneration applications [37, 53, 87, 211]. Similarly, PDMS was chosen as the inorganic component over silica, silane, and other polysiloxanes due to its processability and its intermediate level of hydrophobicity. In addition, PDMS is used extensively in biomedical applications and is considered biocompatible [68, 212-215]. For the present study, PDMS and PEG molecular weights

(Mn) and concentrations were selected to yield scaffolds with moduli within the "osteogenic" range identified in the 2D human MSC studies of Engler et al [68] and the 3D human and mouse MSC studies of Huebsch et al [216].

In analyzing the lineage progression of encapsulated mouse 10T½ MSCs, quantitative immunoassays were performed for mid-to-late term markers associated with osteoblast, chondrocytic, smooth muscle cell (SMC), and adipocytic fates. Furthermore, biochemical and histological analyses were conducted to assess the deposition of ECM components associated with mature bone (e.g. collagen I and calcium phosphate) [217] as well as ECM molecules which would be considered undesirable for bone regeneration (e.g. elastin and collagen type III).

6.3. Material and Methods

6.3.1. Preparation of Diacrylate-Terminated PEG

Diacrylate-terminated PEG (PEGDA, Fig. 25) was prepared in accordance to known methods (23). Briefly, PEG (M_n = 3.4 kDa, Sigma) was dissolved in dry dichloromethane (20 mL $mmol^{-1}$ PEG) in a 250 ml round bottom flask purged with Ar. Triethylamine (2:1 molar ratio, Sigma) was added slowly to the solution, followed by the drop-wise addition of acryloyl chloride (4:1 molar ratio, Sigma). The reaction mixture was allowed to stir at room temperature overnight. Removal of HCl was accomplished by washing the mixture twice with 2M K_2CO_3 and separating into aqueous and organic

phases. The organic phase was then dried with anhydrous $MgSO_4$ and the volatiles removed under reduced pressure. The resulting crude oil was precipitated in diethyl ether in an ice bath, filtered, and dried under vacuum at room temperature overnight. Extent of diacrylation was confirmed to be approximately 85% by ^{1}H NMR.

6.3.2. Synthesis of Methacrylate-Terminated Star PDMS Methacrylate-terminated

Star PDMS ($PDMS_{star}$-MA, M_n = 2 kDa) was prepared via a two-step synthetic strategy per a modification of the methodology in Grunlan et al [218]. A star conformation of PDMS was selected over a linear form in order to reduce phase separation between the hydrophobic PDMS and hydrophilic PEG prior to hydrogel polymerization [219]. In brief, silane (SiH)-terminated star PDMS ($PDMS_{star}$-SiH) was first prepared by the acid-catalyzed equilibration of octamethylcyclotetrasiloxane with tetrakis(dimethylsiloxane)silane (tetra-SiH) [218]. Octamethylcyclotetrasiloxane and tetra- SiH were combined in a 100 mL round bottom flask under N_2 at a 4:1 molar ratio, with the ratio of octamethylcyclotetrasiloxane and tetra-SiH selected to yield a product of the desired M_n. Triflic acid (0.060 µl mmol^{-1} octamethylcyclotetrasiloxane) was then added, and the reaction was allowed to stir for 1 h at 90 ºC. After cooling, the mixture was neutralized by combining with $MgCO_3$ and dichloromethane (0.020 mL mmol^{-1} octamethylcyclotetrasiloxane) and stirring for 2 h. After filtration through a pad of Celite, the volatiles were removed under reduced pressure. The chemical structure and

Mn of the resulting colorless product ($PDMS_{star}$-SiH) were confirmed by ^{1}H NMR, ^{13}C NMR, IR, and gel permeation chromatography (GPC).

The SiH terminal groups of the $PDMS_{star}$-SiH were converted into photo-sensitive methacrylate moieties by the subsequent hydrosilylation reaction with allyl methacrylate [220]. Briefly, $PDMS_{star}$-SiH was dissolved in dry toluene using a 100 ml round bottom flask and purged with N_2. Karstedt's catalyst (Pt-divinyltetramethyldisiloxane complex in xylene, 2% Pt) was added at 33 μl $mmol^{-1}$, and the reaction mixture was heated to 45 ºC. Allyl methacrylate was then added over 15 min in a 4:1 molar ratio, after which the reaction was heated to 90 ºC and stirred overnight. Completion of the reaction was confirmed by the disappearance of the Si-H (~2100 cm^{-1}) absorbance in the IR spectrum. The reaction mixture was decolorized by refluxing with activated carbon for 12 h. After filtration, the volatiles were removed under reduced pressure. The resulting product ($PDMS_{star}$-MA, Fig. 18) was confirmed by ^{1}H-NMR.

6.3.3. Synthesis of Acrylate-Derivatized Cell Adhesion Ligand

Cell adhesion peptide RGDS (American Peptide) was reacted with acryloyl-PEGN- hydroxysuccinimide (ACRL-PEG-NHS, 3.4 kDa; Nektar) at a 1:1 molar ratio for 2 h in 50 mM sodium bicarbonate buffer, pH 8.5 [71, 221]. The product (ACRL-PEG-RGDS) was purified by dialysis, lyophilized, and stored at -20 ºC until use.

6.3.4. Hydrogel Preparation

PEG-$PDMS_{star}$ hybrid hydrogels were prepared by the photopolymerization of aqueous mixtures of PEGDA and $PDMS_{star}$-MA. Five distinct precursor solutions were prepared: i) three with 10 wt% total polymer, but with either a 100:0, 95:5, or 80:20 wt ratio of PEGDA to PDMSstar-MA, and ii) two additional PEGDA formulations containing 9.5 and 8.0 wt% total polymer but no PDMS (referred to as 95:0 and 80:0 constructs, respectively). ACRL-PEG-RGDS was added to each solution so as to yield 1 mM RGDS in the swollen gels. Photoinitiator consisting of a 30 wt% solution of 2,2-dimethyl-2-phenyl-acetophenone in N-vinylpyrrolidone was added to the precursor solutions at 10 μl ml^{-1}. The resulting mixtures were vortexed and passed through 0.22 μm PES filters, which served both to sterilize the solutions as well as to create fine, stable dispersions of hydrophobic $PDMS_{star}$ in the aqueous PEG solutions. The filtered precursor solutions were immediately poured into 0.75 mm thick transparent rectangular molds, and polymerized by 6 min exposure to longwave UV light (~6 mW cm^{-2}, 365 nm; Spectroline).

6.3.5. Evaluation of Initial Scaffold Material Properties

6.3.5.1. Dynamic Light Scattering

The average size of $PDMS_{star}$-MA particles in the PEG-$PDMS_{star}$ hydrogels was estimated by dynamic light scattering (DLS) measurements of aqueous solutions of 0.5

wt% and 2 wt% PDMSstar-MA. Following 0.22 μm filtration, DLS measurements were performed on each solution using a Brookhaven ZetaPALS instrument. A laser with a wavelength of 660 nm was used as the incident beam, and scattered light was detected at a 90° scattering angle at 25 °C. The light scattering data were analyzed with the BI-DLSW control software, and a non-negative constrained least squares algorithm was used to determine the size distributions.

6.3.5.2. Hydrogel Mechanical Properties

Bulk Mechanical Testing. Following 18 h immersion in PBS, four 8-mm discs were cored from each hydrogel formulation and mechanically tested under unconstrained compression using an Instron 3342. Following application of a 0.05 N preload, each hydrogel was subjected to compression at a rate of 1 mm min^{-1}. The compressive modulus of each hydrogel was extracted from the resulting stress-strain data over a 5-25% strain range.

Atomic Force Microscopy. Following 18 h of swelling in deionized water (dIH_2O) [222],_PEG-$PDMS_{star}$ hydrogels were locally, mechanically tested using a Bioscope System AFM (Veeco Instruments) equipped with a Nanoscope IIIa controller and mounted on a Zeiss Axiovert 100 TV inverted optical microscope. Each hydrogel was fixed to a 60-mm diameter polystyrene petri-dish with RP30 instant adhesive (Adhesive Systems, Inc). The hydrogels were then submerged in 1.5 ml of dIH_2O to

reduce tip-adhesion effects and to maintain sample hydration during testing. The gel samples were indented with a 600 nm diameter spherical tip (silicon dioxide glass bead) attached to a silicon-nitride cantilever with a manufacturer-calibrated spring constant of 360 pN nm^{-1} (Novascan). Deflection sensitivity for the AFM probe was determined to be 54 nm V^{-1}. All indentations were performed at a frequency of 0.5 Hz with a z-scan size of 800 nm (speed of 0.8 μm s^{-1}). After recording typically 30 consecutive indentation force-depth curves at each location on the hydrogel, the tip was retracted to its original position. At least ten distinct locations were analyzed per hydrogel sample.

The applied force f^{sphere} (pN) during indentation was taken to be the product of the measured cantilever deflection d (V), cantilever spring constant k (pN nm^{-1}), and deflection sensitivity d_s (nm V^{-1}). The indentation depth δ (nm) of the probe during an approachretraction cycle was calculated as the difference between the piezo displacement z (nm) and effective cantilever deflection $d_s d$ (nm). An effective Young's modulus (E) was determined from AFM force curves based on the Hertzian equation [223-225]. However, the strict use of this equation requires simplifying assumptions, such as a flat, homogeneous, semi-infinite elastic material and a rigid probe [226]. Thus, to accommodate potential nonlinearities, we calculated the point-wise apparent modulus ($E_i \quad \frac{3}{8}\left(\frac{f_i^{sphere}}{\sqrt{R\delta_i^3}}\right)$), or material stiffness, at each point (i) along all post-contact approach curves. All point-wise modulus values appeared to converge upon an asymptotic value at an indentation depth typically less than 30 nm. However, only point-wise moduli

corresponding to indention depths beyond 600 nm were used to calculate an average effective Young's modulus for a particular location [225, 227].

6.3.5.3. Hydrogel Mesh Size

PEG-based hydrogel mesh structure cannot be readily visualized using techniques such as conventional scanning electron microscopy. Thus, a variety of methods to estimate PEGDA hydrogel mesh size have been developed, including correlations linking measurable quantities, such as equilibrium hydrogel swelling and PEGDA Mn, to mesh size [228, 229]. Although these correlations yield reasonable average mesh size estimates for homopolymer hydrogels [228, 229], they cannot readily be applied to PEG-PDMSstar hybrid hydrogels. Thus, in this study, average hydrogel mesh size was characterized via dextran diffusion based on an adaptation of the methodology of Watkins et al [120]. Briefly, four 8-mm discs were cored from each hydrogel formulation following 24 h swelling and immersed in 0.5 mL HBS-azide (HEPES-buffered saline plus 0.05 wt% azide) containing 50 μg ml^{-1} FITC-labeled dextran (10 kDa, Sigma). Dextran was then allowed to diffuse into the hydrogels for 24 h at 37 ºC, after which each disc was gently blotted and transferred to 0.5 ml fresh HBS-azide. After 24 h at 37 ºC, the fluorescence of the HBS-azide solution surrounding each disc was measured at ex/em 488/532. Each fluorescence measure was converted to micrograms dextran using dextran standard curves and then divided by gel weight to yield a quantitative indicator of hydrogel permissivity (C). These permissivity measures

were used to estimate the mesh size ( ) of each hydrogel (x) relative to the 100:0 PEG-PDMSstar formulation as follows: $_x \left(\frac{C_x}{C_{1000\ \text{PEG-PDMS}}} \right)$

6.3.5.4. Serum Protein Adsorption

Following 24 h of swelling, four 36-mm discs were harvested from each PEG-$PDMS_{star}$ hydrogel formulation to evaluate the dependence of bulk serum protein adsorption on increasing $PDMS_{star}$ content. Each disc sample was exposed to 10% fetal bovine serum in PBS for 24 h at 37 °C. Non-adsorbed proteins were then removed by immersing the specimens in dIH_2O at 37 °C for 60 min, with dIH_2O changes every 20 min. Adsorbed proteins were subsequently stripped from the hydrogels by progressive extraction with a series of aqueous isopropanol solutions of increasing hydrophobicity [230]. Specifically, each hydrogel sample was successively immersed in 10%, 30%, 50%, and 70% aqueous isopropanol solutions (I10, I30, I50, I70, respectively) for 20 min per solution at 37 °C. The isopropanol fractions for a particular hydrogel sample were then combined, evaporated under vacuum, and resuspended in 500 μl of PBS. The total amount of protein stripped from each hydrogel sample was quantified using the CBQCA total protein quantitation kit (Invitrogen). For the purpose of comparison, the average protein measures for each gel composition were normalized to the 100:0 PEG-$PDMS_{star}$ formulation.

6.3.5.5. Relative Bulk Hydrophobicity

Contact angle measurements are widely used to analyze differences in the hydrophobic character of material surfaces. However, this method is limited to assessment of surface hydrophobicity, and associated results cannot be readily extended to bulk behavior. We therefore developed a method to assess differences in bulk hydrogel hydrophobicity by comparing the extent of swelling in solvents of varying polarities [231]. Specifically, solvents of higher polarity indices (P) interact preferentially with hydrophilic domains of the bulk material, while solvents of lower P indices show greater affinity for hydrophobic segments of the material. Thus, differences in the relative uptake of solvents of distinct polarities by a given hydrogel formulation can serve as an indicator of its bulk hydrophobicity. In brief, four discs from each hydrogel formulation were submerged in dIH_2O (P =12.1) or I70 (P = 10.0) [232] for 24 h at room temperature, after which the swollen weight (W_s) of each disc was recorded. The samples were then dried under vacuum for 48 h and their corresponding dry weights (W_d) measured. The equilibrium mass swelling ratio (q) of each formulation in each solvent (x) was calculated as $q_x \left(\frac{s}{d}\right)$. The relative bulk hydrophobicity (H) of each hydrogel formulation was estimated as follows: $H \left(\frac{q_{I70}}{q_{dIH2O}}\right)$.

6.3.6. Cell Culture

Cryopreserved 10T½ mouse mesenchymal stem cells (ATCC) were thawed and expanded in monolayer culture. Prior to encapsulation, cells were maintained at 37 ºC and 5% CO_2 in Dulbecco's Modified Eagle's Media (DMEM, Hyclone) supplemented with 10% heat-inactivated fetal bovine serum (FBS, Hyclone).

6.3.7. Fabrication and Culture of Cell-Laden Constructs

Precursor solutions for the 100:0, 95:5, and 80:20 PEG-$PDMS_{star}$ gels and the 95:0 and 80:0 controls were prepared in PBS. ACRL-PEG-RGDS was then added to each precursor solution so as to yield an RGDS concentration of 1 mM in the swollen gels. Following addition of photoinitiator, the mixtures were vortexed and sterilized by 0.22 μm filtration. 10T½ cells were then resuspended in each precursor solution so as to yield a post-swelling cell density of ~2 x 106 cells g^{-1}. The resulting suspensions were polymerized into hydrogel networks by 6 min exposure to longwave UV light (~6 mW cm^{-2}, 365 nm), a process which has previously been demonstrated to be cytocompatible [73, 128, 233]. Gels were immersed in DMEM supplemented with 10% heatinactivated FBS, 100 U ml^{-1} penicillin and 100 mg l^{-1} streptomycin and maintained at 37 ºC and 5% CO2. Following 24 h, samples (n = 4 per formulation) were collected for bulk compressive analyses per the above procedure. Media in the remaining samples was changed every two days for 21 days.

6.3.8. Endpoint Construct Analyses

After 21 days of culture, a series of samples (n = 4 per formulation) were mechanically analyzed under bulk compression. Separate samples were collected from each hydrogel formulation for biochemical and histological analyses. All steps associated with the biochemical and histological procedures described below took place at room temperature unless otherwise noted.

6.3.8.1. Biochemical Analyses

Competitive ELISAs for Differentiation Markers. Proteins extracted by sample homogenization in Trizol followed by protein isolation [194] were evaluated for the housekeeping protein GAPDH as well as for mid-to-late term markers of osteogenesis, chondrogenesis, SMC progression, and adipogenesis via competitive ELISAs. In brief, appropriate primary antibodies and their corresponding peptide antigens were purchased from SCBT. High binding EIA 96 well plates (Costar) were coated overnight at 4 °C with 200 ng per well of peptide for adipocyte-fatty acid binding protein (A-FABP, C-15), PPARγ (I-18), myocardin (M-16), SM22α (P-15), runx2 (S-19), collagen I (Col1A1, D-13), osteocalcin (M-15), sox-9 (C-20), or collagen II (Col2A1, N-19) and 100 ng per well of peptide for GAPDH (V-18). The coated wells were then blocked with BSA. Peptide standards and isolated sample proteins were diluted in PBS containing 3% BSA and 0.05% Tween 20 and incubated with primary antibody for 1 h, after which the mixtures were transferred to coated wells and incubated for an additional hour. Primary

antibody which had bound to each coated well surface was then detected using an appropriate HRP-conjugated secondary antibody (Jackson ImmunoResearch Laboratories, JIRL), followed by application of 2,2'-azino-bis(3-ethylbenzthiazoline-6-sulphonic acid) [ABTS, Sigma]. Resulting sample absorbance was read at 410 nm and translated to a concentration using the associated standard curve. Each target protein was analyzed in duplicate for each sample (n = 3-6 per gel formulation) and normalized to GAPDH. For the purposes of comparison, the resulting protein concentrations for each formulation were further normalized to the 100:0 PEG-$PDMS_{star}$ formulation.

Total Collagen, Sulfated Glycosaminoglycan, Elastin, and Collagen III Assays. Based on the cell marker results, the 100:0, 95:5, and 80:20 gels were further analyzed for various ECM components. Sample proteins isolated by base hydrolysis [83] were used to quantify total collagen, sulfated GAG, elastin, and collagen III. For each of the following assays, the standards used were subjected to the same association with PEGDA and $PDMS_{star}$-MA and the same digestion conditions as the samples.

GAGs production was measured using a modification of the Blyscan assay (Biocolor). In brief, 40 µl of protein from each sample (n 5-6 per formulation) was neutralized, mixed with 60 µl Blyscan dye reagent, and the absorbance immediately read at 525 nm relative to a chondroitin sulfate B standard (Sigma). Similarly, levels of the amino acid hydroxyproline were quantified as an indirect measure of total collagen. Extracted proteins were first further hydrolyzed for 18 h at 110 ºC in 6 M HCl. The samples (n = 5-6 per formulation) were then dried under vacuum followed by

resuspension in dIH_2O and reaction with chloramine T and p-dimethylbenzaldehyde reagents [76]. Sample absorbance was read at 550 nm relative to an L-4-hydroxyproline standard (Sigma). Total collagen content was estimated from measured grams of hydroxyproline by dividing by 0.13.

For collagen III quantification, samples (n = 4-6 per formulation) and standards were applied to a high binding 96 well EIA plate for 3 h, after which the plate was blocked with 3 wt% BSA. Following application of primary antibody for collagen III (Calbiochem), donkey anti-rabbit HRP secondary antibody (JIRL) and ABTS were applied. Absorbance was read at 410 nm, with human collagen III (Sigma) serving as a standard. To quantify elastin, the above procedure was followed except that isolated sample proteins were first exposed to 0.25 M oxalic acid at 100 ºC overnight to convert elastin to α-elastin. Oxalic acid was then removed and exchanged for PBS using Microcon YM-3 centrifugal filters (Millipore). Resulting samples (n = 5-6 per formulation) were then applied to a high binding EIA 96 well plate for 3 h. Adsorbed elastin fragments were detected by applying elastin primary antibody (BA-4, SCBT), with bovine α-elastin (Sigma) serving as a standard.

Measured total collagen, sGAG, collagen III, and elastin levels were normalized to cell number as assessed by the PicoGreen assay (Invitrogen). For the purposes of comparison, the resulting concentrations for each formulation were further normalized to the 100:0 PEG-$PDMS_{star}$ hydrogels.

Total Calcium Deposition. To assess construct calcium levels, hydrogel discs (n = 3-4 per formulation) were homogenized in 640 μl lysis buffer (1% TritonX-100, 0.5% SDS in calcium-free PBS) per 100 mg hydrogel. Total calcium was quantified using 10 μl aliquots of each sample homogenate via the Calcium CPC liquid color kit (Stanbio).

6.3.8.2. Histological Analyses

Samples harvested for histological analyses were fixed with 10% formalin for 30 min, embedded in Tissue-Tek media, and cut into 35 μm sections using a cryomicrotome.

Immunostaining. Immunohistochemical staining was conducted using the same A-FABP, SM22α, osteocalcin, and collagen II primary antibodies used for competitive ELISA analyses. After 10 min treatment with peroxidase (Biocare Medical), sections were blocked with Terminator (Biocare Medical) for 30 min followed by 1 h exposure to primary antibody diluted in HBS. Bound primary antibody (SCBT) was detected by using either AP- or HRP-conjugated secondary antibodies (JIRL) followed by application of an appropriate chromogen (LabVision). Three sections from each sample of each formulation were stained per antibody. Immunostained sections were imaged under brightfield using an Axiovert microscope (Zeiss).

Von Kossa Staining. To detect calcium deposits, three sections per sample of each formulation were stained using a standard von Kossa kit (American MasterTech

Scientific). In brief, rehydrated sections were rinsed with dIH_2O, after which a 5% silver nitrate solution was applied. Sections were then exposed to full spectrum light in a humidified chamber for 45 min. After rinsing with dIH_2O, sections were exposed to 5% sodium thiosulfate for 2.5 min, briefly rinsed, and mounted. Stained sections were imaged as previously described.

6.3.9. Statistical Analyses

Data are reported as mean ± standard deviation. Statistical differences among material property measures (e.g. modulus) were performed using ANOVA followed by a Tukey post-hoc test, $p < 0.05$. Statistical differences in biochemical or cell marker data were assessed via ANOVA followed by the Tamhane T2 post-hoc test for samples with unequal variances, $p < 0.05$ (SPSS software).

6.4. Results

6.4.1. Hydrogel Material Properties

To gain insight into the shifts in scaffold material properties underlying observed alterations in cell behavior across formulations, various hydrogel properties were characterized.

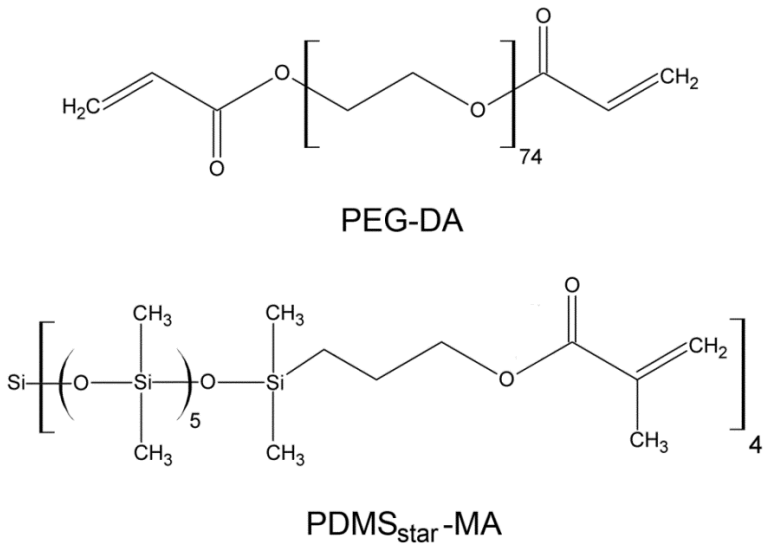

Fig. 25. Schematic of the PEGDA and PDMS$_{star}$-MA components of PEG-PDMS$_{star}$ hydrogels.

6.4.1.1. PDMS$_{star}$ Particle Size

A previous study of PEG-PDMS$_{star}$ hydrogels demonstrated that the phase separation between PDMS$_{star}$ and PEG observed in aqueous solution resulted in PEG hydrogels embedded with spherical PDMS$_{star}$ "particles" [234]. To characterize the average diameter of the PDMS$_{star}$ particles incorporated into the present PEG-PDMS$_{star}$ hydrogels, DLS studies were performed. These assays revealed an average PDMS$_{star}$ particle size of 190 nm with a polydispersity index of 1.4 for both the 0.5% and 2% PDMS$_{star}$ aqueous solutions (representative of the PDMS$_{star}$ concentrations in the 95:5 and 80:20 hydrogels, respectively). A representative DLS curve is provided in Fig. 26. These DLS results indicate that the scaffold inorganic content to which encapsulated cells could potentially be exposed (i.e. the PDMS$_{star}$ total particle surface area) increased monotonically from the 100:0 to the 80:20 gels.

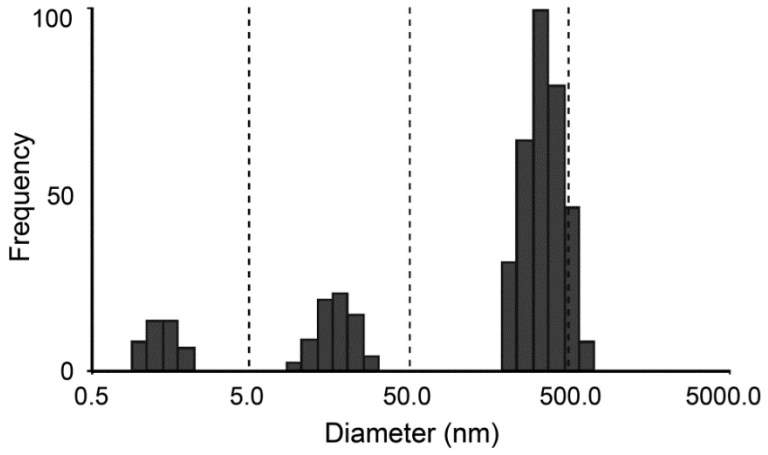

Fig. 26. Representative particle size distribution.

6.4.1.2. Mechanical Properties

As shown in Fig. 20A, hydrogel modulus under bulk compression was not significantly altered by the increase in PDMS content associated with the 100:0 and the 95:5 gels. In contrast, the bulk compressive modulus of the 80:20 PEG-$PDMS_{star}$ hydrogels was approximately 75% of that of the 95:5 formulation ($p < 0.001$). These bulk modulus values were not significantly affected by inclusion of cells (at 2×10^6 cells g^{-1}) (Table 8 vs Fig. 20A). In addition, no significant differences in gel modulus were noted between day 1 and day 21 of culture (Table 8), indicating minimal scaffold degradation over the culture period, consistent with previous PEGDA literature [190]. This resistance to degradation implied that minimal alterations in bulk material properties occurred over the culture period and facilitated the correlation between initial scaffold material properties and observed cell behaviors.

Table 8. Moduli of Cell-Laden PEG-$PDMS_{star}$ Hydrogels under Bulk Compression.

PEG-PDMS Ratio	Modulus at 24 h[†]	Modulus at 21 Days[†]
100:0	148.5 ± 5.1	149.6 ± 16.0
95:5	140.0 ± 5.2	140.4 ± 10.4
80:20	108.8 ± 10.0*,#	111.7 ± 14.2*,#,
95:0	134.7 ± 27.8	144.1 ± 11.7
80:0	100.9 ± 33.0	102.3 ± 31.6

*,statistical difference with the 100:0 formulation, $p < 0.05$; # statistical difference with the 95:5 formulation, $p < 0.05$; statistical difference with the 95:0 formulation, $p < 0.05$ † n = 4 per formulation per assay.

To assess the degree to which the decrease in PEG between the 100:0 and 80:20 gels was contributing to the observed differences in mechanical properties, control hydrogels containing 9.5 wt% PEGDA and 8.0 wt% PEGDA but no $PDMS_{star}$ were prepared. These control gels are referred to as 95:0 and 80:0 PEG-$PDMS_{star}$ hydrogels, respectively. Comparison of the bulk modulus values of the 95:5 and 95:0 gels as well as those of the 80:20 and 80:0 hydrogels (Fig. 27A) suggests that the PEG-containing phase was the primary determinant of the observed bulk compressive modulus values.

To evaluate spatial variations in modulus associated with PEG-$PDMS_{star}$ phase separation, microscale AFM-based compressive measurements were performed. In contrast to the bulk compression results, the average AFM modulus values for the 80:20 and 80:0 hydrogels indicated that $PDMS_{star}$ incorporation substantially altered hydrogel modulus at the microscale (Fig. 27B). This was reflected not only in the change in average modulus between these two formulations but also in the increased standard deviations associated with the average local moduli of the $PDMS_{star}$ containing gels. The difference in the magnitude of the bulk compression and AFM-based modulus values

can be attributed to differences in mechanical testing method and conditions. In particular, the AFM assessments were conducted over a much lower strain range than the bulk compressive tests (0.08-0.1% versus 5-25% strain).

6.4.1.3. Average Mesh Size and Relative Bulk Hydrophobicity

The bulk average mesh size data reflected the AFM-modulus assessments. Namely, average mesh size increased significantly as the ratio of PEG to $PDMS_{star}$ decreased ($p < 0.001$, Table 9). In addition, the average mesh sizes of the 95:0 and the 80:0 control gels were significantly greater than that of the 95:5 ($p = 0.001$) and 80:20 ($p = 0.001$) hydrogels, respectively. These results reflect the inclusion of densely crosslinked nanoparticles of 2 kDa $PDMS_{star}$ within a more loosely crosslinked 3.4 kDa PEG hydrogel network. In terms of relative bulk hydrophobicity, hydrogel H-values were significantly higher in the 80:20 and 95:5 hydrogels than in the 100:0 gels ($p < 0.001$ and $p = 0.003$, respectively; Table 9). However, the H-values for the 80:0 and 95:0 control gels could not be distinguished from those of the 100:0 hydrogels. Thus, the present data suggest that the increase in relative bulk hydrophobicity observed between the 100:0 and 80:20 hydrogels can be attributed to the increased incorporation of $PDMS_{star}$ rather than to decreasing PEGDA levels.

Table 9. Relative Mesh Size, Bulk Hydrophobicity, and Serum Protein Adsorption.

PEG-PDMS Ratio	Relative Mesh Size†	H q_{I70}/q_{dIH2O}†	Relative Adsorbed Protein†
100:0	1.00 ± 0.02	1.04 ± 0.01	1.00 ± 0.15
95:5	1.05 ± 0.03	1.10 ± 0.02*	1.97 ± 0.29*
80:20	1.37 ± 0.04*,#,	1.17 ± 0.03*,#,	5.06 ± 0.48*,#,
95:0	1.10 ± 0.02*	1.04 ± 0.02	1.12 ± 0.02
80:0	1.52 ± 0.02*,#,	1.03 ± 0.03#	2.76 ± 0.33*,

*statistical difference with the 100:0 formulation, $p < 0.05$; #statistical difference with the 95:5 formulation, $p < 0.05$; , statistical difference with the 95:0 formulation, $p < 0.05$. † n = 4 per formulation per assay.

6.4.1.4. Serum Protein Adsorption

A primary mechanism by which scaffold hydrophobicity impacts cell behavior is through modulation of the levels, identities, and orientations of absorbed proteins [31, 34, 235, 236]. We therefore measured the amount of serum proteins adsorbed by the various hydrogel formulations. The levels of serum protein adsorbed onto the 95:5 and 80:20 hydrogels were approximately 2-fold and 5-fold greater than the 100:0 gels ($p = 0.021$ and $p < 0.001$, respectively; Table 9). Importantly, this increase in adsorbed serum proteins could not be attributed solely to the associated decrease in PEG levels from the 100:0 to the 80:20 gels. Namely, the serum protein adsorption by the 80:20 gels was 80% greater than that of the 80:0 hydrogels ($p < 0.001$). Thus, the presence of hydrophobic $PDMS_{star}$ particles within the PEG-$PDMS_{star}$ hydrogels altered bulk serum protein adsorption.

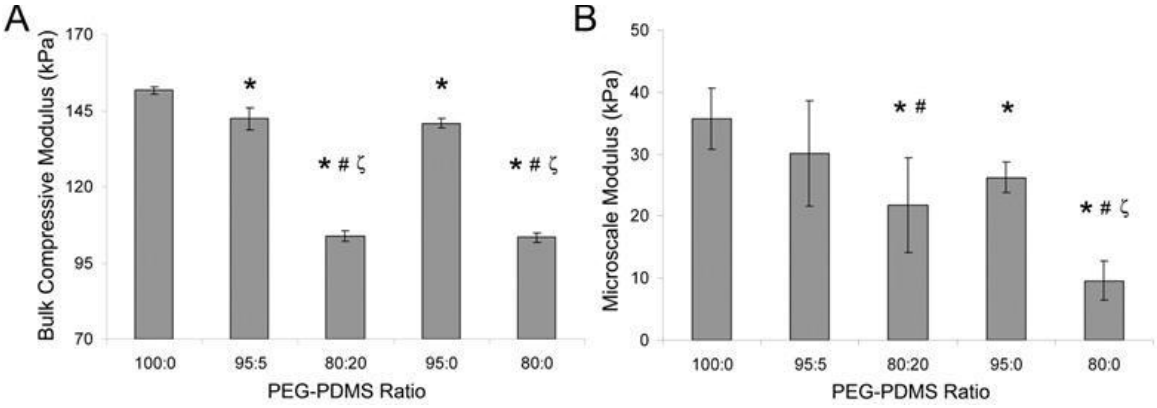

Figure 27. Average mechanical property measures of PEG-PDMS$_{star}$ hydrogels obtained from (A) bulk compression and (B) AFM-based local compression tests. *significantly different from 100:0 gels; #significantly different from 95:5 gels; significantly different from 95:0 gels. Samples for bulk compressive tests: n = 3-5 per formulation. Sample locations for AFM-based tests: n = 10 per formulation.

6.4.2. Cell Phenotypic Markers and ECM Production

To investigate the potential influence of alterations in PEG-PDMSstar hydrogel composition on 10T½ fate decisions, markers associated with chondrocyte-, osteoblast-, SMC-, and adipocyte-like fates were examined via competitive ELISA. Specifically, isolated sample proteins were evaluated for mid-to-late term markers of osteogenesis (runx2, osteocalcin), chondrogenesis (sox-9, collagen II), SMC progression (myocardin, SM22α), and adipogenesis (PPARγ, A-FABP).

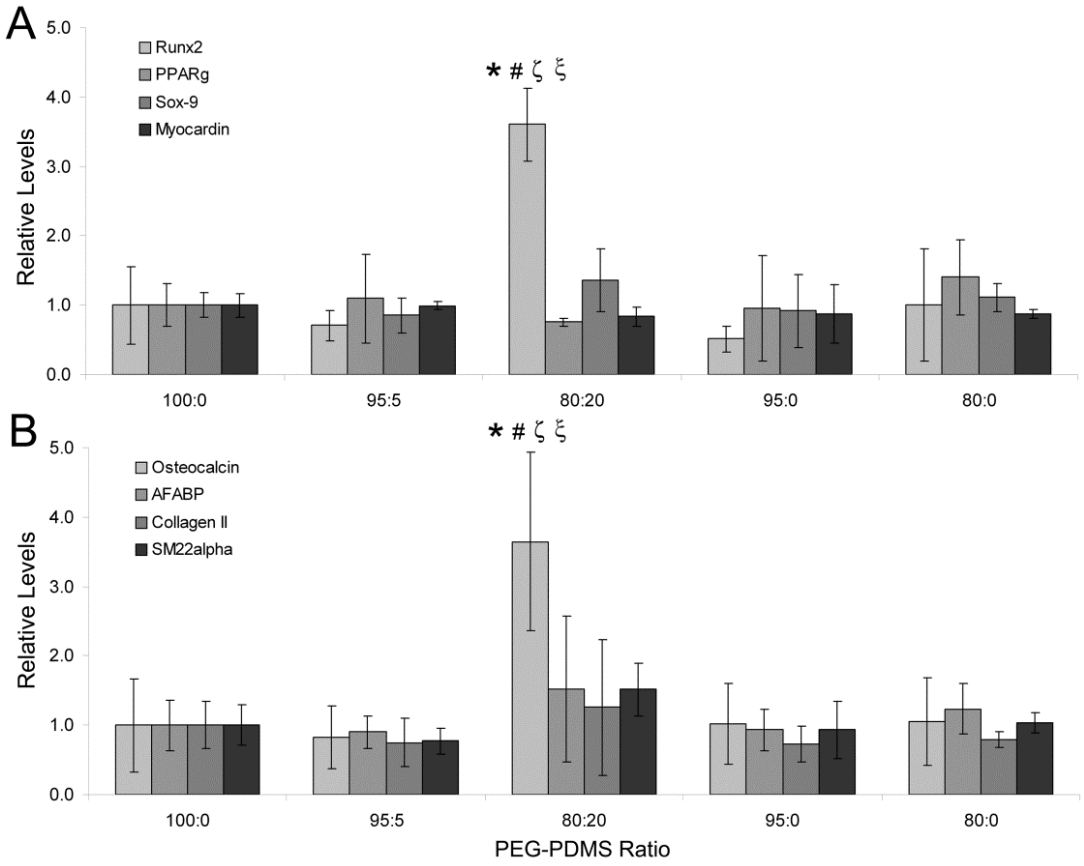

Figure 28. Analyses of cell differentiation markers. (A) Levels of runx2, PPARγ, sox-9, and mycoardin per PEG-$PDMS_{star}$ formulation, and (B) levels of osteocalcin, A-FABP, collagen II, and SM22α per PEG-$PDMS_{star}$ gel type. Results were normalized to the 100:0 PEG-$PDMS_{star}$ formulation for the purpose of comparison. *significantly different from 100:0 gels; $^{\#}$significantly different from 95:5 gels; significantly different from 95:0 gels; $^{\xi}$significantly different from 80:0 gels. Samples per assay: n = 3-6 per formulation.

ELISA analyses revealed that expression of transcription factors sox-9, myocardin, and PPARγ did not vary significantly across formulations (Fig. 28A). In agreement with the sox-9 data, collagen II production was also not significantly altered with increasing $PDMS_{star}$ content (Fig. 28B). Similarly, although A-FABP and SM22α levels appeared to increase slightly in the 80:20 hydrogels relative to the 100:0 hydrogels, these differences fell below statistical significance. However, levels of the

osteogenic transcription factor runx2 increased approximately 4-fold as PDMS levels increased from the 100:0 gels to the 80:20 gels ($p < 0.001$). In addition, osteocalcin deposition was approximately 400 percent greater in the 80:20 hydrogels than in the 100:0 hydrogels ($p < 0.001$). Immunostaining results for collagen II, osteocalcin, SM22α, and A-FABP were consistent with these ELISA results. A subset of these immunostaining images are shown in Fig. 29.

Based on the above differentiation marker results, the 100:0, 95:5, and 80:20 gels were further analyzed for ECM molecules associated with osteogenesis (collagen I, calcium deposits), chondrogenesis (GAGs), adipogenesis (elastin, collagen III), and SMC-lineage progression (collagen III, elastin). As shown in Fig. 30, collagen III deposition did not vary significantly with increasing $PDMS_{star}$ content. Similarly, elastin and GAGs concentrations could not be distinguished across hydrogel formulations (Fig. 30). However, collagen I levels were significantly higher in the 80:20 hydrogels relative to remaining formulations ($p < 0.016$). These collagen I results were reflected in the total collagen data ($p < 0.010$ for all pairwise comparisons). Furthermore, quantitative CPC assays revealed a marked increase in calcium deposits in the 80:20 gels relative to the 100:0 and 95:5 gels ($p < 0.002$, Fig. 22A). Qualitative von Kossa staining supported these quantitative CPC results (Fig. 22B). Cumulatively, the cell marker and ECM data indicated increased MSC osteogenic differentiation with increasing scaffold $PDMS_{star}$ content.

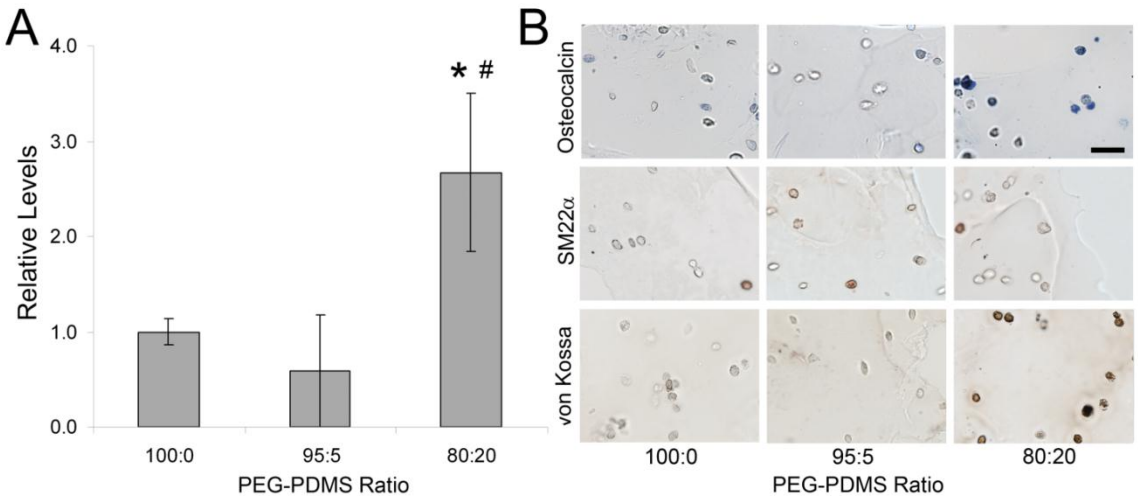

Figure 29. (A) Calcium measures per hydrogel formulation (n = 3-4 per formulation). *significantly different from 100:0 gels; #significantly different from 95:5 gels. (B) Representative images of PEG-$PDMS_{star}$ hydrogel sections stained for osteocalcin (blue), SM22α (red), and calcium deposits (brown-black), n = 3 per gel type. The scale bar in the upper right-hand image equals 40 μm and applies to all images.

6.5. Discussion

In the present study, mouse 10T½ MSCs were encapsulated in a series of PEG-$PDMS_{star}$ hydrogels of varying inorganic content and hydrophobicity. Quantitative analyses indicated marked increases in a range of osteogenic markers with increasing PDMS levels. Specifically, runx2, osteocalcin, and calcium deposits were each 3-4 times greater in the 80:20 formulation versus the 100:0 control gels. Expression of collagen I, the primary collagen type in bone, was also elevated in hydrogels with increased PDMS content. In addition, the agreement in the collagen I and total collagen profiles suggests that collagen I was the dominant collagen type synthesized by the encapsulated cells.

In contrast, intracellular markers for adipogenesis (PPARγ, A-FABP), chondrogenesis (sox-9), and SMC lineage progression (myocardin, SM22α) were not altered in scaffolds with increased PDMS content, indicating that the observed osteogenic response was specific. To further confirm this, the levels of ECM molecules collagen III, elastin, and GAGs were quantified. Specifically, elastin- and collagen III-rich matrices are generally associated with smooth muscle [183] and loose connective tissues [38, 237], whereas increased production of sGAG is generally associated with chondrogenesis [238]. Levels of these ECM moieties were similar across gel formulations, supporting the specificity of the associated osteogenic response. Since introduction of $PDMS_{star}$-MA into the PEGDA hydrogel network could potentially alter bulk hydrogel modulus and mesh structure, the observed cell responses could not be attributed directly to the hydrophobic-inorganic character of PDMS without further material property assessments. Based on the collected modulus data, the decrease in average modulus from ~35 kPa in the 100:0 hydrogels to ~22 kPa in the 80:20 gels did not appear to play a significant role in the observed osteogenic response. Specifically, although osteogenic markers runx2 and osteocalcin were significantly greater in the 80:20 gels than in the 80:0 control gels, the average modulus values (both bulk and AFM-based) could not be distinguished between these gels. The apparent independence of cell responses on average gel modulus is consistent with literature in that each of the analyzed PEG-$PDMS_{star}$ scaffolds fell within the "osteogenic" modulus range identified by Huebsch et al [216] for both mouse and human MSCs in 3D culture. By a similar

argument, the variations in mesh size across hydrogel formulations are an unlikely source of the osteogenic response associated with the 80:20 gels.

Thus, the hydrophobic-inorganic character of PDMS itself appears to promote the observed cellular responses. This would be consistent with prior studies linking increased scaffold silane [36] or siloxane [38] content to increased osteogenic responses. It is likely that both the inorganic nature of PDMS as well as its hydrophobicity played critical roles in the present results. In particular, silica, which is inorganic but hydrophilic, has been associated with increased osteogenesis [33, 34]. Similarly, the introduction of hydrophobic but non-inorganic species within scaffolds has been linked to bone formation [33].

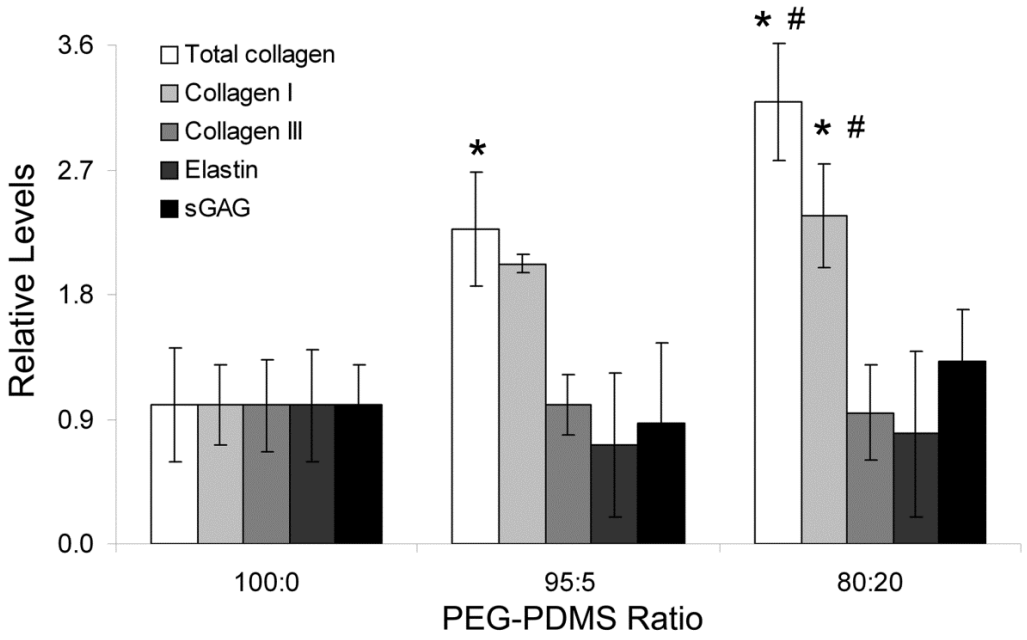

Figure 30. Levels of total collagen, collagen I, collagen III, GAGs and elastin in each PEG-PDMS$_{star}$ formulation. Results were normalized to the 100:0 PEG-PDMS$_{star}$ formulation for the purpose of comparison. *significantly different from 100:0 gels; $^{\#}$significantly different from 95:5 gels. Samples per assay: n = 4-6 per formulation.

Several limitations of the present study merit comment. First, the potential influence of the nanotopography introduced by the PDMS nanoparticles on observed cell responses requires further examination. In addition, the sample number per formulation and the range of PDMS levels examined were limited. More extensive in vitro studies followed by in vivo work would be required to definitely demonstrate that increased PDMS incorporation intrinsically promotes osteogenesis.

CHAPTER VII

INFLUENCE OF CYCLIC STRETCH AND ENDOTHELIAL CELL PRESENCE ON MESENCHYMAL STEM CELL OSTEOGENIC COMMITMENT

7.1. Overview

MSCs are increasingly recognized as a viable cell source for bone regeneration applications. In addition to soluble factors, cyclic stretch has been shown to have a profound effect on mesenchymal stem cell (MSC) osteogenesis. Similarly, EC presence has been demonstrated to enhance MSC osteogenic differentiation. However, potential synergistic interactions between mechanical stimulation and EC presence remain to be elucidated. The aim of the present manuscript was therefore to examine the simultaneous influence of cyclic stretch and EC paracrine signaling on MSC osteogenesis in the context of scaffolds with "osteogenic" moduli.

To accomplish this, 10T½ multipotent stem cells were encapsulated in PEGDA hydrogels with moduli within the "osteogenic" range. Half of the constructs were fabricated with a luminal EC layer. EC+ and EC- constructs were then subjected to continuous cyclic stretch. Following 10 days of culture, both EC+ and EC- constructs were associated with significantly elevated levels of chondrogenic transcription factor sox9 relative to initial (day 0) expression levels. By day 22 of culture, however, sox9 levels in both the EC+ and EC- constructs had returned to or fallen below day 0 levels.

In contrast, osteocalcin expression was significantly higher in Day 22 EC+ constructs relative to EC- constructs and relative to day 0. Similarly, osteopontin and alkaline phosphatase levels were elevated in Day 22 EC+ constructs relative to EC- constructs. Cumulatively, the present results suggest that EC paracrine signaling enhances MSC osteogenesis in the presence of cyclic stretch. In addition, the observed transition from chondrogenic to osteogenic protein expression associated with the EC+ constructs would be consistent with the neovascularization-dependent transition from cartilage matrix to osteoid matrix associated with endochondral bone formation.

7.2. Introduction

Neovascularization and mechanical stress play critical roles in endochondral ossification, a key bone formation mechanism during bone growth and fracture healing [40]. Indeed, in endochondral ossification, blood vessels invade hyaline cartilage, and MSCs associated with invading vessels differentiate into osteoblasts which begin depositing bone matrix [40]. In addition, physiological loading during endochondral ossification enhances the rate and quality of bone matrix deposition [41, 42]. Consistent with the endochondral ossification process, studies have shown MSC osteogenic differentiation to be separately influenced by cyclic loading [43, 44] and EC presence [45-47]. However, potential synergistic interactions between mechanical stimulation and EC presence on MSC osteogenesis remain to be elucidated. This is significant since a deeper understanding of such interactions could lead to improved MSC-based bone

regeneration strategies. The goal of the present study was therefore to evaluate potential synergistic effects of EC paracrine signaling and cyclic stretch on MSC osteogenesis within the context of scaffolds with "osteogenic" moduli.

To accomplish this, 10T½ MSCs were encapsulated within tubular PEGDA hydrogels. The molecular weight and concentration of PEGDA were selected to yield constructs with moduli within the "osteogenic" range identified by Parekh et al. [239]. Specifically, Parekh et al. found that MSC osteogenesis increased with increasing modulus from ~11 kPa through at least 59 kPa. Thus, the present PEGDA constructs were fabricated with moduli of ~60 kPa. Initial MSC interactions with the hydrogel matrix were enabled by the conjugation of adhesion peptide RGDS to the hydrogel network. In addition, half of the constructs were fabricated with a luminal EC layer to allow for evaluation of the influence of EC paracrine signals on MSC differentiation. Tubular scaffold geometry was selected to enable construct mounting within a pulsatile flow bioreactor. This bioreactor setup allowed for simultaneous application of cyclic stretch while exposing luminal ECs to physiological wall shear stress. After 10 and 22 days of culture, the levels of various differentiation markers expressed by encapsulated 10T½ MSCs were characterized in order to evaluate MSC lineage progression.

7.3. Materials and Methods

7.3.1. Polymer Synthesis

PEGDA was prepared as previously described [191] by combining 0.1 mmol ml^{-1} dry PEG (6 kDa, Sigma), 0.4 mmol ml^{-1} acryloyl chloride, and 0.2 mmol ml^{-1} triethylamine in anhydrous DCM and stirring under argon overnight at 4 °C. The resulting solution was washed with 2 M K_2CO_3 and separated into aqueous and DCM phases to remove HCl. The DCM phase was subsequently dried with anhydrous $MgSO_4$, and PEGDA was precipitated in diethyl ether, filtered, and dried under vacuum. Acrylation of the PEG end hydroxyl groups was characterized by ^{1}H-NMR to be ~85%.

Cell adhesion peptide RGDS (American Peptide) was conjugated to acryloyl-PEG-N-hydroxysuccinimide (ACRL-PEG-NHS, 3.4 kDa, Laysan) at a 1:1 molar ratio for 2 h in 50 mM sodium bicarbonate buffer, pH 8.5 [221]. The product (ACRL-PEG-RGDS) was purified by dialysis, lyophilized, and stored at -20 ºC until use.

7.3.2. Cell Culture and Construct Fabrication

Cryopreserved bovine aortic ECs (BAECs, Cell Applications) at passage 3-5 were thawed and expanded at 37 ºC and 5% CO2. During expansion, cells were cultured in Dulbecco's Modified Eagle's Media (DMEM, Hyclone) containing 10% iron-supplemented bovine calf serum (BCS, Hyclone), 100 U/mL penicillin, and 100 mg l^{-1}

streptomycin (Hyclone). Cryopreserved 10T½ mouse MSCs (ATCC) at passage 2-5 were thawed and expanded in DMEM supplemented with 10% heat-inactivated fetal bovine serum (FBS, Hyclone).

10T½ cells were harvested from 4 separate populations, each at passage 5-7. A fraction of each population was allocated for "day 0" protein extraction. The remaining portions of each cell population were then combined and allocated for encapsulation within tubular PEGDA constructs. Similarly, BAECs at passage 5-8 were harvested, combined, and processed to form stable EC layers within the lumens of half of the tubular constructs. Protein extraction and construct fabrication procedures are described further in the following subsections.

7.3.2.1. Day 0 Protein Extraction

Proteins were extracted from Day 0 10T½ cell populations (n = 4) by the addition of Trizol (Invitrogen) per manufacture's protocols. The resulting solutions were centrifuged, and the supernatants were mixed with chloroform (Sigma), vigorously shaken for 15 s, and centrifuged. Ethanol was then added to the lower, protein-rich phenol-chloroform phase of each mixture to precipitate residual DNA. The resulting phenol-ethanol phase was transferred to a 3.4 kDa SnakeSkin dialysis membrane (Pierce). Each solution was dialyzed for ~60 h at 4 °C against an aqueous solution of 0.1% sodium dodecyl sulfate (SDS), with buffer exchange every 18 h. By the end of third 18 h dialysis period, the samples had partitioned into three phases: (1) a supernatant, (2) a globular mass, and (3) a colorless, viscous liquid. The globular mass

of each sample contained the bulk of sample proteins [194] and was resuspended in PBS containing 0.5% SDS and 1% Triton X-100. The isolated sample proteins were subsequently used in quantitative ELISA assays.

7.3.2.2. Fabrication of Bilayered Hydrogels

A series of constructs were fabricated for two experimental time points – day 0, day 10 and day 22. Since ECs seeded onto the surface of PEGDA hydrogels containing cell adhesion peptide RGDS tend to form cell layers that are unstable under flow conditions [240]. Day 0 EC+ constructs were prepared by a unique sequential polymerization process, termed "cementing". In this process, luminal PEGDA served as a "grout" between adjacent ECs rather than as an encapsulating agent[240]. This process effectively prevents EC layer delamination under flow while allowing the "cemented" ECs to directly experience the luminal flow environment [240]. In brief, a precursor solution containing 0.1 g ml^{-1} PEGDA and 1 mM ACRL-PEG-RGDS in 10% sucrose was first prepared. Ten μl of a 300 mg ml^{-1} solution of 2,2- dimethoxy-2-phenyl-acetophenone (DMAP) dissolved in N-vinyl pyrrolidone (NVP) was then added per mL of mixture, and the resulting solution was sterilized by filtration. BAECs were harvested and resuspended at high density ($125x10^6$ cells ml^{-1}) in the PEGDA precursor solution. Fifty μL of the resulting mixture was spread evenly onto a 3 mm glass rod over a 5.5 cm length and was then dried as a thin layer by 8 min application of a sterile air stream. During air stream application, the rod was held horizontally and constantly rotated to facilitate the fabrication of an even coating.

Each EC coated rod was inserted as the inner mandrel of a double-walled cylindrical mold, the outer wall of which was composed of a hollow UV transparent plastic cylinder (5 mm ID). A separate precursor solution containing 0.1 g ml^{-1} PEGDA and 1 mM ACRL-PEG-RGDS in HBS-TEOA (10 mM HEPES, 150 mM NaCl, 115 mM triethanolamine, pH 7.4) was then prepared. Following the addition of 10 µl of a 300 mg ml^{-1} solution of DMAP in NVP, the solution was sterilized by filtration. Harvested 10T½ cells were then resuspended in the precursor solution at ~$5x10^6$ cells ml^{-1}, and the resulting cell suspension was gently pipetted into the cylindrical molds and polymerized by exposure to UV light (365 nm, ~10 mW cm^{-2}, UVP model B-100SP) for 6 min. The resulting bilayered hydrogels were removed from their molds and briefly rinsed in PBS containing 1% PSA (PSA: 10,000 U ml^{-1} Penicillin, 10,000 mg l^{-1} Streptomycin, and 25 mg l^{-1} Amphotericin). Day 0 EC+ constructs (n = 11) were then transferred to DMEM containing 10% BCS and 1% PSA. Day 10 EC+ (n = 8) and Day 22 EC+ constructs (n = 3) were prepared in a similar manner.

Day 0 EC- constructs (n = 8), Day 10 EC- constructs (n = 5) and Day 22 EC- constructs (n = 3) were prepared as above, except that the PEGDA precursor solution for the luminal layer contained no BAECs. BAEC viability through the above construct fabrication process has previously been shown to be similar to BAEC viability following standard encapsulation in PEGDA gels [240]. In addition, “cemented” BAECs have previously been demonstrated to display a phenotype similar to that of BAECs seeded onto the surface of RGDS-containing PEGDA hydrogels [240]. In the present study, we

also confirmed an appropriate phenotype for “cemented” ECs by comparison with ECs seeded onto PEGDA hydrogels containing 1 mM ACRL-PEG-RGDS (Fig. 31).

7.3.3. Day 0 Construct Characterization

After 24 post-fabrication, constructs were harvested for mechanical and histological analyses. Each harvested EC+ and EC- construct was then cut into 6 ring segments approximately 4-6 mm in length. The two end ring segments of each construct were discarded. One of the 4 remaining segments of each construct was transferred to PBS for immediate mechanical testing, and a separate segment was processed for histological analyses.

7.3.3.1. Mechanical Assessment

Twenty-four hours post-fabrication, ring segments ~ 4mm in width were harvested from a subset of each construct set (n = 3 per construct type) to assess initial mechanical properties as well as to confirm similar moduli across gels. Mechanical analyses were conducted using a modification of the circumferential property testing technique validated in Johnson et al. [192] and Hiles et al. [193]. In brief, the dimensions of ring segments were measured using digital calipers. These measures served as dimension inputs for subsequent stress and strain calculations. Each ring was mounted onto an Instron 3342 by threading opposing stainless steel hooks through the segment lumen. The hooks were then uniaxially separated at a rate of 6 mm/min until construct

failure. As hook separation increased, the mounted ring was drawn into an increasingly oblong conformation. Johnson et al. [192] confirmed that the force applied by the hooks to this oblong oval could be approximated as being equally distributed between two rectangles, each with sides equal to the width and wall thickness, h_v, of the ring. The gauge length, l_g, was taken to be the inner diameter, D_v, of the unstretched ring plus h_v, and the elastic modulus, E, of each sample was defined as the slope of the resulting stress–strain curve at a reference stress σ of 20 kPa [84]. Samples remained immersed in PBS until immediately prior to mechanical analyses, and testing was completed rapidly to avoid sample dehydration.

7.3.4. Mechanical Conditioning

After 3 days of static culture, EC+ and EC- constructs were mounted onto the inner ports of separate bioreactor graft chambers. These graft chambers were then connected to separate bioreactor flow loops, described in further detail in the following section.

7.3.4.1. Bioreactor Flow Loop

Constructs were exposed to pulsatile flow conditions using a modification of the bioreactor system previously described in Bulick et al. [117]. In brief, a peristaltic pump drew media from a reservoir, generating the desired flow rate of media through the system. The media flow was then passed through a compliance chamber, and a CellMax

pump (Spectrum Labs) was used to overlay the desired pulsatile waveform. The flow was then passed through the constructs. Pressure profiles were monitored immediately upstream and downstream of each construct using sterile transducers (Merit Medical) equipped with inlet and outlet valves. After exiting the constructs, the media was passed back to the media reservoir, completing the flow circuit. Both the graft chamber and the media reservoir were fitted with vent ports.

7.3.4.2. Mechanical Stimulation Regimen

The graft chamber baths and the inner flow loops were filled with DMEM supplemented with 10% BCS and 1% PSA. At day 4 of culture, flow was initiated at 20 ml min^{-1} per construct. After 3 h, the flow was ramped to 40 mL/min per construct. Following 24 h of flow, the mean pressure (Pavg) in each construct lumen was adjusted ~ 90 mmHg using the pressure transducer valves. At day 7 of culture, pulsation at 120 beats per minute [bmp] and a ΔP ~ 15 mmHg was initiated. After an additional 24 h, flow was increased to 120 ml min^{-1} per construct and a ΔP of ~25 mmHg. Continuous pulsatile flow was then applied through 22 days total culture time, with media changes every two days.

7.3.4.3. Shear Stress Estimates and Viscosity Measures

To estimate the shear stress experienced by ECs on the luminal surface of EC+ constructs, the Womersley number was first calculated [195, 196]. Specifically, rigorous estimates of the wall shear stress, τ_w, associated with the above pulsatile flow conditions

can be obtained from the mathematical descriptions of pulsatile flow in rigid pipes developed by Womersley [195, 196] and the associated dimensionless Womersley number, $\alpha = R\sqrt{\frac{}{\mu}}$, where R vessel inner radius, frequency of oscillation, media density, and μ media viscosity. The magnitude of α is an indicator of the impact of pulsatile flow frequency relative to viscous effects on fluid flow.

To estimate the Womersley number, the viscosity of DMEM containing 10% BCS and 1% PSA was determined using a Physica MCR 300 Modular Compact Rheometer fitted with a CP50-1 cone plate [197]. During testing, the temperature was held constant at 37 oC using a Peltier temperature controller. The change in media shear stress with increasing shear rate from 0.5-200 s^{-1} was monitored by the device and was used to calculate media viscosity. Through this technique, the viscosity of DMEM containing 10% BCS and 1% PSA was determined to be ~0.65 cP at 37 °C, in good agreement with previous literature [198].

Thus, for R 0.165 cm and 4π s^{-1}, α was approximately 5.4. For α in the range of 3-10, the Hagen-Poiseuille equation can be assumed to provide a useful estimate of wall shear stress [199]. Specifically, the Hagen-Poiseuille equation predicts that $\tau_w = \frac{4\mu Q}{\pi R^3}$, where Q = volumetric flow rate.

7.3.4.4. Circumferential Strain Estimates

To estimate the circumferential strain experienced by the constructs, the measured elastic moduli and vessel dimensions were input into the Bernoulli equation

$\sim \frac{(P)R}{h_v E}$, where R = inner vessel radius, h_v = wall thickness, and E = construct modulus [201]. This equation has previously been shown to be in good agreement with actual strains experienced by PEGDA constructs in the present bioreactor setup [84].

7.3.5. Endpoint Analyses

After 10 and 22 days total culture time, constructs were harvested for mechanical, histological, and biochemical analyses. In addition, constructs were harvested at 24 h post-fabrication for mechanical (Day 0 mechanical assesmensts) and histological analyses. Each EC+ construct was examined using a Leica stereomicroscope to confirm that the luminal EC layer was intact. Each harvested EC+ and EC- construct was then cut into 6 ring segments approximately 4-6 mm in length. The two end ring segments of each construct were discarded. One of the 4 remaining segments of each construct was transferred to PBS for immediate mechanical testing per the "Day 0" protocol, and a separate segment was processed for histological analyses. The two remaining segments per construct were immersed in formalin for 30 min, after which they were allocated for quantitative biochemical assays. For these segments, the luminal layer was removed using a dremel, and the remaining 10T½ layer was processed for biochemical analyses. For the EC+ segments, the removed luminal layer was also collected for further assessment. Details regarding the biochemical and histological assessments are given in the following subsections.

7.3.5.1. Biochemical Analyses

Day 10 and Day 22 10T½ layers and Day 10 and Day 22 EC layers were homogenized in Trizol. Sample proteins were then isolated as described for the Day 0 10T½ cell populations. The sample proteins isolated from Day 10 10T½ layers were evaluated for early-to-mid term markers of osteogenesis, chondrogenesis, adipogenesis, and myogenesis via competitive ELISAs. Based on Day 10 results, proteins extracted from Day 22 10T½ layers were analyzed for mid-to-late term markers of chondrogenesis and osteogenesis. Similarly, sample proteins isolated from the luminal layers of Day 10 and Day 22 EC + constructs were evaluated for various EC phenotypic markers.

For each antibody examined, high binding EIA 96 well plates (Costar) were coated overnight at 4 °C with appropriate competitive peptide. The concentration of the applied competitive peptide was 200 ng/well, except for β-actin (50 ng/well). The coated wells were then blocked with BSA and rinsed with PBS. Aliquots of each sample were incubated with primary antibody for 1 h, after which the sample-antibody mixtures were applied to coated wells for 1 h. Standard curves were similarly prepared by incubating primary antibody with varying levels of competitive peptide for 1 h, followed by solution application to coated wells. For both samples and standards, primary antibody which had bound to the coated wells was detected using an appropriate HRP-conjugated secondary antibody (Jackson Immunoresearch), followed by application of 2,2'-azino-bis(3-ethylbenzthiazoline-6-sulphonic acid) (Sigma) and monitoring of absorbance at 410 nm.

Each target protein was analyzed in duplicate for each sample and normalized to the average of housekeeping proteins β-actin and GAPDH. For the purpose of comparison, the resulting proteins concentrations for the Day 10 and Day 22 10T½ layers were normalized to Day 0 10T½ expression levels.

7.3.5.2. Histological Analyses

Construct segments reserved for immunostaining were fixed in formalin for 30 min. Each sample was then transferred to Tissue-Tek freezing media, snap frozen, and cut into 35 μm sections using a cryotome. Rehydrated sections were blocked with peroxidase for 30 min followed by 30 min exposure to Terminator (Biocare Medical). Primary antibodies for sox9, alkaline phosphatase, and osteopontin were diluted in PBS containing 3% BSA and then applied to the sections for 1 h. Bound primary antibody was detected either using HRP-conjugated secondary antibody (Jackson ImmunoResearch) followed by application of chromogen AEC (LabVision) or using AP-conjugated secondary antibody followed by application of chromogen Ferangi Blue (Biocare Medical). EC+ constructs were also stained for VE-cadherin, PECAM-1, and thrombomodulin per the above procedure. Further details regarding the antibodies employed are given in Table 10.

Table 10. Antibodies Employed in Immunostaining and ELISA Assessments.

Antibody†	Clone	Immunostaining	ELISA
Runx2	S-19		√
Osterix	M-15		√
Alkaline Phosphatase	N-18	√	
Osteopontin	AKm2A1	√	
Osteocalcin	M-15		√
PPARγ	I-18		√
A-FABP	C-15		√
Sox 9	C-20	√	√
Collagen II	N-19		√
Myocardin	M-16		√
SM22α	P-15		√
VE-Cadherin	C-19	√	√
PECAM-1	M-20	√	√
Thrombomodulin	M-17		√
GAPDH	V-15		√
β-actin	13E5		√

†all antibodies were obtained from Santa Cruz Biotechnology.

Stained sections were imaged using a Zeiss Axiovert microscope, and cell counts were carried out to semi-quantitatively evaluate immunostaining results for intracellular markers sox9 and alkaline phosphatase. These counting assessments were conducted according to established methods [53, 88, 89] on sections from each sample. For each cell, i, in a given section, a staining intensity, di, was recorded on a scale of 0–3, 0 "no staining" and 3 "highest intensity among both treatment groups for that antibody" by a single observer blinded to outcome. The cumulative staining intensity, d, for a given antibody in a particular section was calculated using the following equation: $d \quad \frac{d_i}{\text{total cell number}}$. In addition, since deposited ECM remained localized around the parent cells in each construct, as is characteristic for PEGDA gels [12], the relative expression

of the ECM protein osteopontin was also evaluated by cell counts per the above procedure. Sox9 counts were used to internally validate the counting approach by direct comparison with corresponding quantitative ELISA data (Fig. 37). The degree of correlation between the two assessment techniques was 98.9% by Pearson's correlation coefficient method.

7.3.6. Statistical Analyses

Results are reported as mean ± standard error of the mean. Comparisons among hydrogel treatment groups were conducted using ANOVA and Tukey's post-hoc test (SPSS software), $p < 0.05$.

7.4. Results

7.4.1. Construct Modulus and Applied Stress Conditions

As shown in Table 11, the initial moduli of the EC+ and EC- constructs were statistically indistinguishable at 64.4 ± 3.1 kPa and 70.3 ± 3.8, respectively. Importantly, these initial moduli were within the osteogenic r ange identified in the 3D studies of Parekh et al. [239]. Specifically, Parekh et al. found that MSC osteogenesis increased monotonically with increasing modulus from ~11 kPa through at least 59 kPa. Construct moduli in both treatment groups remained within the osteogenic range throughout the 22

day culture period. Furthermore, the similarity in the moduli of the EC+ and EC- constructs observed at day 0 was also observed at day 10 and day 22 (Table 11), indicating that modulus was not a source of difference between treatment groups.

Similarly, gel dimension assessments indicated the inner radius and wall thickness of both the EC+ and EC- constructs were maintained at 1.65 ± 0.02 mm and 1.18 ± 0.03 mm, respectively, over the culture period. These measures are consistent with the slow degradation rate (1-2 years) and resistance to cell-mediated compaction characteristic of PEGDA hydrogels [72, 84, 90-92]. Based on the construct moduli, dimension data, and the applied ΔP, the cyclic tensile strain experienced by the encapsulated 10T½ cells was ≈ 7.2% at full pulsation. Similarly, the average wall shear stress experienced by the luminal ECs was ≈ 3.7 dyn cm^{-2}, within the physiological range for the microvessels [241] associated with developing bone.

Table 11. Modulus for the EC+ and EC- Constructs with Time in Culture.[†]

	Day 0	**Day 10**	**Day 22**
EC+	64.4 ± 3.1	58.8 ± 2.1	62.0 ± 10.9
EC-	70.3 ± 3.8	63.9 ± 2.0	62.0 ± 3.8

[†]no significant differences between treatment groups or between time points were detected.

7.4.2. EC Phenotype

ECs seeded onto the surface of PEGDA hydrogels containing cell adhesion peptide RGDS tend to form cell layers that are unstable under flow conditions [240]. Therefore, the ensure stable, luminal EC layers for the EC+ constructs, a novel "cementing" technique was employed. In brief, this method uses PEGDA as a "grout" between adjacent cells rather than as an encapsulating agent [240]. Before evaluating the lineage progression associated with the 10T½ construct layers, it was important to confirm that ECs within the "cemented" EC layers were expressing an appropriate phenotype. Thus, the phenotype of "cemented" ECs was evaluated relative to conventionally "seeded" ECs, i.e. "cemented" ECs were compared to ECs which had been seeded as a confluent monolayer on the surface of PEGDA hydrogels containing cell adhesion ligand RGDS. Cells in both contexts expressed similar levels of the molecule VE-Cadherin and PECAM-1 (Fig. 31), markers associated with EC intercellular junctions and permeability regulation. To further understand the impact of "cementing" on EC phenotype, competitive ELISAs were conducted for thrombomodulin, a protein downregulated following EC damage. As for VE-Cadherin and PECAM-1, levels of thrombomodulin were similar in "cemented" versus conventionally "seeded" constructs (Fig. 31). These results are consistent with a previous study demonstrating that "cemented" BAECs display a similar phenotype as conventionally "seeded" BAECs [240].

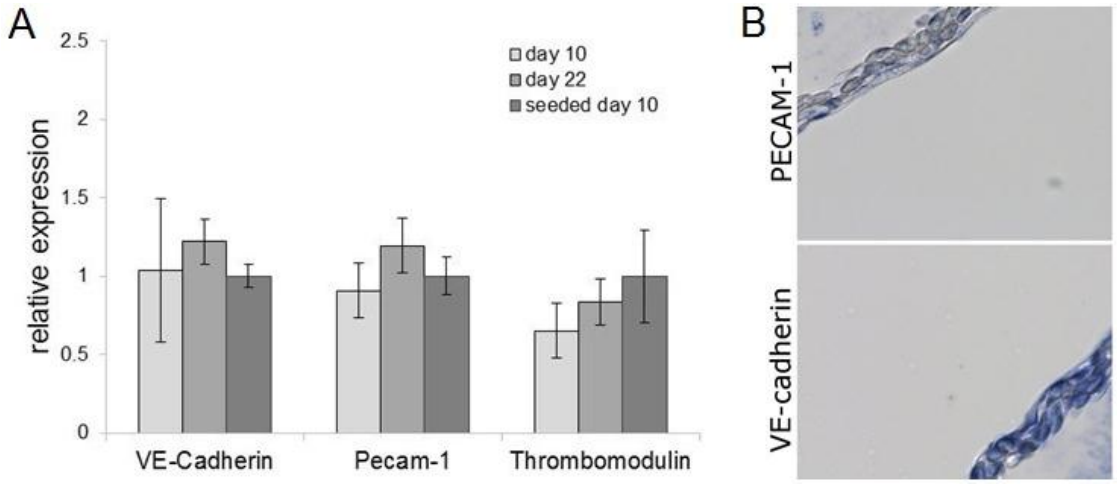

Fig. 31. (A) Elisa analyses of EC functional and damage-associated markers (VE-Cadherin, Pecam-1 and Thrombomdulin). (B) Representative images of EC funtional markers immunostaining. Positive staining is indicated by blue coloration. Scale bar = 20 μm.

7.4.3. Day 10 10T½ MSC Differentiation

Following 10 days of culture, subsets of constructs were harvested to evaluate 10T½ MSC lineage progression between treatment groups (EC+ and EC- constructs) and relative to day 0. To assess the specificity of potential osteogenic responses, early-to-mid-term markers of chondrogenesis, smooth muscle progression, and adipogenesis were evaluated in addition to markers for osteogenesis. As shown in Fig. 32B, day 10 expression of the smooth muscle transcription factor myocardin was similar between EC+ and EC- constructs (Fig. 33) and relative to day 0 (Fig. 32B). In addition, day 10 levels of the smooth muscle cytoskeletal protein SM22α were indistinguishable from day 0 levels in both EC+ and EC- constructs. Similarly, day 10 levels of adipogenic transcription factor PPARγ as well as of the adipocyte intracellular protein A-FABP

were statistically indistinguishable across treatment groups (Fig. 33) and relative to day 0 (Fig. 32A).

As with the adipogenic markers, 10T½ expression of osteogenic transcription factors runx2 and osterix at day 10 could not be distinguished between EC+ and EC- constructs (Fig. 33) or from day 0 levels (Fig. 34 B). Although day 10 expression of bone ECM protein osteocalcin appeared to be elevated in the EC+ constructs relative to day 0, this difference fell below statistical significance (data no show). In contrast, day 10 expression of chondrogenic transcription factor sox9 was increased approximately 2-fold relative to day 0 in both the EC+ and EC- constructs ($p < 0.016$). This increase in sox9 expression relative to day 0 levels had not yet translated to substantial increases in the cartilage ECM protein collagen II (Fig. 34A), suggesting initial stages of chondrogenesis.

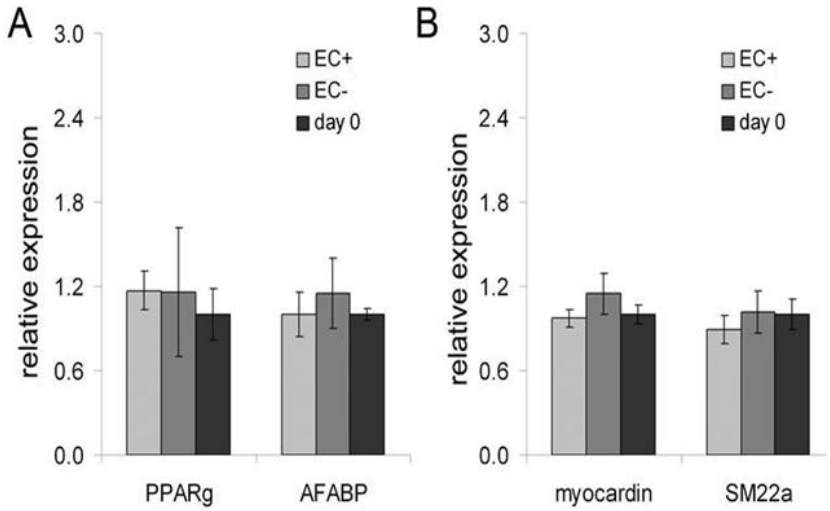

Fig. 32. ELISA analyses of day 10 expression of (A) smooth muscle lineage markers (myocardin and SM22a) relative to day 0 and (B) adipogenic markers (PPARg and A-FABP). n = 5-8 samples per day 10 treatment group, n = 4 for day 0.

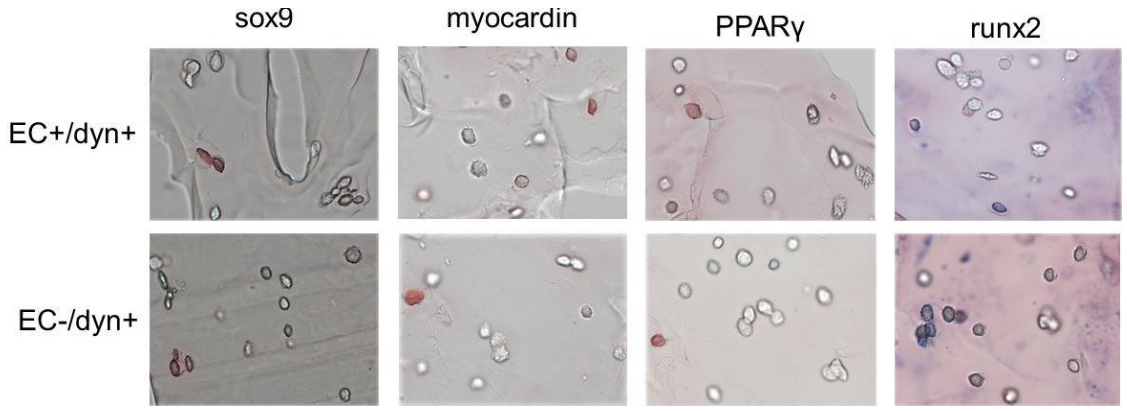

Fig. 33. Representative images of day 10 immunostaining for sox9, myocardin, PPARγ, and runx2. Positive staining is indicated by red (sox9, myocardin and PPARγ) or blue (rux2) coloration. Scale bar = 20 μm.

7.4.4. Day 22 Cell Differentiation

Based on the day 10 sox9 and osteocalcin results, day 22 analyses focused on chondrogenic markers in addition to osteogenic markers. As for day 10, no differences in collagen II levels were noted between day 0 and day 22 (Fig. 35A). However, in contrast to day 10 data, sox9 levels in EC+ and EC- constructs at day 22 were no longer elevated relative to day 0. Specifically, sox9 expression in the Day 22 EC+ constructs had returned to day 0 levels, whereas sox9 expression in the Day 22 EC- constructs was 2.5-fold lower than day 0 levels ($p = 0.036$). Furthermore, semi-quantitative cell counts results indicated that sox9 levels in the Day 22 EC+ and EC- constructs were approximately 2.0-fold lower than levels in the Day 0 EC- constructs (Fig. 36A, [Day 0 EC+ and EC- constructs did not show significant differences between them for sox9, AP and osteopontin, data not showed]).

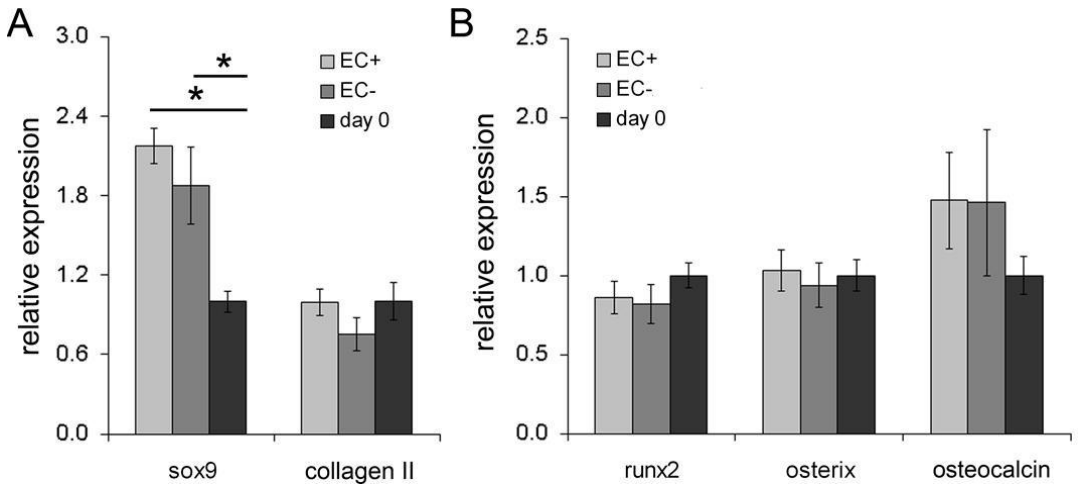

Fig. 34. ELISA analyses of day 10 expression of (A) chondrogenic markers (sox9 and collagen II) and (B) osteogenic markers (runx2 and osterix) relative to day 0. n = 5-8 samples per day 10 treatment group, n = 4 for day 0. * indicates a significant difference from EC+, $p < 0.05$.

Evaluation of osteogenic transcription factor osterix indicated no significant differences at day 22 between the EC+ and EC- groups or relative to day 0 (Fig. 35B). Conversely, day 22 expression of bone ECM protein osteocalcin was approximately 1.6-fold higher in EC+ constructs than at day 0 ($p = 0.025$). In addition, day 22 osteocalcin levels were approximately 1.6-fold greater in EC+ constructs than in EC- constructs ($p = 0.018$). These osteocalcin ELISA assessments were underscored by semi-quantitative cell counts for mid-term bone markers alkaline phosphatase (AP) and osteopontin. In particular, AP and osteopontin levels were 1.7-fold ($p = 0.002$) and 2.1-fold ($p = 0.005$) greater, respectively, in Day 22 EC+ constructs than in Day 22 and Day 0 EC- constructs (Fig. 35 B and C). These results cumulatively suggest that the early chondrogenesis observed for EC+ constructs at day 10 had transitioned to osteogenesis by day 22.

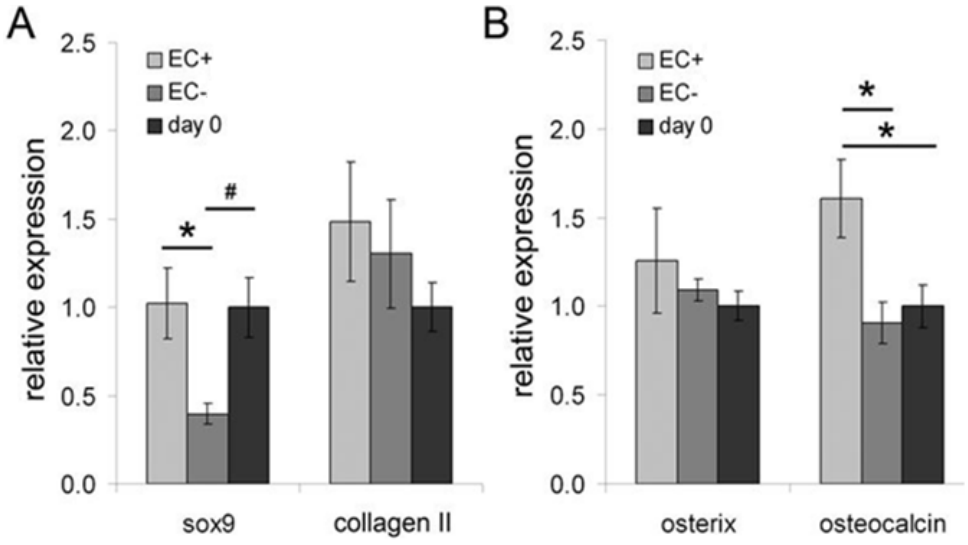

Fig. 35. ELISA analyses of day 22 expression of (A) chondrogenic markers (sox9 and collagen II) and (B) osteogenic markers (osterix and osteocalcin) relative to day 0. n = 3-4 samples per day 22 treatment group and per day 0.

7.5. Discussion

In the present study, the simultaneous influence of cyclic stretch and EC paracrine signaling on MSC osteogenesis was examined in the context of scaffolds with "osteogenic" moduli. To accomplish this goal, tubular constructs were prepared, half of which contained a luminal EC lining. These constructs were then mounted within a pulsatile flow bioreactor which enabled exposure of 10T½ MSCs to cyclic stretch while also exposing luminal ECs to physiological shear stress. Following 10 days and 22 days of culture, 10T½ MSC lineage progression was analyzed in both EC+ and EC- constructs.

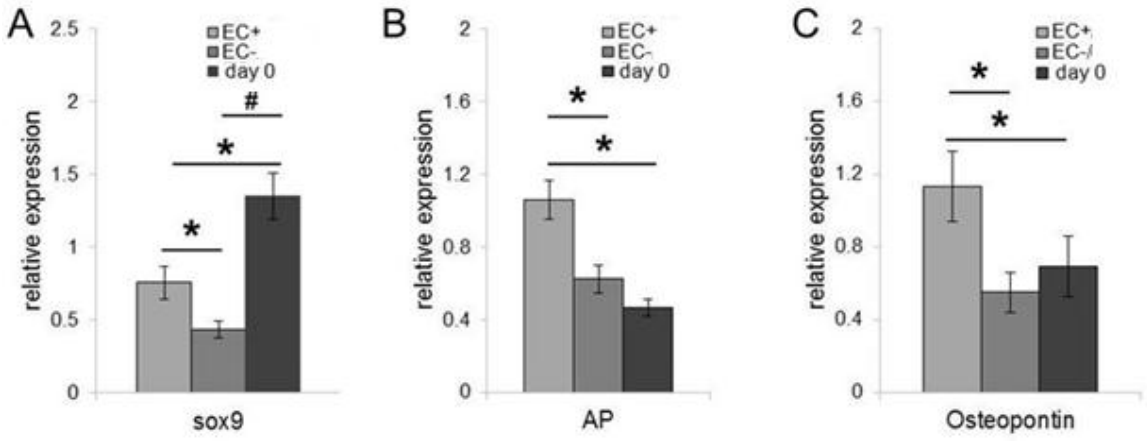

Fig. 36. Cell counting assessments of day 22 EC+ and EC- and day 0 EC- constructs expression of sox9, alkaline phosphatase (AP) and osteopontin. Sections from 3 separate samples of each treatment group were evaluated. Validation of the cell counting assessment method is given in Fig. 37. * indicates a significant difference from EC+/dyn+, # indicates a significant difference from EC- day 0.

Day 10 data indicated an initial chondrogenic response, as evidence by increased 10T½ sox9 expression in both EC+ and EC- constructs relative to day 0. The independence of this response on EC presence indicates that this initial chondrogenic behavior was either due to the rounded cell phenotype imposed by the tight crosslink density and slow degradation rate of PEGDA hydrogels Fig. 37 and/or due to the mechanical stresses experience by the 10T½ MSCs. Specifically, rounded cell morphologies have previously been associated with chondrogenesis [242]. In addition, the 10T½ cells in both treatment groups experienced cyclic stretch as well as dynamic hydrostatic pressure imparted by the pressurized media passing through the construct lumens. Although generally associated with cyclic compression [243-246], MSC chondrogenesis has also recently been shown to be stimulated by cyclic stretch. Indeed, McMahon et al. [247, 248] and Connelly et al. [249] found that 10% cyclic tensile strain

increased chondrogenic differentiation relative to static controls. Similarly, hydrostatic pressure has been shown to stimulate MSC chondrogenesis [250, 251]. In particular, Kisiday et al. demonstrated that hydrostatic pressure was able to induce a chondrogenic response of similar magnitude as that induced by chondrogenic media supplements [251] Thus, the initial increase in sox9 expression may represent the combined effects of rounded cell morphology, cyclic tensile strain, and hydrostatic pressure.

By day 22, however, sox9 expression in both EC+ and EC- constructs had returned to or fallen below day 0 levels. In addition, sox 9 levels in both EC+ and EC- constructs were lower than levels in EC- constructs at Day 0. This result is consistent with the work of Connelly et al. who found that increases in sulfated glycosaminoglycan production following 1 week of MSC exposure to cyclic tension and chondrogenic media were lost after 2 weeks of loading [249]. In contrast, levels of bone ECM protein osteocalcin were 1.6-fold greater in Day 22 EC+ constructs relative to EC- constructs and relative to day 0. In addition, mid-term osteogenic markers AP and osteopontin were 1.7-to-2 fold higher in EC+ constructs than in EC- constructs and Day 0 EC- constructs. Cumulatively, these results suggest that the applied cyclic stretch and associated hydrostatic pressure were not alone sufficient to induce osteogenesis. In agreement with these results, previous literature indicates that pure hydrostatic pressure loading inhibits MSC osteogenesis even in the presence of osteogenic media supplements [250]. In addition, although literature regarding the effects of cyclic stretch on MSC osteogenesis is mixed [43, 44, 252, 253], the present data are in agreement with those of Shi et al.[252] and Steinmetz et al. [253]. Specifically, Shi et al. found that continuous cyclic

mechanical stretch inhibited runx2 expression when MSCs were cultured in the presence of osteogenic supplements. Similarly, Steinmetz et al. found that an intermittent 15% cyclic strain inhibited osteogenesis even in the presence of osteoinductive media [253].

Given that osteocalcin, osteopontin, and AP were each elevated in EC+ constructs relative to EC- constructs, the current data imply either that EC paracrine signaling stimulates osteogenesis and/or that EC paracrine signaling alters the manner in which MSCs interpret the applied mechanical stimuli. Although EC presence has previously been linked to increased MSC osteogenesis, these osteogenic responses have generally occurred following direct EC-MSC contact and/or in the presence of osteogenic supplements [46, 47, 254]. For instance, Saleh et al. found that MSC osteogenic differentiation was significantly elevated in EC-MSC spheroid co-cultures relative to MSC spheroids not containing ECs when cultured under osteogenic conditions [46]. In addition, Kaigler et al. found that ECs significantly increased MSC osteogenic differentiation in vitro in the absence of osteogenic media supplements only when ECs and MSCs were cultured in direct contact [45]. In contrast, only paracrine signaling between ECs and MSCs was enabled by the current culture setup. Therefore, the exact mechanism of EC influence on the present MSC responses requires further investigation. That said, the observed transition from chondrogenic to osteogenic protein expression associated with the EC+ constructs would be consistent with the neovascularization-dependent transition from a cartilage matrix to an osteoid matrix associated with endochondral ossification [255].

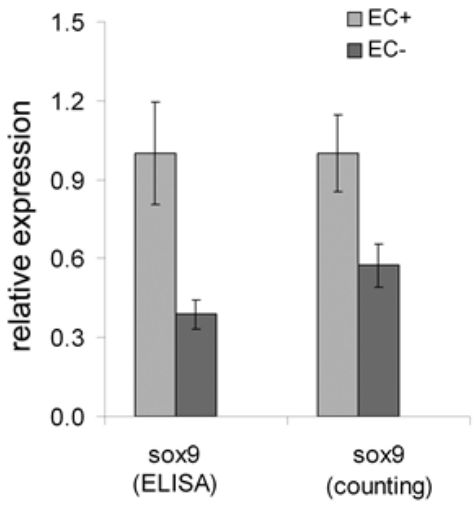

Fig. 37. Sox9 counts used to internally validate the counting approach by direct comparison with corresponding quantitative ELISA data. The degree of correlation between the two assessment techniques was 98.9% by Pearson's correlation coefficient method.

Several limitations of the present study merit comment. Osteogenesis represents a complex set of processes that are mediated by a number of factors. The interplay between these factors and the precise sequences leading to osteogenic commitment are not fully understood, and the present study examined only a limited subset of the interactions that mark osteogenesis. In addition, the present study examined mouse MSCs and thus, the current results may not be indicative of human MSC responses. Despite these limitations, the cumulative ECM and phenotypic data indicate EC paracrine signaling enhances MSC osteogenesis in the presence of cyclic stretch and hydrostatic pressure. Future studies explore a broader range of time points as well as varying mechanical stimulation regimens.

CHAPTER VIII

CONCLUSIONS

8.1. Summary

This work has shown that scaffold properties and paracrine EC-MSC interactions impact cell phenotype and cell differentiation. Specifically, PEG-GAG hydrogels have been shown to impact VFF and SMC behavior. Results indicate that subtle alterations in the biochemical stimuli presented to VFF cells (HA_{IMW} versus HA_{HMW}) altered VFF behavior. In particular, HA_{IMW} increased VFF myofibroblastic phenotype, suggesting that, among the examined formulations, the HA_{HMW} gels would be the most suitable system for VF regeneration. Moreover, the present results are in agreement with a previous 3D study of VFF responses to HA_{IMW} relative to alginate in collagen-based scaffolds permissive of cell elongation, indicating that PEGDA hydrogels prove useful as VF regeneration scaffolds despite the fact that they impose non-native VFF morphologies. In addition, PEG–HA gels may be the most appropriate for vocal fold SLP regeneration of the formulations examined, at least for the sulfated GAG types (CSC, HS and HA) and molecular weights investigated. Specifically, since collagen I, fibronectin, and SM-α-actin (myofibroblast marker) are generally elevated in scarred lamina propria these results suggest that CSC and HS may be undesirable for vocal fold implants relative to HA. Based on the results from these two vocal fold studies, future

work will explore a broader range of HA molecular weights on VFF function toward identifying suitable vocal fold regeneration scaffolds.

In contrast to VFFs, cell shape is known to strongly impact SMC function. Indeed, SMCs take on rounded phenotypes as they transform into foam cells during early atherosclerosis. Thus, we exploited the fact that PEGDA hydrogel enforce rounded cell morphologies to examine SMC responses to biochemical stimuli in an atherosclerotic-mimetic environment. Results from the present study supported the hypothesis that specific GAG types have differential influences on SMC foam cell formation. Specifically, DS was associated with greater phagocytosis of apoB, sustained increases in A-FABP expression, and an increased synthetic phenotype as well as a decreased expression of contractile marker MHC. The present PEG-base model system can be expanded to probe the impact of a range of atherogenic stimuli on SMC phenotype, potentially leading to more effective treatments for atherosclerosis.

In addition, EC paracrine signaling was demonstrated to induce MSC osteogenesis in the presence of cyclic stretch. Furthermore, we employed a novel class of hydrogels formed from the photocrosslink of PEG-DA and $PDMS_{star}$-MA to examine the influence of simultaneous increases in scaffold hydrophobicity and inorganic content on the osteogenic responses of encapsulated MSCs. Based on ECM and cell phenotypic data, elevated scaffold inorganic content and hydrophobicity were indeed correlated with increased osteogenic differentiation, indicating that PEG-$PDMS_{star}$ hydrogels may be promising scaffolds for bone regeneration. Future studies will seek to elucidate the influence of PDMS chemistry versus nanotopography (form PEG-PDMS phase

separation) on MSC osteogenic differentiation. To further probe MSC osteogenesis, the impact of EC paracrine signaling on MSC osteogenic lineage progression was examined in the presence of physiological loading. Results indicated that EC paracrine signaling enhances MSC osteogenesis in the presence of cyclic stretch. Moreover, the observed temporal transition from chondrogenic to osteogenic protein expression associated with the EC^{+} constructs would be consistent with the neovascularization-dependent transition from cartilage matrix to osteoid matrix associated with endochondral bone formation. A potential limitation of this study is that the EC layers were formed using a novel method for fabricating mechanically stable EC layers in bi-layered TEVGs through the use of PEGDA as an intercellular ‘‘cementing’’ agent rather than as an encapsulating agent. These ECs, although exposed to luminal stresses associated with fluid flow, did not appear to respond to these mechanical signals in terms of increases in various EC markers. Since the ECs within these layers do not directly contact each other, it is possible that the lack of direct cell-cell communication limited normal responses to mechanical stress. Thus, future work will examine MSC osteogenesis in the presence of EC paracrine signaling both in the presence and absence of cyclic stretch so that the contribution of mechanical conditioning to observed cell responses can be understood. In addition, alternate strategies for forming stable EC layers will be explored.

8.2. Recommendations

PEGDA hydrogels have been shown to be a useful tool in the study of the impact of biochemical stimuli and EC paracrine signaling on cell behavior. The blank slate nature of PEGDA hydrogels as well as the ability to tightly control of their material properties opens the possibility to design more efficient scaffolds for tissue engineering applications. For instance, in this work the PEGDA blank slate was modified by the incorporation of hydrophobic, inorganic $PDMS_{star.}$ This modification was demonstrated to be promising for inducing mouse MSC osteogenic differentiation and may potentially be applicable for human MSC osteogenic differentiation.

Although, PEGDA-based hydrogels have benefits as scaffolds for tissue engineering, the tight cross-link density and slow degradation rate of PEGDA gels provide some limitations that need to be addressed. For example, despite the presence of the cell adhesion ligand RGDS in the PEGDA hydrogels VFF take rounded/stellate morphologies, which are non-native for a number of cell types. In addition, direct intercellular contact is limited in PEGDA hydrogels. Thus, this scaffold system may not be appropriate for instances where the formation of intercellular junctions are critical to function. For instance, EC response to shear stress may be limited if direct EC-EC contact is limited. Furthermore, the microstructure of native ECM cannot be replicated in PEGDA hydrogels because deposited ECM is localized around individual cells due to tight crosslink density of PEGDA gels.

Several of these limitations could be addressed with the use of a degradable PEG based hydrogels which will allow the cells to have more freedom inside the hydrogel network. Modulation of PEG based hydrogels degradation rate can be achieved through the conjugation of degradable domains to PEG chains. For instance, the conjugation of polycaprolactone, polylactic acid or glycolide to PEG modulates the number of available ester hydrolysis sites which increase degradation rate. An alternative route involves the inclusion of enzymatically degradable peptides in which degradation rate is regulated by cell native enzyme release.

In addition, the role of the proteoglycan core protein in modulating SMC responses to CSC or DS signals was not accounted for. In addition, GAG chain length and charge densities are determining factors in the levels of bound lipid per chain. Although we have attempted to mimic the GAG chain lengths associated with atherosclerotic vessels in the present work, the CSC and DS chains conjugated to the hydrogel networks may not have charge densities appropriate to the atherogenic environment. Future work will probe a broader range of GAG charge densities and molecular weights on SMC foam cell formation.

Moreover, the potential influence of the nanotopography introduced by the PDMS nanoparticles on observed cell responses requires further examination. In addition, the sample number per formulation and the range of PDMS levels examined were limited. More extensive in vitro studies followed by in vivo work would be required to definitely demonstrate that increased PDMS incorporation intrinsically promotes osteogenesis. Future studies will probe the impact of a broader range of $PDMS_{star}$ levels and will

investigate the primary mechanisms through which they alter MSC behavior. In addition, various solvents will be employed to modulate the presence of PDMS nanoparticles within the hydrogel matrix, so that the impact of scaffold hydrophobicity and inorganic content can be more clearly parsed from the influence of nanotopography.

Furthermore, the cumulative ECM and phenotypic data indicate that EC paracrine signaling enhances MSC osteogenesis in the presence of cyclic stretch and hydrostatic pressure. However, osteogenesis represents a complex set of processes that are mediated by a number of physiological factors. The interplay between these factors and the precise sequences leading to osteogenic commitment are not fully understood, and the present study examined only a limited subset of the interactions that mark osteogenesis. In addition, the present study examined mouse MSCs and thus, the current results may not be indicative of human MSC responses. Future studies will explore a broader range of time points as well as varying mechanical stimulation regimens.

REFERENCES

1. Schultheiss J, Seebach C, Henrich D, Wilhelm K, Barker J, Frank J. Mesenchymal stem cell (MSC) and endothelial progenitor cell (EPC) growth and adhesion in six different bone graft substitutes. European Journal of Trauma and Emergency Surgery 2011; 37: 635-644.
2. Chan RW, Titze IR. Viscosities of implantable biomaterials in vocal fold augmentation surgery. Laryngoscope 1998; 108: 725-31.
3. Chan RW, Titze IR. Hyaluronic acid (with fibronectin) as a bioimplant for the vocal fold mucosa. Laryngoscope 1999; 109: 1142-9.
4. Hallen L, Johansson C, Laurent C. Cross-linked hyaluronan (Hylan B gel): a new injectable remedy for treatment of vocal fold insufficiency--an animal study. Acta Otolaryngol 1999; 119: 107-11.
5. Hallen L, Testad P, Sederholm E, Dahlqvist A, Laurent C. DiHA (dextranomers in hyaluronan) injections for treatment of insufficient closure of the vocal folds: early clinical experiences. Laryngoscope 2001; 111: 1063-7.
6. Jia X, Burdick JA, Kobler J, Clifton RJ, Rosowski JJ, Zeitels SM, et al. Synthesis and Characterization of in Situ Cross-Linkable Hyaluronic Acid-Based Hydrogels with Potential Application for Vocal Fold Regeneration. Macromolecules 2004; 37: 3239-3248.

7. Finck C, Lefebvre P. Implantation of esterified hyaluronic acid in microdissected Reinke's space after vocal fold microsurgery: first clinical experiences. Laryngoscope 2005; 115: 1841-7.

8. Hansen JK, Thibeault SL, Walsh JF, Shu XZ, Prestwich GD. In vivo engineering of the vocal fold extracellular matrix with injectable hyaluronic acid hydrogels: early effects on tissue repair and biomechanics in a rabbit model. Ann Otol Rhinol Laryngol 2005; 114: 662-70.

9. Burns JA, Kim KH, Kobler JB, deBoer JF, Lopez-Guerra G, Zeitels SM. Real-time tracking of vocal fold injections with optical coherence tomography. Laryngoscope 2009; 119: 2182-6.

10. Kutty JK, Cho E, Soo Lee J, Vyavahare NR, Webb K. The effect of hyaluronic acid incorporation on fibroblast spreading and proliferation within PEG-diacrylate based semi-interpenetrating networks. Biomaterials 2007; 28: 4928-38.

11. Kutty JK, Webb K. Mechanomimetic hydrogels for vocal fold lamina propria regeneration. J Biomater Sci Polym Ed 2009; 20: 737-56.

12. Liao H, Munoz-Pinto D, Qu X, Hou Y, Grunlan MA, Hahn MS. Influence of hydrogel mechanical properties and mesh size on vocal fold fibroblast extracellular matrix production and phenotype. Acta Biomater 2008; 4: 1161-71.

13. Thibeault SL, Klemuk SA, Chen X, Quinchia Johnson BH. In Vivo engineering of the vocal fold ECM with injectable HA hydrogels-late effects on tissue repair and biomechanics in a rabbit model. J Voice 2011; 25: 249-53.

14. Zeitels SM HR, Karajanagi SS, Langer RS. Hydrogels for vocal cord and soft tissue augmention and repair. US patent 20100055184; 2010.

15. Klemuk SA, Titze IR. Viscoelastic properties of three vocal-fold injectable biomaterials at low audio frequencies. Laryngoscope 2004; 114: 1597-603.

16. Munoz-Pinto DJ, Jimenez-Vergara AC, Gelves LM, McMahon RE, Guiza-Arguello V, Hahn MS. Probing vocal fold fibroblast response to hyaluronan in 3D contexts. Biotechnol Bioeng 2009; 104: 821-31.

17. Sahiner N, Jha AK, Nguyen D, Jia X. Fabrication and characterization of cross-linkable hydrogel particles based on hyaluronic acid: potential application in vocal fold regeneration. J Biomater Sci Polym Ed 2008; 19: 223-43.

18. Kimura M, Mau T, Chan RW. Viscoelastic properties of phonosurgical biomaterials at phonatory frequencies. Laryngoscope 2010; 120: 764-8.

19. Klemuk SA, Lu X, Hoffman HT, Titze IR. Phonation threshold pressure predictions using viscoelastic properties up to 1,400 Hz of injectables intended for Reinke's space. Laryngoscope 2010; 120: 995-1001.

20. Hahn MS, Jao CY, Faquin W, Grande-Allen KJ. Glycosaminoglycan composition of the vocal fold lamina propria in relation to function. Ann Otol Rhinol Laryngol 2008; 117: 371-81.

21. Tateya T, Tateya I, Sohn JH, Bless DM. Histologic characterization of rat vocal fold scarring. Ann Otol Rhinol Laryngol 2005; 114: 183-91.

22. Nakashima Y, Wight TN, Sueishi K. Early atherosclerosis in humans: role of diffuse intimal thickening and extracellular matrix proteoglycans. Cardiovasc Res 2008; 79: 14-23.

23. Nakashima Y, Fujii H, Sumiyoshi S, Wight TN, Sueishi K. Early human atherosclerosis: accumulation of lipid and proteoglycans in intimal thickenings followed by macrophage infiltration. Arterioscler Thromb Vasc Biol 2007; 27: 1159-65.

24. Khalil MF, Wagner WD, Goldberg IJ. Molecular interactions leading to lipoprotein retention and the initiation of atherosclerosis. Arterioscler Thromb Vasc Biol 2004; 24: 2211-8.

25. Vijayagopal P, Menon PV. Varied low density lipoprotein binding property of proteoglycans synthesized by vascular smooth muscle cells cultured on extracellular matrix. Atherosclerosis 2005; 178: 75-82.

26. Williams KJ, Tabas I. The response-to-retention hypothesis of early atherogenesis. Arterioscler Thromb Vasc Biol 1995; 15: 551-61.

27. Camejo G, Hurt-Camejo E, Wiklund O, Bondjers G. Association of apo B lipoproteins with arterial proteoglycans: pathological significance and molecular basis. Atherosclerosis. 1998; 139: 205-22.

28. Thompson MM, Budd JS, Eady SL, James RF, Bell PR. Effect of pulsatile shear stress on endothelial attachment to native vascular surfaces. Br J Surg 1994; 81: 1121-7.

29. Zhang ZX, Xi TF, Wang YJ, Chen XS, Zhang J, Wang CR, et al. In vitro study of endothelial cells lining vascular grafts grown within the recipient's peritoneal cavity. Tissue Eng Part A 2008; 14: 1109-20.

30. Salacinski HJ, Tiwari A, Hamilton G, Seifalian AM. Cellular engineering of vascular bypass grafts: role of chemical coatings for enhancing endothelial cell attachment. Med Biol Eng Comput 2001; 39: 609-18.

31. Ducheyne P, Qiu Q. Bioactive ceramics: the effect of surface reactivity on bone formation and bone cell function. Biomaterials 1999; 20: 2287-303.

32. Kretlow JD, Mikos AG. Review: mineralization of synthetic polymer scaffolds for bone tissue engineering. Tissue Eng 2007; 13: 927-38.

33. Khan Y, Yaszemski MJ, Mikos AG, Laurencin CT. Tissue engineering of bone: material and matrix considerations. J Bone Joint Surg Am 2008; 1: 36-42.

34. Garcia AJ, Ducheyne P, Boettiger D. Effect of surface reaction stage on fibronectin-mediated adhesion of osteoblast-like cells to bioactive glass. J Biomed Mater Res. 1998; 40: 48-56.

35. Song JH, Yoon BH, Kim HE, Kim HW. Bioactive and degradable hybridized nanofibers of gelatin-siloxane for bone regeneration. J Biomed Mater Res A 2008; 84: 875-84.

36. Curran JM, Chen R, Hunt JA. The guidance of human mesenchymal stem cell differentiation in vitro by controlled modifications to the cell substrate. Biomaterials 2006; 27: 4783-93.

37. Ayala R, Zhang C, Yang D, Hwang Y, Aung A, Shroff SS, et al. Engineering the cell-material interface for controlling stem cell adhesion, migration, and differentiation. Biomaterials 2011; 32: 3700-11.

38. Fischer GM, Cox RH, Detweiler DK. Altered arterial connective tissue in racing greyhound dogs. Experientia 1975; 31: 1426-7.

39. Jansen EJ, Sladek RE, Bahar H, Yaffe A, Gijbels MJ, Kuijer R, et al. Hydrophobicity as a design criterion for polymer scaffolds in bone tissue engineering. Biomaterials 2005; 26: 4423-31.

40. Maes C, Kobayashi T, Selig MK, Torrekens S, Roth SI, Mackem S, et al. Osteoblast precursors, but not mature osteoblasts, move into developing and fractured bones along with invading blood vessels. Dev Cell 2010; 19: 329-44.

41. Reich A, Jaffe N, Tong A, Lavelin I, Genina O, Pines M, et al. Weight loading young chicks inhibits bone elongation and promotes growth plate ossification and vascularization. J Appl Physiol 2005; 98: 2381-9.

42. Carter DR, Wong M. Mechanical stresses and endochondral ossification in the chondroepiphysis. J Orthop Res 1988; 6: 148-54.

43. Sumanasinghe RD, Bernacki SH, Loboa EG. Osteogenic differentiation of human mesenchymal stem cells in collagen matrices: effect of uniaxial cyclic tensile strain on bone morphogenetic protein (BMP-2) mRNA expression. Tissue Eng 2006; 12: 3459-65.

44. Simmons CA, Matlis S, Thornton AJ, Chen S, Wang CY, Mooney DJ. Cyclic strain enhances matrix mineralization by adult human mesenchymal stem cells

via the extracellular signal-regulated kinase (ERK1/2) signaling pathway. J Biomech 2003; 36: 1087-96.

45. Kaigler D, Krebsbach PH, West ER, Horger K, Huang YC, Mooney DJ. Endothelial cell modulation of bone marrow stromal cell osteogenic potential. Faseb J 2005; 19: 665-7.

46. Saleh FA, Whyte M, Genever PG. Effects of endothelial cells on human mesenchymal stem cell activity in a three-dimensional in vitro model. Eur Cell Mater 2011; 22: 242-57.

47. Rouwkema J, de Boer J, Van Blitterswijk CA. Endothelial cells assemble into a 3-dimensional prevascular network in a bone tissue engineering construct. Tissue Eng 2006; 12: 2685-93.

48. Zhu J. Bioactive modification of poly(ethylene glycol) hydrogels for tissue engineering. Biomaterials 2010; 31: 4639-56.

49. Dawson E, Mapili G, Erickson K, Taqvi S, Roy K. Biomaterials for stem cell differentiation. Adv Drug Deliv Rev 2008; 60: 215-28.

50. Hwang NS, Varghese S, Elisseeff J. Controlled differentiation of stem cells. Adv Drug Deliv Rev 2008; 60: 199-214.

51. Singh A, Elisseeff J. Biomaterials for stem cell differentiation. Journal of Materials Chemistry 2010; 20: 8832-8847.

52. Kalakkunnath S, Kalika DS, Lin H, Raharjo RD, Freeman BD. Molecular relaxation in cross-linked poly(ethylene glycol) and poly(propylene glycol) diacrylate networks by dielectric spectroscopy. Polymer 2007; 48: 579-589.

53. Benoit DS, Schwartz MP, Durney AR, Anseth KS. Small functional groups for controlled differentiation of hydrogel-encapsulated human mesenchymal stem cells. Nat Mater 2008; 7: 816-23.

54. Armstrong N, Hardin J, McClay DR. Cell-cell interactions regulate skeleton formation in the sea urchin embryo. Development 1993; 119: 833-40.

55. Ball SG, Shuttleworth AC, Kielty CM. Direct cell contact influences bone marrow mesenchymal stem cell fate. Int J Biochem Cell Biol 2004; 36: 714-27.

56. Clarkin CE, Emery RJ, Pitsillides AA, Wheeler-Jones CP. Evaluation of VEGF-mediated signaling in primary human cells reveals a paracrine action for VEGF in osteoblast-mediated crosstalk to endothelial cells. J Cell Physiol 2008; 214: 537-44.

57. Grellier M, Bordenave L, Amedee J. Cell-to-cell communication between osteogenic and endothelial lineages: implications for tissue engineering. Trends Biotechnol 2009; 27: 562-71.

58. Ramig LO, Verdolini K. Treatment efficacy: voice disorders. J Speech Lang Hear Res 1998; 41: S101-16.

59. Benninger MS, Alessi D, Archer S, Bastian R, Ford C, Koufman J, et al. Vocal fold scarring: current concepts and management. Otolaryngol Head Neck Surg 1996; 115: 474-82.

60. Dailey SH, Ford CN. Surgical management of sulcus vocalis and vocal fold scarring. Otolaryngol Clin North Am 2006; 39: 23-42.

61. Rosen CA. Phonosurgical vocal fold injection: procedures and materials. Otolaryngol Clin North Am 2000; 33: 1087-96.

62. Titze IR, Hitchcock RW, Broadhead K, Webb K, Li W, Gray SD, et al. Design and validation of a bioreactor for engineering vocal fold tissues under combined tensile and vibrational stresses. J Biomech 2004; 37: 1521-9.

63. David-Raoudi M, Tranchepain F, Deschrevel B, Vincent JC, Bogdanowicz P, Boumediene K, et al. Differential effects of hyaluronan and its fragments on fibroblasts: relation to wound healing. Wound Repair Regen 2008; 16: 274-87.

64. Joddar B, Ramamurthi A. Elastogenic effects of exogenous hyaluronan oligosaccharides on vascular smooth muscle cells. Biomaterials 2006; 27: 5698-707.

65. Joddar B, Ramamurthi A. Fragment size- and dose-specific effects of hyaluronan on matrix synthesis by vascular smooth muscle cells. Biomaterials 2006; 27: 2994-3004.

66. Meran S, Thomas D, Stephens P, Martin J, Bowen T, Phillips A, et al. Involvement of hyaluronan in regulation of fibroblast phenotype. J Biol Chem 2007; 282: 25687-97.

67. Hui TY, Cheung KM, Cheung WL, Chan D, Chan BP. In vitro chondrogenic differentiation of human mesenchymal stem cells in collagen microspheres: influence of cell seeding density and collagen concentration. Biomaterials 2008; 29: 3201-12.

68. Engler AJ, Sen S, Sweeney HL, Discher DE. Matrix elasticity directs stem cell lineage specification. Cell 2006; 126: 677-89.

69. Mann BK, Tsai AT, Scott-Burden T, West JL. Modification of surfaces with cell adhesion peptides alters extracellular matrix deposition. Biomaterials 1999; 20: 2281-6.

70. Gombotz WR, Wang GH, Horbett TA, Hoffman AS. Protein adsorption to poly(ethylene oxide) surfaces. J Biomed Mater Res 1991; 25: 1547-62.

71. Hahn MS, Miller JS, West JL. Laser Scanning Lithography for Surface Micropatterning on Hydrogels. Advanced Materials 2005; 17: 2939-2942.

72. Munoz-Pinto DJ, Bulick AS, Hahn MS. Uncoupled investigation of scaffold modulus and mesh size on smooth muscle cell behavior. J Biomed Mater Res A 2009; 90: 303-16.

73. Bryant SJ, Anseth KS. Hydrogel properties influence ECM production by chondrocytes photoencapsulated in poly(ethylene glycol) hydrogels. J Biomed Mater Res 2002; 59: 63-72.

74. Bryant SJ, Arthur JA, Anseth KS. Incorporation of tissue-specific molecules alters chondrocyte metabolism and gene expression in photocrosslinked hydrogels. Acta Biomater 2005; 1: 243-52.

75. Elisseeff J, Anseth K, Sims D, McIntosh W, Randolph M, Yaremchuk M, et al. Transdermal photopolymerization of poly(ethylene oxide)-based injectable hydrogels for tissue-engineered cartilage. Plast Reconstr Surg 1999; 104: 1014-22.

76. Hahn MS, Teply BA, Stevens MM, Zeitels SM, Langer R. Collagen composite hydrogels for vocal fold lamina propria restoration. Biomaterials 2006; 27: 1104-9.

77. Humphries JD, Byron A, Humphries MJ. Integrin ligands at a glance. J Cell Sci 2006; 119: 3901-3.

78. Slevin M, Kumar S, Gaffney J. Angiogenic oligosaccharides of hyaluronan induce multiple signaling pathways affecting vascular endothelial cell mitogenic and wound healing responses. J Biol Chem 2002; 277: 41046-59.

79. Slevin M, Krupinski J, Gaffney J, Matou S, West D, Delisser H, et al. Hyaluronan-mediated angiogenesis in vascular disease: uncovering RHAMM and CD44 receptor signaling pathways. Matrix Biol 2007; 26: 58-68.

80. Turley EA, Noble PW, Bourguignon LY. Signaling properties of hyaluronan receptors. J Biol Chem 2002; 277: 4589-92.

81. Masters KS, Shah DN, Leinwand LA, Anseth KS. Crosslinked hyaluronan scaffolds as a biologically active carrier for valvular interstitial cells. Biomaterials 2005; 26: 2517-25.

82. Garrett CG, Coleman JR, Reinisch L. Comparative histology and vibration of the vocal folds: implications for experimental studies in microlaryngeal surgery. Laryngoscope 2000; 110: 814-24.

83. Buxton AN, Zhu J, Marchant R, West JL, Yoo JU, Johnstone B. Design and characterization of poly(ethylene glycol) photopolymerizable semi-

interpenetrating networks for chondrogenesis of human mesenchymal stem cells. Tissue Eng 2007; 13: 2549-60.

84. Hahn MS, McHale MK, Wang E, Schmedlen RH, West JL. Physiologic pulsatile flow bioreactor conditioning of poly(ethylene glycol)-based tissue engineered vascular grafts. Ann Biomed Eng 2007; 35: 190-200.

85. Gregory TR. Nucleotypic effects without nuclei: genome size and erythrocyte size in mammals. Genome 2000; 43: 895-901.

86. Luo Y, Kobler JB, Zeitels SM, Langer R. Effects of growth factors on extracellular matrix production by vocal fold fibroblasts in 3-dimensional culture. Tissue Eng 2006; 12: 3365-74.

87. Burdick JA, Anseth KS. Photoencapsulation of osteoblasts in injectable RGD-modified PEG hydrogels for bone tissue engineering. Biomaterials 2002; 23: 4315-23.

88. Salinas CN, Anseth KS. The enhancement of chondrogenic differentiation of human mesenchymal stem cells by enzymatically regulated RGD functionalities. Biomaterials 2008; 29: 2370-7.

89. Salinas CN, Anseth KS. The influence of the RGD peptide motif and its contextual presentation in PEG gels on human mesenchymal stem cell viability. J Tissue Eng Regen Med 2008; 2: 296-304.

90. Bryant SJ, Anseth KS. Controlling the spatial distribution of ECM components in degradable PEG hydrogels for tissue engineering cartilage. J Biomed Mater Res A 2003; 64: 70-9.

91. Bryant SJ, Durand KL, Anseth KS. Manipulations in hydrogel chemistry control photoencapsulated chondrocyte behavior and their extracellular matrix production. J Biomed Mater Res A 2003; 67: 1430-6.

92. Peyton SR, Raub CB, Keschrumrus VP, Putnam AJ. The use of poly(ethylene glycol) hydrogels to investigate the impact of ECM chemistry and mechanics on smooth muscle cells. Biomaterials 2006; 27: 4881-93.

93. Munoz-Pinto D, Whittaker P, Hahn MS. Lamina propria cellularity and collagen composition: an integrated assessment of structure in humans. Ann Otol Rhinol Laryngol 2009; 118: 299-306.

94. Culav EM, Clark CH, Merrilees MJ. Connective tissues: matrix composition and its relevance to physical therapy. Phys Ther 1999; 79: 308-19.

95. Light ND. Estimation of types I and III collagens in whole tissue by quantitation of CNBr peptides on SDS-polyacrylamide gels. Biochim Biophys Acta 1982; 702: 30-6.

96. Bogatkevich GS, Tourkina E, Silver RM, Ludwicka-Bradley A. Thrombin differentiates normal lung fibroblasts to a myofibroblast phenotype via the proteolytically activated receptor-1 and a protein kinase C-dependent pathway. J Biol Chem 2001; 276: 45184-92.

97. Broadley C, Gonzalez DA, Nair R, Koriwchak MJ, Ossoff RH, Davidson JM. A tissue-culture model for the study of canine vocal fold fibroblasts. Laryngoscope 1995; 105: 23-7.

98. Chailley-Heu B, Boucherat O, Barlier-Mur AM, Bourbon JR. FGF-18 is upregulated in the postnatal rat lung and enhances elastogenesis in myofibroblasts. Am J Physiol Lung Cell Mol Physiol 2005; 288: L43-51.

99. Hoff CR, Perkins DR, Davidson JM. Elastin gene expression is upregulated during pulmonary fibrosis. Connect Tissue Res 1999; 40: 145-53.

100. Mariani TJ, Crouch E, Roby JD, Starcher B, Pierce RA. Increased elastin production in experimental granulomatous lung disease. Am J Pathol 1995; 147: 988-1000.

101. Rishikof DC, Lucey EC, Kuang PP, Snider GL, Goldstein RH. Induction of the myofibroblast phenotype following elastolytic injury to mouse lung. Histochem Cell Biol 2006; 125: 527-34.

102. Hahn MS, Kobler JB, Starcher BC, Zeitels SM, Langer R. Quantitative and comparative studies of the vocal fold extracellular matrix. I: Elastic fibers and hyaluronic acid. Ann Otol Rhinol Laryngol 2006; 115: 156-64.

103. Catten M, Gray SD, Hammond TH, Zhou R, Hammond E. Analysis of cellular location and concentration in vocal fold lamina propria. Otolaryngol Head Neck Surg 1998; 118: 663-7.

104. Koh WG, Itle LJ, Pishko MV. Molding of hydrogel microstructures to create multiphenotype cell microarrays. Anal Chem 2003; 75: 5783-9.

105. Liu VA, Bhatia SN. Three-Dimensional Photopatterning of Hydrogels Containing Living Cells. Biomedical Microdevices 2002; 4: 257-266.

106. Shah DN, Recktenwall-Work SM, Anseth KS. The effect of bioactive hydrogels on the secretion of extracellular matrix molecules by valvular interstitial cells. Biomaterials 2008; 29: 2060-72.

107. Hahn MS, Teply BA, Stevens MM, Zeitels SM, Langer R. Collagen composite hydrogels for vocal fold lamina propria restoration. Biomaterials 2006; 27: 1104-1109.

108. Gray SD, Titze IR, Alipour F, Hammond TH. Biomechanical and histologic observations of vocal fold fibrous proteins. Ann Otol Rhinol Laryngol 2000; 109: 77-85.

109. Hansen JK, Thibeault SL. Current understanding and review of the literature: vocal fold scarring. J Voice 2006; 20: 110-20.

110. Titze IR, Broadhead K, Tresco P, Gray S. Strain distribution in an elastic substrate vibrated in a bioreactor for vocal fold tissue engineering. J Biomech 2005; 38: 2406-14.

111. Kutty JK, Webb K. Tissue engineering therapies for the vocal fold lamina propria. Tissue Eng Part B Rev 2009; 15: 249-62.

112. Thibeault SL, Klemuk SA, Smith ME, Leugers C, Prestwich G. In vivo comparison of biomimetic approaches for tissue regeneration of the scarred vocal fold. Tissue Eng Part A 2009; 15: 1481-7.

113. Iozzo RV, Schaefer L. Proteoglycans in health and disease: novel regulatory signaling mechanisms evoked by the small leucine-rich proteoglycans. Febs J 2010; 277: 3864-75.

114. Thibeault SL, Bless DM, Gray SD. Interstitial protein alterations in rabbit vocal fold with scar. J Voice 2003; 17: 377-83.

115. Hahn MS, Kobler JB, Zeitels SM, Langer R. Midmembranous vocal fold lamina propria proteoglycans across selected species. Ann Otol Rhinol Laryngol 2005; 114: 451-62.

116. Scott PG, Dodd CM, Tredget EE, Ghahary A, Rahemtulla F. Chemical characterization and quantification of proteoglycans in human post-burn hypertrophic and mature scars. Clin Sci (Lond) 1996; 90: 417-25.

117. Bulick AS, Munoz-Pinto DJ, Qu X, Mani M, Cristancho D, Urban M, et al. Impact of endothelial cells and mechanical conditioning on smooth muscle cell extracellular matrix production and differentiation. Tissue Eng Part A 2009; 15: 815-25.

118. Benoit DS, Anseth KS. Heparin functionalized PEG gels that modulate protein adsorption for hMSC adhesion and differentiation. Acta Biomater 2005; 1: 461-70.

119. Qu X, Jimenez-Vergara AC, Munoz-Pinto DJ, Ortiz D, McMahon RE, Cristancho D, et al. Regulation of smooth muscle cell phenotype by glycosaminoglycan identity. Acta Biomater 2011; 7: 1031-9.

120. Watkins AW, Anseth KS. Investigation of Molecular Transport and Distributions in Poly(ethylene glycol) Hydrogels with Confocal Laser Scanning Microscopy. Macromolecules 2005; 38: 1326-1334.

121. Armstrong JK, Wenby RB, Meiselman HJ, Fisher TC. The hydrodynamic radii of macromolecules and their effect on red blood cell aggregation. Biophys J 2004; 87: 4259-70.

122. Anseth KS, Bowman CN, Brannon-Peppas L. Mechanical properties of hydrogels and their experimental determination. Biomaterials 1996; 17: 1647-57.

123. Elbert DL, Hubbell JA. Conjugate addition reactions combined with free-radical cross-linking for the design of materials for tissue engineering. Biomacromolecules 2001; 2: 430-41.

124. Miller EJ, Gay S. Collagen: an overview. Methods Enzymol 1982; 82: 3-32.

125. Chan RW. Measurements of vocal fold tissue viscoelasticity: approaching the male phonatory frequency range. J Acoust Soc Am 2004; 115: 3161-70.

126. Chan RW, Rodriguez ML. A simple-shear rheometer for linear viscoelastic characterization of vocal fold tissues at phonatory frequencies. J Acoust Soc Am 2008; 124: 1207-19.

127. Amadeu TP, Braune AS, Porto LC, Desmouliere A, Costa AM. Fibrillin-1 and elastin are differentially expressed in hypertrophic scars and keloids. Wound Repair Regen 2004; 12: 169-74.

128. Bryant SJ, Nuttelman CR, Anseth KS. Cytocompatibility of UV and visible light photoinitiating systems on cultured NIH/3T3 fibroblasts in vitro. J Biomater Sci Polym Ed 2000; 11: 439-57.

129. Gabbiani G. The myofibroblast in wound healing and fibrocontractive diseases. J Pathol 2003; 200: 500-3.

130. Burd A. Hyaluronan and scarring. In: Garg HG, Hales CA, editors. Chemistry and biology of hyaluronan. Oxford: Elsevier Science Ltd.; 2004. p. 367–94.

131. Hahn MS, Kobler JB, Zeitels SM, Langer R. Quantitative and comparative studies of the vocal fold extracellular matrix II: collagen. Ann Otol Rhinol Laryngol 2006; 115: 225-32.

132. Fan SQ, Qin LY, Cai JL, Zhu GY, Bin X, Yan HS. Effect of heparin on production of basic fibroblast growth factor and transforming growth factor-beta1 by human normal skin and hyperplastic scar fibroblasts. J Burn Care Res 2007; 28: 734-41.

133. Entwistle J, Hall CL, Turley EA. HA receptors: regulators of signalling to the cytoskeleton. J Cell Biochem 1996; 61: 569-77.

134. Fujimoto T, Kawashima H, Tanaka T, Hirose M, Toyama-Sorimachi N, Matsuzawa Y, et al. CD44 binds a chondroitin sulfate proteoglycan, aggrecan. Int Immunol 2001; 13: 359-66.

135. Yang B, Hall CL, Yang BL, Savani RC, Turley EA. Identification of a novel heparin binding domain in RHAMM and evidence that it modifies HA mediated locomotion of ras-transformed cells. J Cell Biochem 1994; 56: 455-68.

136. Ishiguro S, Akasaka Y, Kiguchi H, Suzuki T, Imaizumi R, Ishikawa Y, et al. Basic fibroblast growth factor induces down-regulation of alpha-smooth muscle actin and reduction of myofibroblast areas in open skin wounds. Wound Repair Regen 2009; 17: 617-25.

137. Bondi CD, Manickam N, Lee DY, Block K, Gorin Y, Abboud HE, et al. NAD(P)H oxidase mediates TGF-beta1-induced activation of kidney myofibroblasts. J Am Soc Nephrol 2010; 21: 93-102.

138. Chen A, Zhang L, Xu J, Tang J. The antioxidant (-)-epigallocatechin-3-gallate inhibits activated hepatic stellate cell growth and suppresses acetaldehyde-induced gene expression. Biochem J 2002; 368: 695-704.

139. Rider CC. Heparin/heparan sulphate binding in the TGF-beta cytokine superfamily. Biochem Soc Trans 2006; 34: 458-60.

140. Fthenou E, Zafiropoulos A, Katonis P, Tsatsakis A, Karamanos NK, Tzanakakis GN. Chondroitin sulfate prevents platelet derived growth factor-mediated phosphorylation of PDGF-Rbeta in normal human fibroblasts severely impairing mitogenic responses. J Cell Biochem 2008; 103: 1866-76.

141. Rolny C, Spillmann D, Lindahl U, Claesson-Welsh L. Heparin amplifies platelet-derived growth factor (PDGF)- BB-induced PDGF alpha -receptor but not PDGF beta -receptor tyrosine phosphorylation in heparan sulfate-deficient cells. Effects on signal transduction and biological responses. J Biol Chem 2002; 277: 19315-21.

142. Ashikari-Hada S, Habuchi H, Kariya Y, Kimata K. Heparin regulates vascular endothelial growth factor165-dependent mitogenic activity, tube formation, and its receptor phosphorylation of human endothelial cells. Comparison of the effects of heparin and modified heparins. J Biol Chem 2005; 280: 31508-15.

143. Smith SM, West LA, Govindraj P, Zhang X, Ornitz DM, Hassell JR. Heparan and chondroitin sulfate on growth plate perlecan mediate binding and delivery of FGF-2 to FGF receptors. Matrix Biol 2007; 26: 175-84.

144. Lloyd-Jones D, Adams RJ, Brown TM, Carnethon M, Dai S, De Simone G, et al. Heart disease and stroke statistics--2010 update: a report from the American Heart Association. Circulation 2010; 121: e46-e215.

145. Katsuda S, Boyd HC, Fligner C, Ross R, Gown AM. Human atherosclerosis. III. Immunocytochemical analysis of the cell composition of lesions of young adults. Am J Pathol 1992; 140: 907-14.

146. Davies JD, Carpenter KL, Challis IR, Figg NL, McNair R, Proudfoot D, et al. Adipocytic differentiation and liver x receptor pathways regulate the accumulation of triacylglycerols in human vascular smooth muscle cells. J Biol Chem 2005; 280: 3911-9.

147. Rong JX, Shapiro M, Trogan E, Fisher EA. Transdifferentiation of mouse aortic smooth muscle cells to a macrophage-like state after cholesterol loading. Proc Natl Acad Sci USA 2003; 100: 13531-6.

148. Wada Y, Sugiyama A, Yamamoto T, Naito M, Noguchi N, Yokoyama S, et al. Lipid accumulation in smooth muscle cells under LDL loading is independent of LDL receptor pathway and enhanced by hypoxic conditions. Arterioscler Thromb Vasc Biol 2002; 22: 1712-9.

149. Papakonstantinou E, Karakiulakis G, Eickelberg O, Perruchoud AP, Block LH, Roth M. A 340 kDa hyaluronic acid secreted by human vascular smooth muscle cells regulates their proliferation and migration. Glycobiology 1998; 8: 821-30.

150. Stevens RL, Colombo M, Gonzales JJ, Hollander W, Schmid K. The glycosaminoglycans of the human artery and their changes in atherosclerosis. J Clin Invest 1976; 58: 470-81.

151. Wagner WD. Proteoglycan structure and function as related to atherosclerosis. Ann N Y Acad Sci 1985; 454: 52-68.

152. Tammi M, Seppala PO, Lehtonen A, Mottonen M. Connective tissue components in normal and atherosclerotic human coronary arteries. Atherosclerosis 1978; 29: 191-4.

153. Theocharis AD, Theocharis DA, De Luca G, Hjerpe A, Karamanos NK. Compositional and structural alterations of chondroitin and dermatan sulfates during the progression of atherosclerosis and aneurysmal dilatation of the human abdominal aorta. Biochimie 2002; 84: 667-74.

154. Papakonstantinou E, Roth M, Block LH, Mirtsou-Fidani V, Argiriadis P, Karakiulakis G. The differential distribution of hyaluronic acid in the layers of human atheromatic aortas is associated with vascular smooth muscle cell proliferation and migration. Atherosclerosis 1998; 138: 79-89.

155. Glukhova MA, Frid MG, Koteliansky VE. Phenotypic changes of human aortic smooth muscle cells during development and in the adult vessel. Am J Physiol 1991; 261: 78-80.

156. Raines EW, Ross R. Smooth muscle cells and the pathogenesis of the lesions of atherosclerosis. Br Heart J 1993; 69: S30-7.

157. Orlandi A, Bochaton-Piallat ML, Gabbiani G, Spagnoli LG. Aging, smooth muscle cells and vascular pathobiology: implications for atherosclerosis. Atherosclerosis 2006; 188: 221-30.

158. Bobryshev YV, Lord RS. Langhans cells of human arterial intima: uniform by stellate appearance but different by nature. Tissue Cell 1996; 28: 177-94.

159. Kruse R, Merten M, Yoshida K, Schmidt A, Volker W, Buddecke E. Cholesterol-dependent changes of glycosaminoglycan pattern in human aorta. Basic Res Cardiol 1996; 91: 344-52.

160. Hasegawa H KH, Koiwa Y, Ichiki M, Tezuka F. Measurement of elastic moduli of tissue components in atherosclerotic plaques by ultrasonic phased tracking method. In: Proceedings of the ultrasonics symposium, Vol. 2. New York: IEEE; 2002 p. 1847–50.

161. Bryant SJ, Davis-Arehart KA, Luo N, Shoemaker RK, Arthur JA, Anseth KS. Synthesis and Characterization of Photopolymerized Multifunctional Hydrogels: Water-Soluble Poly(Vinyl Alcohol) and Chondroitin Sulfate Macromers for Chondrocyte Encapsulation. Macromolecules 2004; 37: 6726-6733.

162. Masters KS, Shah DN, Walker G, Leinwand LA, Anseth KS. Designing scaffolds for valvular interstitial cells: cell adhesion and function on naturally derived materials. J Biomed Mater Res A 2004; 71: 172-80.

163. Benoit DS, Durney AR, Anseth KS. The effect of heparin-functionalized PEG hydrogels on three-dimensional human mesenchymal stem cell osteogenic differentiation. Biomaterials 2007; 28: 66-77.

164. Ford MC, Bertram JP, Hynes SR, Michaud M, Li Q, Young M, et al. A macroporous hydrogel for the coculture of neural progenitor and endothelial cells to form functional vascular networks in vivo. Proc Natl Acad Sci USA 2006; 103: 2512-7.

165. Weirich J, Seiler L, Hug MJ, Fleckenstein-Grun G. Ca(2+) entry into primary cultured pig coronary smooth muscle cells after previous store depletion by repetitive P2Y purinoceptor stimulation. Cell Calcium 2001; 29: 359-67.

166. Gockerman A, Clemmons DR. Porcine aortic smooth muscle cells secrete a serine protease for insulin-like growth factor binding protein-2. Circ Res 1995; 76: 514-21.

167. Calabro A, Hascall VC, Midura RJ. Adaptation of FACE methodology for microanalysis of total hyaluronan and chondroitin sulfate composition from cartilage. Glycobiology 2000; 10: 283-93.

168. Zhang G, Wang X, Wang Z, Zhang J, Suggs L. A PEGylated fibrin patch for mesenchymal stem cell delivery. Tissue Eng 2006; 12: 9-19.

169. Munoz-Pinto DJ, McMahon RE, Kanzelberger MA, Jimenez-Vergara AC, Grunlan MA and Hahn MS. Inorganic-organic hybrid scaffolds for osteochondral regeneration. J Biomed Mater Res A 2010; 94: 112-21.

170. Zhang Z, Apse K, Pang J, Stanton RC. High glucose inhibits glucose-6-phosphate dehydrogenase via cAMP in aortic endothelial cells. J Biol Chem 2000; 275: 40042-7.

171. Goodrich RP, Sowemimo-Coker SO, Zerez CR, Tanaka KR. Preservation of metabolic activity in lyophilized human erythrocytes. Proc Natl Acad Sci USA 1992; 89: 967-71.

172. Keeley F, Todorovich L, Rabinovitch M. Elastin and elastases in the pathology of the arterial wall. In: Robert L, Hornebeck W, editors. Elastin and elastases. Boca Raton, FL: CRC Press; 1989. p. 169–84.

173. Andreeva ER, Pugach IM, Orekhov AN. Collagen-synthesizing cells in initial and advanced atherosclerotic lesions of human aorta. Atherosclerosis 1997; 130: 133-42.

174. Kratky RG, Ivey J, Roach MR. Local changes in collagen content in rabbit aortic atherosclerotic lesions with time. Atherosclerosis 1999; 143: 7-14.

175. Handa S, Sadi AM, Cybulsky MI, Stewart DJ, Husain M. Region-specific patterns of vascular remodelling occur early in atherosclerosis and without loss of smooth muscle cell markers. Atherosclerosis 2008; 196: 617-23.

176. Gutierrez MDP, O'Brien MDKD, Ferguson M, Nikkari MDPST, Alpers MDCE, Wight PTN. Differences in the Distribution of Versican, Decorin, and Biglycan in Atherosclerotic Human Coronary Arteries. Cardiovascular Pathology 1997; 6: 271-278.

177. Wight TN, Merrilees MJ. Proteoglycans in atherosclerosis and restenosis: key roles for versican. Circ Res 2004; 94: 1158-67.

178. O'Brien KD, Olin KL, Alpers CE, Chiu W, Ferguson M, Hudkins K, et al. Comparison of apolipoprotein and proteoglycan deposits in human coronary atherosclerotic plaques: colocalization of biglycan with apolipoproteins. Circulation 1998; 98: 519-27.

179. Evanko SP, Raines EW, Ross R, Gold LI, Wight TN. Proteoglycan distribution in lesions of atherosclerosis depends on lesion severity, structural characteristics, and the proximity of platelet-derived growth factor and transforming growth factor-beta. Am J Pathol 1998; 152: 533-46.

180. Rodriguez-Lee M, Ostergren-Lunden G, Wallin B, Moses J, Bondjers G, Camejo G. Fatty acids cause alterations of human arterial smooth muscle cell proteoglycans that increase the affinity for low-density lipoprotein. Arterioscler Thromb Vasc Biol 2006; 26: 130-5.

181. Lloyd-Jones D, Adams R, Carnethon M, De Simone G, Ferguson TB, Flegal K, et al. Heart disease and stroke statistics--2009 update: a report from the American Heart Association Statistics Committee and Stroke Statistics Subcommittee. Circulation 2009; 119: e21-181.

182. McKee JA, Banik SS, Boyer MJ, Hamad NM, Lawson JH, Niklason LE, et al. Human arteries engineered in vitro. EMBO Rep 2003; 4: 633-8.

183. Schmedlen RH, Elbjeirami WM, Gobin AS, West JL. Tissue engineered small-diameter vascular grafts. Clin Plast Surg 2003; 30: 507-17.

184. Isenberg BC, Tranquillo RT. Long-term cyclic distention enhances the mechanical properties of collagen-based media-equivalents. Ann Biomed Eng 2003; 31: 937-49.

185. Seliktar D, Black RA, Vito RP, Nerem RM. Dynamic mechanical conditioning of collagen-gel blood vessel constructs induces remodeling in vitro. Ann Biomed Eng 2000; 28: 351-62.

186. Solan A, Mitchell S, Moses M, Niklason L. Effect of pulse rate on collagen deposition in the tissue-engineered blood vessel. Tissue Eng 2003; 9: 579-86.

187. Fung YC. Biomechanics: Mechanical Properties of Living Tissues. New York: Springer-Verlag; 1993. p 321–391.

188. Lemson MS, Tordoir JH, Daemen MJ, Kitslaar PJ. Intimal hyperplasia in vascular grafts. Eur J Vasc Endovasc Surg 2000; 19: 336-50.

189. West JL, Hubbell JA. Separation of the arterial wall from blood contact using hydrogel barriers reduces intimal thickening after balloon injury in the rat: the roles of medial and luminal factors in arterial healing. Proc Natl Acad Sci USA 1996; 93: 13188-93.

190. Sawhney AS, Pathak CP, Hubbell JA. Bioerodible hydrogels based on photopolymerized poly(ethylene glycol)-co-poly(.alpha.-hydroxy acid) diacrylate macromers. Macromolecules 1993; 26: 581-587.

191. Hahn MS, Taite LJ, Moon JJ, Rowland MC, Ruffino KA, West JL. Photolithographic patterning of polyethylene glycol hydrogels. Biomaterials 2006; 27: 2519-24.

192. Johnson CP, How T, Scraggs M, West CR, Burns J. A biomechanical study of the human vertebral artery with implications for fatal arterial injury. Forensic Sci Int 2000; 109: 169-82.

193. Hiles MC, Badylak SF, Lantz GC, Kokini K, Geddes LA, Morff RJ. Mechanical properties of xenogeneic small-intestinal submucosa when used as an aortic graft in the dog. J Biomed Mater Res 1995; 29: 883-91.

194. Hummon AB, Lim SR, Difilippantonio MJ, Ried T. Isolation and solubilization of proteins after TRIzol extraction of RNA and DNA from patient material following prolonged storage. Biotechniques 2007; 42: 467-70, 472.

195. Womersley JR. Oscillatory flow in arteries: the constrained elastic tube as a model of arterial flow and pulse transmission. Phys Med Biol. 1957; 2: 178-87.

196. Womersley JR. Method for the calculation of velocity, rate of flow and viscous drag in arteries when the pressure gradient is known. J Physiol 1955; 127: 553-63.

197. Wechezak AR, Coan DE, Viggers RF, Sauvage LR. Dextran increases survival of subconfluent endothelial cells exposed to shear stress. Am J Physiol 1993; 264: H520-5.

198. Rinker KD, Kirkpatrick AP, Ting-Beall HP, Shepherd RD, Levin JD, Irick J, et al. Linoleic acid increases monocyte deformation and adhesion to endothelium. Atherosclerosis 2004; 177: 275-85.

199. Wolf S, Werthessen NT. Dynamics of arterial flow. Adv Exp Med Biol 1979; 115: 1-472.

200. Soulis JV, Farmakis TM, Giannoglou GD, Louridas GE. Wall shear stress in normal left coronary artery tree. J Biomech 2006; 39: 742-9.

201. Posey J, Geddes L. Measurement of the modulus of elasticity of the arterial wall. Cardiovasc. Res Ctr Bull 1973: 83–88.

202. Bryant SJ, Anseth KS, Lee DA, Bader DL. Crosslinking density influences the morphology of chondrocytes photoencapsulated in PEG hydrogels during the application of compressive strain. J Orthop Res 2004; 22: 1143-9.

203. Hastings NE, Simmers MB, McDonald OG, Wamhoff BR, Blackman BR. Atherosclerosis-prone hemodynamics differentially regulates endothelial and smooth muscle cell phenotypes and promotes pro-inflammatory priming. Am J Physiol Cell Physiol 2007; 293: C1824-33.

204. Raeber GP, Lutolf MP, Hubbell JA. Molecularly engineered PEG hydrogels: a novel model system for proteolytically mediated cell migration. Biophys J 2005; 89: 1374-88.

205. Reddy SK, Sebra RP, Anseth KS, Bowman CN. Living radical photopolymerization induced grafting on thiol–ene based substrates. Journal of Polymer Science Part A: Polymer Chemistry 2005; 43: 2134-2144.

206. Rydholm AE, Anseth KS, Bowman CN. Effects of neighboring sulfides and pH on ester hydrolysis in thiol-acrylate photopolymers. Acta Biomater 2007; 3: 449-55.

207. Ning CQ, Mehta J, El-Ghannam A. Effects of silica on the bioactivity of calcium phosphate composites in vitro. J Mater Sci Mater Med 2005; 16: 355-60.

208. Gupta G, El-Ghannam A, Kirakodu S, Khraisheh M, Zbib H. Enhancement of osteoblast gene expression by mechanically compatible porous Si-rich nanocomposite. J Biomed Mater Res B Appl Biomater 2007; 81: 387-96.

209. Ren L, Tsuru K, Hayakawa S, Osaka A. In vitro Evaluation of Osteoblast Response to Sol-Gel Derived Gelatin-Siloxane Hybrids. Journal of Sol-Gel Science and Technology 2003; 26: 1137-1140.

210. Fisher JP, Lalani Z, Bossano CM, Brey EM, Demian N, Johnston CM, et al. Effect of biomaterial properties on bone healing in a rabbit tooth extraction socket model. J Biomed Mater Res A 2004; 68: 428-38.

211. Yang F, Williams CG, Wang DA, Lee H, Manson PN, Elisseeff J. The effect of incorporating RGD adhesive peptide in polyethylene glycol diacrylate hydrogel on osteogenesis of bone marrow stromal cells. Biomaterials 2005; 26: 5991-8.

212. Hron P. Hydrophilisation of silicone rubber for medical applications. Polymer International 2003; 52: 1531-1539.

213. Bradley SG, Munson AE, McCay JA, Brown RD, Musgrove DL, Wilson S, et al. Subchronic 10 day immunotoxicity of polydimethylsiloxane (silicone) fluid, gel and elastomer and polyurethane disks in female B6C3F1 mice. Drug Chem Toxicol 1994; 17: 175-220.

214. Rowe VK, Spencer HC, Bass SL. Toxicological studies on certain commercial silicones and hydrolyzable silane intermediates. J Ind Hyg Toxicol 1948; 30: 332-52.

215. Curtis J, Colas A. Medical applications of silicones. In: Ratner BD, Schoen FJ, Lemons JE, Editors. Biomaterials Science: An Introduction to Materials in Medicine. San Diego: Elsevier Ademic Press; 2004. p 697-707.

216. Huebsch N, Arany PR, Mao AS, Shvartsman D, Ali OA, Bencherif SA, et al. Harnessing traction-mediated manipulation of the cell/matrix interface to control stem-cell fate. Nat Mater 2010; 9: 518-26.

217. Thomopoulos S, Williams GR, Gimbel JA, Favata M, Soslowsky LJ. Variation of biomechanical, structural, and compositional properties along the tendon to bone insertion site. J Orthop Res 2003; 21: 413-9.

218. Grunlan MA, Lee NS, Mansfeld F, Kus E, Finlay JA, Callow JA, et al. Minimally adhesive polymer surfaces prepared from star oligosiloxanes and star oligofluorosiloxanes. Journal of Polymer Science Part A: Polymer Chemistry 2006; 44: 2551-2566.

219. Gong C, Fréchet JMJ. End functionalization of hyperbranched poly(siloxysilane): Novel crosslinking agents and hyperbranched–linear star block copolymers. Journal of Polymer Science Part A: Polymer Chemistry 2000; 38: 2970-2978.

220. Boutevin B, Guida-Pietrasanta F, Ratsimihety A. Synthesis of photocrosslinkable fluorinated polydimethylsiloxanes: Direct introduction of acrylic pendant groups via hydrosilylation. Journal of Polymer Science Part A: Polymer Chemistry 2000; 38: 3722-3728.

221. Hahn MS, Miller JS, West JL. Three-Dimensional Biochemical and Biomechanical Patterning of Hydrogels for Guiding Cell Behavior. Advanced Materials 2006; 18: 2679-2684.

222. Nemir S, Hayenga HN, West JL. PEGDA hydrogels with patterned elasticity: Novel tools for the study of cell response to substrate rigidity. Biotechnol Bioeng 2010; 105: 636-44.

223. Engler AJ, Richert L, Wong JY, Picart C, Discher DE. Surface probe measurements of the elasticity of sectioned tissue, thin gels and polyelectrolyte multilayer films: Correlations between substrate stiffness and cell adhesion. Surface Science 2004; 570: 142-154.

224. Costa KD. Imaging and probing cell mechanical properties with the atomic force microscope. Methods Mol Biol 2006; 319: 331-61.

225. Costa KD, Sim AJ, Yin FC. Non-Hertzian approach to analyzing mechanical properties of endothelial cells probed by atomic force microscopy. J Biomech Eng 2006; 128: 176-84.

226. Johnson K. Contact Mechanics. Cambridge: Cambridge University Press: 1985.

227. Engler AJ, Rehfeldt F, Sen S, Discher DE. Microtissue elasticity: measurements by atomic force microscopy and its influence on cell differentiation. Methods Cell Biol 2007; 83: 521-45.

228. Canal T, Peppas NA. Correlation between mesh size and equilibrium degree of swelling of polymeric networks. J Biomed Mater Res 1989; 23: 1183-93.

229. Mellott MB, Searcy K, Pishko MV. Release of protein from highly cross-linked hydrogels of poly(ethylene glycol) diacrylate fabricated by UV polymerization. Biomaterials 2001; 22: 929-41.

230. Faucheux N, Haye B, Nagel MD. Activation of the cyclic AMP pathway in cells adhering to biomaterials: regulation by vitronectin- and fibronectin-integrin binding. Biomaterials 2000; 21: 1031-8.

231. Munoz-Pinto D. Hybrid Polyethylene Glycol Hydrogels for Tissue Engineering Applications. College Station: Chemical Engineering, Texas A&M University; 2011.

232. Freed BK, Biesecker J, Middleton WJ. Spectral polarity index: a new method for determining the relative polarity of solvents [1]. Journal of Fluorine Chemistry 1990; 48: 63-75.

233. Williams CG, Malik AN, Kim TK, Manson PN, Elisseeff JH. Variable cytocompatibility of six cell lines with photoinitiators used for polymerizing hydrogels and cell encapsulation. Biomaterials 2005; 26: 1211-8.

234. Hou Y, Schoener CA, Regan KR, Munoz-Pinto D, Hahn MS, Grunlan MA. Photo-cross-linked PDMSstar-PEG hydrogels: synthesis, characterization, and potential application for tissue engineering scaffolds. Biomacromolecules 2010; 11: 648-56.

235. Lim JY, Shaughnessy MC, Zhou Z, Noh H, Vogler EA, Donahue HJ. Surface energy effects on osteoblast spatial growth and mineralization. Biomaterials 2008; 29: 1776-84.

236. Anselme K. Osteoblast adhesion on biomaterials. Biomaterials 2000; 21: 667-81.

237. Sires BS, Lemke BN, Dortzbach RK, Gonnering RS. Characterization of human orbital fat and connective tissue. Ophthal Plast Reconstr Surg 1998; 14: 403-14.

238. Stevens MM, Marini RP, Martin I, Langer R, Prasad Shastri V. FGF-2 enhances TGF-beta1-induced periosteal chondrogenesis. J Orthop Res 2004; 22: 1114-9.

239. Parekh SH, Chatterjee K, Lin-Gibson S, Moore NM, Cicerone MT, Young MF, et al. Modulus-driven differentiation of marrow stromal cells in 3D scaffolds that is independent of myosin-based cytoskeletal tension. Biomaterials 2011; 32: 2256-64.

240. Jimenez-Vergara AC, Guiza-Arguello V, Becerra-Bayona S, Munoz-Pinto DJ, McMahon RE, Morales A, et al. Approach for fabricating tissue engineered vascular grafts with stable endothelialization. Ann Biomed Eng 2010; 38: 2885-95.

241. Koutsiaris AG, Tachmitzi SV, Batis N, Kotoula MG, Karabatsas CH, Tsironi E, et al. Volume flow and wall shear stress quantification in the human conjunctival capillaries and post-capillary venules in vivo. Biorheology 2007; 44: 375-86.

242. Gao L, McBeath R, Chen CS. Stem cell shape regulates a chondrogenic versus myogenic fate through Rac1 and N-cadherin. Stem Cells 2010; 28: 564-72.

243. Terraciano V, Hwang N, Moroni L, Park HB, Zhang Z, Mizrahi J, et al. Differential response of adult and embryonic mesenchymal progenitor cells to mechanical compression in hydrogels. Stem Cells 2007; 25: 2730-8.

244. Huang CY, Hagar KL, Frost LE, Sun Y, Cheung HS. Effects of cyclic compressive loading on chondrogenesis of rabbit bone-marrow derived mesenchymal stem cells. Stem Cells 2004; 22: 313-23.

245. Thorpe SD, Buckley CT, Kelly DJ. Can Dynamic Compression in the Absence of Growth Factors Induce Chondrogenic Differentiation of Bone Marrow Derived MSCs Encapsulated in Agarose Hydrogels?. In: Haj A, Bader D, Editors. 8th International Conference on Cell & Stem Cell Engineering (ICCE), Vol. 30. Dublin: Springer Berlin Heidelberg; 2011. p 43-46.

246. Pelaez D, Huang CY, Cheung HS. Cyclic compression maintains viability and induces chondrogenesis of human mesenchymal stem cells in fibrin gel scaffolds. Stem Cells Dev 2009; 18: 93-102.

247. McMahon LA, Campbell VA, Prendergast PJ. Involvement of stretch-activated ion channels in strain-regulated glycosaminoglycan synthesis in mesenchymal stem cell-seeded 3D scaffolds. J Biomech 2008; 41: 2055-9.

248. McMahon LA, Reid AJ, Campbell VA, Prendergast PJ. Regulatory effects of mechanical strain on the chondrogenic differentiation of MSCs in a collagen-GAG scaffold: experimental and computational analysis. Ann Biomed Eng 2008; 36: 185-94.

249. Connelly JT, Vanderploeg EJ, Mouw JK, Wilson CG, Levenston ME. Tensile loading modulates bone marrow stromal cell differentiation and the development of engineered fibrocartilage constructs. Tissue Eng Part A 2010; 16: 1913-23.

250. Wagner DR, Lindsey DP, Li KW, Tummala P, Chandran SE, Smith RL, et al. Hydrostatic pressure enhances chondrogenic differentiation of human bone marrow stromal cells in osteochondrogenic medium. Ann Biomed Eng 2008; 36: 813-20.

251. Kisiday JD, Frisbie DD, McIlwraith CW, Grodzinsky AJ. Dynamic compression stimulates proteoglycan synthesis by mesenchymal stem cells in the absence of chondrogenic cytokines. Tissue Eng Part A 2009; 15: 2817-24.

252. Shih YR, Tseng KF, Lai HY, Lin CH, Lee OK. Matrix stiffness regulation of integrin-mediated mechanotransduction during osteogenic differentiation of human mesenchymal stem cells. J Bone Miner Res 2011; 26: 730-8.

253. Steinmetz NJ, Bryant SJ. The effects of intermittent dynamic loading on chondrogenic and osteogenic differentiation of human marrow stromal cells encapsulated in RGD-modified poly(ethylene glycol) hydrogels. Acta Biomater 2011; 7: 3829-40.

254. Bidarra SJ, Barrias CC, Barbosa MA, Soares R, Amedee J, Granja PL. Phenotypic and proliferative modulation of human mesenchymal stem cells via crosstalk with endothelial cells. Stem Cell Res 2011; 7: 186-97.

255. Kanczler JM, Oreffo RO. Osteogenesis and angiogenesis: the potential for engineering bone. Eur Cell Mater 2008; 15: 100-14.

VITA

Andrea Carolina Jimenez Vergara received her Bachelor degree in chemical engineering from The Universidad Industrial de Santander, Colombia, in 2005. She entered the Materials Science and Engineering graduate program at Texas A&M University in fall 2008 and received her Doctor of Philosophy degree in August 2012. Her research interests include the study of cell-material and cell-cell interactions and influence of dynamic stimuli for tissue engineering applications. She plans to continue her research in a postdoctoral position at Rensselaer Polytechnic Institute (RPI), in the area of mesenchymal stem cell research.

Mrs. Jimenez Vergara may be reached at 200 Jack E. Brown Engineering Building, Chemical Engineering Department, Texas A&M University, College Station TX 77843-3122. Her email address is andreacjv@tamu.edu.